UNIVERSIDADE FEDERAL DO CEARÁ
CENTRO DE TECNOLOGIA
PROGRAMA DE PÓS-GRADUAÇÃO EM ENGENHARIA CIVIL: ESTRUTURAS E CONSTRUÇÃO CIVIL

DANIEL LIRA LOPES TARGINO

INFLUENCE OF MICROSTRUCTURE AND CEMENT FORMULATION ON STIFFNESS AND FATIGUE BEHAVIOR OF CEMENTITIOUS MATERIALS

FORTALEZA
2023

DANIEL LIRA LOPES TARGINO

INFLUENCE OF MICROSTRUCTURE AND CEMENT FORMULATION ON STIFFNESS AND FATIGUE BEHAVIOR OF CEMENTITIOUS MATERIALS

M.Sc. Thesis presented to the Post-Graduate Program in Structures and Civil Construction, as a partial fulfillment of the requirements for the Master's degree in Civil Engineering at the Federal University of Ceará.

Area within the Graduate Program: Building Materials

Advisor: Lucas Feitosa de Albuquerque Lima Babadopulos, Ph.D.

Co-advisor: Yassine El-Mendili, Ph.D.

FORTALEZA

2023

Dados Internacionais de Catalogação na Publicação
Universidade Federal do Ceará
Sistema de Bibliotecas
Gerada automaticamente pelo módulo Catalog, mediante os dados fornecidos pelo(a) autor(a)

T192i Targino, Daniel Lira Lopes.
Influence of Microstructure and Cement Formulation on Stiffness and Fatigue Behavior of Cementitious Materials / Daniel Lira Lopes Targino. – 2023.
158 f. : il. color.

Dissertação (mestrado) – Universidade Federal do Ceará, Centro de Tecnologia, Programa de Pós-Graduação em Engenharia Civil: Estruturas e Construção Civil, Fortaleza, 2023.
Orientação: Prof. Dr. Lucas Feitosa de Albuquerque Lima Babadopulos.
Coorientação: Prof. Dr. Yassine El-Mendili.

1. fatigue behavior. 2. quasi-static characterization. 3. cementitious materials. 4. microstructure. 5. supplementary cementitious materials. I. Título.

CDD 624.1

DANIEL LIRA LOPES TARGINO

INFLUENCE OF MICROSTRUCTURE AND CEMENT FORMULATION ON STIFFNESS AND FATIGUE BEHAVIOR OF CEMENTITIOUS MATERIALS

M.Sc. Thesis presented to the Post-Graduate Program in Structures and Civil Construction, as a partial fulfillment of the requirements for the Master's degree in Civil Engineering at the Federal University of Ceará.

Area within the Graduate Program: Building Materials

Advisor: Lucas Feitosa de Albuquerque Lima Babadopulos, Ph.D.

Co-advisor: Yassine El-Mendili, Ph.D.

Approved in: 10/11/2023.

COMMITTEE

_____
Prof. Lucas Feitosa de Albuquerque Lima Babadopulos, Ph.D. (Advisor)
Federal University of Ceará

_____
Prof. Yassine El-Mendili, Ph.D. HDR. (Co-advisor)
École Spéciale des Travaux Publics, ESTP Paris

_____
Prof. Marcelo Silva Medeiros Júnior, Ph.D.
Federal University of Ceará

_____
Prof. Cédric Sauzéat, Ph.D. HDR.
University of Lyon, ENTPE

À minha mãe Lúcia, por me ensinar a ser a pessoa que sou.
À Diana, por ser meu suporte e sempre estar ao meu lado.

ACKNOWLEDGEMENTS

The following paragraphs are presented in both Portuguese and English, allowing me to properly express my gratitude to everyone involved in this achievement. To all of you, my deepest thanks.

Os seguintes parágrafos são apresentados em português e inglês, permitindo que eu expresse adequadamente minha gratidão a todos os envolvidos nesta conquista. A todos vocês, o meu mais profundo obrigado.

Os últimos anos de trabalho foram tão intensos que é difícil pensar que o esse mestrado foi concluído em pouco mais de dois anos. Foram vários obstáculos, vários desafios, contudo quanto maior o obstáculo melhor a sensação de dever cumprido após. Gratidão é o sentimento que tenho por todos que fizeram parte dessa jornada. Tenho certeza de que essa trajetória não seria possível sem a participação de todos os envolvidos.

Agradeço a Deus por Sua constante orientação, determinação e força durante esta jornada acadêmica, essencial para minha perseverança e conclusão de mais essa etapa. Agradeço por tudo que me foi dado e por todas as pessoas que Ele colocou nessa trajetória. Considero a família ser a base de tudo, por isso tenho muito a agradecer.

Agradeço aos meus pais, em especial minha mãe Lúcia e meu pai Targino, por serem o meu suporte em todo momento e me ensinar a ser a pessoa que sou hoje, valorizando trabalho duro, caráter, moral e a vida. Minha vida sempre foi um conjunto de altos e baixos, mas vocês sempre foram meu constante ao longo de tudo. Sem sombra de dúvida, não teria alcançado o que tenho hoje sem seu apoio. Agradeço e lembro também de meus avós que já não estão mais conosco. Agradeço também aos meus tios, meu irmão, meus primos e sobrinhos. Todos vocês contribuíram para a pessoa que sou hoje.

Agradeço à Diana, a quem escolhi para estar ao meu lado e o tem feito tão bem. Não foram meses ou anos, já temos uma história juntos de algumas ‘vidas’ e aventuras juntos. Sua dedicação me fez alcançar mais esse marco e sem sombra de dúvida essa conquista é nossa. Essa jornada não seria possível sem você ao meu lado. Agradeço também à sua família, Dona Anália, seus irmãos, tios e primos que me fizeram parte do seu todo.

De maneira especial agradeço ao meu orientador, Prof. Lucas Babadopulos. Lembro que ao entrar no mestrado era alguém com o objetivo de atuar no exterior, e posso dizer ao final dessa montanha russa dos últimos anos que esse objetivo está mais que bem atendido. Sua

orientação, críticas e forma de pensar moldaram um pesquisador mais preciso e aplicado. Obrigado por sua dedicação e compromisso com meu crescimento acadêmico.

Fadiga não é um trabalho de uma pessoa, mas sim de várias. Sem uma ótima equipe as várias noites viradas e turnos de trabalho no laboratório não seriam possíveis e para isso tive os melhores: Ingrid Lourany, Dulce Holanda e Pablo Martinez.

Agradeço ao Laboratório de Misturas e Pavimentação (LMP) da Universidade Federal do Ceará, em especial à Profª. Juceline Batista, pela confiança e pela liberação de utilização do laboratório de misturas, em especial pelos inúmeros agendamentos da prensa dinâmica. Agradeço também ao prof. Jorge, Annie e Iolanda, por tornarem possível e viabilizar o bom andamento de tudo.

Agradeço ao grupo de pesquisa em Reologia de Materiais (ReoM), pela rica experiência, compartilhamento de ideias, pensamentos e suporte.

Agradeço ao Prof. Eduardo Cabral e o Laboratório de Materiais e Construção Civil (LMCC) da Universidade Federal do Ceará pela extração de corpos de prova e liberação de ensaios de caracterização mecânica.

Agradeço à Fundação Cearense de Apoio ao Desenvolvimento Científico e Tecnológico (FUNCAP) através do projeto FUNCAP/INSA-ROUEN pelo financiamento do estágio de mestrado na França.

A vocês meu muito Obrigado.

When I first arrived in France, I was used to saying I was starting from scratch, knowing nobody, and being completely unfamiliar with a new place. It was a daunting experience, stepping into the unknown, but it was also an opportunity for growth and learning. But when I came back, I left behind friends who became like family that I am going to cherish for life.

I would like to express my sincere gratitude to my co-advisor Yassine El Mendili. Thank you for the opportunity to be in France, for the immense support during my stay in Caen, for the guidance, and especially for all the support after I came back. I truly hope this partnership continues in the upcoming years and hopefully, we can work together soon.

I would like to express my sincere thanks to Fouad Boukhelf, for the immense support during my stay. Thank you for the invite to contribute to your ongoing research, for the valuable contributions to this current achievement and for being extremely supportive during all my staying in France. Your kindness and generosity have made this time more memorable.

Furthermore, Faraj, Meriem, Lally, Camila, Felipe, Marcela, Mohamed, Hitchem, are all names part of this memorable stay. Each one of you has contributed to making a great time of mine, being a rich and fulfilling experience.

This achievement is not just mine, but ours.

I would like to thank the Builders Ecole d'Ingénieurs and the FONDEOL Project for the opportunity to have a six-month internship, for the support and funding. This experience has been instrumental in my academic journey, providing me invaluable skills and knowledge.

To you all my sincere thanks.

"Gratitude is not only the greatest of virtues, but the parent of all others."

(Cícero 106 a.C. - 43 a.C.)

ABSTRACT

This master's thesis investigates the influence of microstructural aspects and cement formulations, particularly with the incorporation of supplementary cementitious materials (SCMs), on stiffness and fatigue behavior of cementitious materials. The contributions are formatted as three scientific papers. Firstly, (i) an investigation of the glass powder (GP) influence as a SCM on the mechanical, physical and microstructural behavior of mortars is presented. The results show improvements in several aspects, including heat of hydration, porosity, and strength parameters. The sustainability also had significant improvement, demonstrating the GP a feasible SCM addition for cementitious materials. Secondly, (ii) a characterization method that accounts for the viscoelasticity of cementitious materials is proposed. This method led to accurate and consistent findings when assessing the complex modulus of cementitious materials. Finally, in the third paper, (iii) the influence of microstructure and SCM additions on mechanic, quasi-static and fatigue behavior is addressed. The findings demonstrate that the improved microstructural results, such as low heat of hydration, denser pore size structures, and higher CSH content, for example, were aligned with a lower cracks' incidence and microstructural voids (up to 61.58%), higher absolute value of complex modulus (up to 24%), lower phase angle (up to 0.56° in average), and improved endurance limit by 19.80%. It is possible to address the influence of those aspects on mechanical behavior and fatigue resistance. Additionally, methods were proposed for mechanical characterization and fatigue tests in pure compression and tension, as well as for data processing the results. Those validations demonstrated their consistency, resulting in accurate measures and in agreement with the literature of complex modulus. This research provides a more comprehensive perspective on fatigue, accounting for feasible optimization parameters on the microstructure and SCMs incorporation, promoting the development of more resistant, durable, and sustainable cementitious materials.

Keywords: fatigue behavior; quasi-static characterization; cementitious materials; microstructure; supplementary cementitious materials.

RESUMO

Esta tese de mestrado investiga a influência de aspectos microestruturais e formulações de cimento, especialmente com a incorporação de materiais cimentícios suplementares (MCSs), na rigidez e no comportamento de fadiga de materiais cimentícios. As contribuições estão formatadas em três artigos científicos. Em primeiro lugar, (i) é apresentada uma investigação da influência do pó de vidro (PV) como MCS no comportamento mecânico, físico e microestrutural das argamassas. Os resultados mostram melhorias em vários aspectos, incluindo parâmetros de calor de hidratação, porosidade e resistência. A sustentabilidade também teve uma melhora significativa, demonstrando que o PV é uma adição viável como MCS para materiais cimentícios. Em segundo lugar, (ii) é proposto um método de caracterização que leva em conta a viscoelasticidade dos materiais cimentícios. Esse método levou a resultados precisos e consistentes ao avaliar o módulo complexo de materiais cimentícios. Por fim, no terceiro artigo, (iii) é abordada a influência da microestrutura e das adições MCS no comportamento mecânico, quase estático e de fadiga. As descobertas demonstram que os resultados microestruturais aprimorados, como baixo calor de hidratação, estruturas de poros mais densas e maior teor de CSH, por exemplo, são alinhados com menores incidência de trincas e vazios microestruturais (até 61,58%), maior valor absoluto do módulo complexo (até 24%), menor ângulo de fase (até 0,56° em média) e limite de resistência aprimorado em 19,80%. É possível abordar a influência desses aspectos no comportamento mecânico e na resistência à fadiga. Além disso, foram propostos métodos para caracterização mecânica e testes de fadiga em compressão e tensão puras, bem como para o processamento de dados dos resultados. Essas validações demonstraram sua consistência, resultando em medidas precisas e em concordância com a literatura de módulo complexo. Esta pesquisa fornece uma perspectiva mais abrangente sobre fadiga, levando em conta os parâmetros de otimização viáveis na microestrutura e na incorporação de MCSs, promovendo o desenvolvimento de materiais cimentícios mais resistentes, duráveis e sustentáveis.

Palavras-chave: comportamento de fadiga; caracterização dinâmica; materiais cimentícios; microestrutura; materiais cimentícios suplementares.

LIST OF FIGURES

LIST OF TABLES

TABLE OF CONTENTS

1 INTRODUCTION

This chapter serves as an introduction to the primary subject of the current study. It explains its relevance, addresses research gaps and hypotheses, outlines both general and specific objectives, and defines the study's scope. This approach is designed to offer a comprehensive understanding of the theme's significance and purpose, facilitating better engagement with the upcoming chapters.

1.1 Context

The examination of fatigue behavior in cementitious materials is an ongoing research topic of materials' durability applied to structural applications, and it is especially relevant for those subjected to cyclic loads. This encompasses applications including aerogenerators (towers and foundations), pavements, and bridges.

Fatigue assessment allows for the evaluation of their mechanical properties over time as well as the progression of degradation through cycles and years. These characteristics are intrinsic to these materials and gradually compromise their load-bearing capacity. This degradation increases the risk of failure and potentially can lead to collapse.

The fatigue phenomenon in cementitious materials is complex, influenced by several factors, and further complicated by their inherent heterogeneity. Despite sustained efforts and recent research progress, critical scientific gaps remain to be addressed (Gan *et al*., 2022). Advancements in this field promise to improve design methods and enhance mechanical performance, durability and fatigue resistance (Anglani; Tulliani; Antonaci, 2020; Shah *et al*., 2023), aligning with sustainability goals.

Fatigue assessment is important for several aspects. Understanding the mechanical performance of cementitious materials under cyclic loads is vital for their safe use in structural and non-structural applications (Müller; Mechtcherine, 2017). Examining their mechanical response across loading cycles can provide insights into degradation, microstructural inhomogeneities and cracks' propagation (coalescence) (Han *et al*., 2014).

Furthermore, the development of accurate models is crucial for predicting fatigue life and durability, aiming for durable and resistant structures (Ciavarella; Carbone; Vinogradov, 2018), assessing the effects of loading, simulating its implications on composites (Vassilopoulos, 2015), and optimizing their designs. The development of cementitious composites with strain-hardening properties has also shown promise in enhancing structural performance and durability (Huang *et al*., 2017; Zerbst; Madia, 2021).

Fatigue resistance itself is influenced by numerous factors. These factors include structural imperfections such as pores, deficiencies in particles' adhesion, surface roughness, microstructural anisotropy and even residual stresses (Zerbst; Madia, 2021). As a result, these elements can reduce load-bearing capacity, impacting fatigue resistance and increasing the stress-strain variability of their mechanical responses.

The inherent heterogeneity poses a challenge in determining representative properties (Ding *et al*., 2019), necessitating the consideration of defects, surface irregularities, and residual stresses in the experimental assessment (Huang *et al*., 2017). Mitigating these factors is crucial for accurate evaluation and the preservation of structural integrity (Correia; De Jesus; Calçada, 2017). Furthermore, amplifying load-bearing capacity and materials' stiffness can culminate in improved fatigue resistance (Wang, 2012).

Microstructural attributes also exert a profound influence on fatigue. Microscale features such as fillers' and aggregates' surface smoothness, grain boundary, void content, and micropores can directly govern crack initiation, affecting the degradation mechanisms (Chan, 2010). In this context, materials more fatigue-resistant result from the optimization of the microstructure by reducing void content, introducing finer fillers, strengthening interfacial transition zone (ITZ) bonding properties, and improving stiffness (Qiu; Yang, 2017).

Additionally, microstructure can also influence the viscoelastic properties. Finer particles exhibit reduced creep behavior, enhancing aggregates-cement interfacial transition zone (ITZ) (Giorla; Dunant, 2018). The presence of deformations caused by internal stress, such as those resulting from drying shrinkage, can affect the residual deformations and stress accumulation in materials subjected to cyclic loads (Corrado; Molinari, 2016).

In summary, microstructural parameters play a crucial role in fatigue, influencing cracks initiation (nucleation), stiffness behavior, viscoelastic traits, and residual deformations, directly impacting fatigue and mechanical response.

Furthermore, the use of supplementary cementitious materials (SCMs) such as blast furnace slag, fly ash, metakaolin, and limestone has shown the potential to enhance fatigue life (Anurag *et al*., 2021). The incorporation of these materials can affect both the fresh and hardened properties of cementitious materials and result in the production of low-carbon cementitious composites (Weng; Liao, 2021).

The development of low-clinker binders aligns with global initiatives for more sustainable solutions. The addition of SCMs in cementitious materials has the potential to enhance microstructure, reduce drying and autogenous shrinkage and improve compressive

strength (Sagar; Sivakumar, 2021), thereby positively impacting fatigue, mechanical performance and durability (Kemer *et al*., 2021; Qian *et al*., 2022).

According to the literature on SCMs, several additions have demonstrated the potential to improve fatigue life, with a focus on microstructure and mechanical behavior. The incorporation of glass powder (GP) and silica fume (SF) as SCMs has a profound influence on the fresh state, mechanical attributes, and microstructure (Boukhelf *et al*., 2021).

The addition of GP enhances workability while reducing thermal conductivity and specific heat. It refines the porous structure, increases density, and improves water resistance (Boukhelf *et al*., 2021; Fu *et al*., 2021). Similarly, SF enhances mechanical properties through the improvement of the nucleation resistance and pozzolanic effects. By promoting cement hydration, SF consumes more $Ca(OH)_2$ and precipitates a higher content of calcium silicate hydrate (CSH) and calcium aluminosilicate hydrates (CASH), resulting in increased strength (Guo *et al*., 2021).

The synergistic application of GP and SF can further enhance microstructure through its densification, internal stress alleviation, improved stability and increased water resistance (Keerio *et al*., 2022). In general, the incorporation of GP and SF can improve microstructural properties, potentially leading to improved fatigue resistance.

Furthermore, when assessing the literature on fatigue behavior, it is evident that there are gaps concerning testing methodologies, including variation in loading conditions (Becks *et al*., 2022, 2023), environmental contexts, fatigue modeling and analysis methods. Similarly, assessing the experimental results available, loading regimes such as tensile and shear loading remain underexplored.

There is also a growing demand for research to focus on modulus characterization in this field, with a particular emphasis on accounting for viscoelastic aspects (Chu *et al*., 2023b; Wang; Duan; Zhu, 2021; Zhao *et al*., 2013). This parameter, intrinsic to fatigue, requires comprehensive investigation, having significant implications for both fatigue behavior and the mechanical performance of these materials. Viscoelastic stress modeling and modulus characterization are important for understanding their mechanical behavior and performance under different loading conditions (Bažant; Jirásek, 2018; Zhao *et al*., 2013).

The current investigation is connected to three research initiatives: (i) the FONDEOL project (*Problématiques propres aux Fondations d'éoliennes en zone littorale*), dedicated to aerogenerator tower foundations , a collaborative effort involving French agencies, companies, academic institutions, with the contribution of the Federal University of Ceará (from October 2019 to March 2023), (ii) the BLUEPRINT project, pursuing the creation

of a model of circular economy, focusing on sustainable solutions and materials, traversing the France Channel England expanse in both British and French contexts, and (iii) the FUN-CAP/INSA-Rouen project (“Challenges with respect to aerogenerators' foundation in coastal zones”), an international cooperative endeavor, from Ceará, Brazil, and Normandy, France.

These initiatives coalesce within a broader framework focused on establishing Franco-Brazilian research cooperation in Civil Engineering, imparting a decisive focus on renewable energies. This partnership facilitated a six-month academic mobility in Caen, France, at the laboratories of Builders Ecole d’ingénieurs.

1.2 Problem Statement

The investigation of fatigue behavior is a continuous endeavor to ensure structural integrity and durability. The growing demands of various industries present an escalating need for more sustainable solutions and enhanced materials performance.

Fatigue assessment holds relevance across a wide range of applications. Dynamic and cyclic loads require a comprehensive understanding of their impact on mechanical performance and degradation. The development of materials with enhanced durability, with improved fatigue resistance, holds the potential to extend service life and enhance durability, ultimately contributing to more sustainable structures.

The incorporation of SCMs has garnered significant attention due to their ability to enhance both mechanical and microstructural aspects while addressing environmental concerns. Research exploring the relationships between material composition, microstructure, and fatigue, reveals that the incorporation of SCMs such as GP and SF leads to positive results in terms of microstructure and mechanical properties, potentially influencing fatigue resistance. Further investigation into those influences is essential to provide a comprehensive overview.

Moreover, given the multifaceted nature of these factors, it is essential to establish methodologies for assessing fatigue, requiring accurate models and reliable analytical tools to yield precise results. Mechanical characterization is a crucial prerequisite in fatigue investigations. Stiffness characterization provides insights into the elastic and viscous behavior, which are relevant for fatigue investigations. This comprehensive understanding guides the development of improved cementitious materials with enhanced fatigue resistance.

Despite the relevance of cementitious materials in construction and their usage in dynamic applications, the influence of SCM additions and microstructure aspects on fatigue remains poorly understood. This lack of comprehensive knowledge hinders the optimization of these materials and makes it difficult to obtain enhanced durability and performance.

By elucidating these influences, this study aims to address critical gaps in the current state-of-the-art literature. With this problem research in mind, it is intended to explore the following topics on the identified literature gaps:

- What is the potential of incorporating SCMs for improving mechanical and microstructural properties and enhancing mechanical and fatigue behavior?
- How can testing technologies and analysis methods better characterize cementitious materials under cyclic or dynamic loads?
- What is the influence of microstructural aspects of cementitious materials on the mechanical and fatigue behavior?
- What contributions can be found from the evaluation of the fatigue behavior of cementitious materials in pure tension?

By gaining a deep understanding of how cementitious materials behave under dynamic and cyclic loads, this research can provide valuable knowledge into the development of more fatigue-resistant materials with improved strain response and durability.

1.3 Research Objectives

1.3.1 Main Objectives

The primary objective of this study is to investigate the influence of microstructure and cement formulations, particularly with the incorporation of supplementary cementitious materials (SCMs), on the stiffness and fatigue behavior of cementitious materials. In addition, this study intends to propose an optimized cement formulation for enhanced fatigue behavior and address a literature gap on the fatigue behavior of cementitious materials in pure tension.

Through a comprehensive examination of these research questions, this study aims to contribute to a deeper understanding of the fatigue behavior of cementitious materials. The insights gained from this research have the potential to inform the development of fatigue-resistant composites, with improved durability, and contribute to the creation of structures better equipped to withstand the challenges of cyclic loading conditions.

1.3.2 Specific Objectives

To achieve the main objective, specific objectives should be attended to providing the conceptual knowledge to assess fatigue behavior in the current primary goal. Those include:

1. To evaluate the potential of GP and SF additions, as potentially beneficial SCMs, in cementitious materials, to improve mechanical aspects, physical parameters, and fatigue behavior focusing on the influence of the microstructural changes;
2. To propose and validate a mechanical characterization method able to assess the viscoelasticity of cementitious materials under cyclic loads for both compression and pure tension;
3. To investigate the influences and direct implications of microstructural aspects on the mechanic, quasi-static, and fatigue behaviors while evaluating optimization potential;
4. To evaluate fatigue behavior in pure tension and degradation curves, comparing them with available literature and standard codes.

1.4 Structure Of The Dissertation

The current research is structured into five chapters, each contributing to a comprehensive exploration of the subject matter. Chapter 1 contextualizes the research problem, outlines objectives, and underscores its relevance. Chapters 2 to 4 are presented in the format of scientific articles. These chapters streamline the organization and publication of research findings, offering a focused understanding of specific subjects. Finally, Chapter 5 serves as the summary of the findings, providing a thorough synthesis of the results achieved, and their significance to the state-of-the-art.

Chapter 2 was published in the Materials journal with an open access content (Boukhelf *et al*., 2023), Chapter 3 was published in the Journal of Building Pathology and Rehabilitation (Targino *et al*., 2023), and Chapter 4 is planned to be submitted to the International Journal of Fatigue.

Chapter 2 involves an experimental investigation focused on the influence of GP on the mechanical and physical properties of mortar compositions. The primary objectives encompass a comprehensive overview of its influence over a 3 to 90-day range and elucidate the interplay between GP incorporation and short-term mechanical strength. Additionally, it explores the potential for long-term strength evolution due to underlying pozzolanic reactions.

An innovative aspect of this study lies in the analysis of the heat of hydration through a refined ANN model, to identify the cement hydration modes. By delineating the GP effects, the main contribution of the chapter is to provide an overview of the understanding of its implication on microstructure and physical aspects, while providing initial experimental evidence for further assessment of fatigue behavior.

Chapter 3 focuses on the mechanical characterization of cementitious materials and their implications on durability and mechanical performance. It evaluates a proposed cement fatigue-enhanced formulation using SCMs applied to mortars and concretes, aiming to improve stiffness under cyclic loads. Methodologically, it entails static tests for compressive and tensile strengths and proposes an innovative cyclic stiffness test, assessing elastic and viscous components of the cementitious materials under sinusoidal loads in the frequency domain. The experimental program includes tests in pure compression and pure tension across frequencies from 0.1 Hz up to 25 Hz. Findings suggest that the fatigue-enhanced formulation resulted in a stiffer material with 23% improved modulus and 13.8% higher loss modulus, affecting the energy dissipation. These findings can extend durability, and provide insights into improved fatigue life. The main contribution of this chapter is the proposition of a reliable characterization method, for both compressive and tensile loading regimes, able to assess the viscoelastic behavior of cementitious materials. This testing methodology can be applied both for complex modulus assessments and fatigue tests.

Chapter 4 focuses on the assessment of fatigue behavior in pure tension, with a comprehensive investigation of the influence of microstructural and physical aspects on fatigue life. This objective fills a gap in the literature, as it explores the influence of SCMs on fatigue and provides experimental data in pure tension. The proposed cement formulation shows a 19.80% improvement in endurance limits, up to a 24.64% increase in the absolute value of complex modulus, a stiffer material, and up to a 0.56° decrease in the phase angle, based on the reference formulation comparison, indicating a more elastic behavior with a reduced viscous component. The main contribution of this chapter is the evaluation of the interlink between microstructure and fatigue behavior, in addition to the experimental findings in pure tension and the extended fatigue life findings of the proposed cement formulation.

The concluding thoughts regarding the results achieved are in Chapter 5. This chapter summarizes the research, outlining advancements, potential enhancements, and prospects for future endeavors.

2 INSIGHT INTO THE BEHAVIOR OF MORTARS CONTAINING GLASS POWDER: AN ARTIFICIAL NEURAL NETWORK ANALYSIS APPROACH TO CLASSIFY THE HYDRATION MODES

The main content of this chapter is also available with open access at BOUKHELF; TARGINO; BENZAAMA; BABADOPULOS; EL MENDILI, (2023), published in the Materials journal.

ABSTRACT

In this paper, an artificial neural network (ANN) model is proposed to predict the hydration process of proposed cement formulations. This model overcomes the lack of input parameters of physical models, providing a realistic explanation of hydration with few inputs and fast calculations. Indeed, four mortars were studied based on ordinary Portland cement (CEM I), blast-furnace cement (CEM III), and glass powder (GP) as a cement replacement. These mortars were named CEM I + GP and CEM III + GP. The properties of the mortars were characterized and their life cycle assessment (LCA) was established. Indeed, a decrease in porosity was observed at 90 days by 4.6%, 2.5%, 12.4%, and 7.9% compared to 3 days for CEM I, CEM III, CEM I + GP, and CEM III + GP respectively. In addition, the use of GP resulted in a reduction of mechanical strength in the short term. At 90 days, CEM I + GP and CEM III + GP demonstrated a decrease of 28% and 57% in compressive strength compared to CEM I and CEM III respectively. Nevertheless, the strength evolution did not cease with an increasing over time, due to the continuous pozzolanic reactions between $Ca(OH)_2$ and silica content (Si^+) in GP and slag present in CEM III, demonstrated by a thermo-gravimetrical (TG) analysis. To summarize, the CEM III mortar achieved similar performance compared to the CEM I + GP mortar in the long term. Moreover, the ANN model proposed was able to identify the cement hydration modes with the resulting model having an R^2 score accuracy from 0.968 up to 0.997 compared to the experimental data, allowing a precise identification of the hydration modes. The proposed ANN model poses as a powerful tool to allow cement manufacturers to quickly identify differences in cement hydration by using a simple input parameter, the heat of hydration.

Keywords: artificial neural network; data processing; cement; glass powder valorization; life cycle assessment.

2.1 Introduction

With a production of about 10 Gm³/year, concrete is the most relevant building material, having a notable contribution to the world's environmental problems and greenhouse gases emissions (GHGe) due to its production of more than 4 billion tons/year, at temperatures higher than 1450 °C (Gencel *et al*., 2021; Miller; Horvath; Monteiro, 2016). Indeed, concrete is responsible for 4 to 8% of the world's CO_2 and GHGe corresponding to 50% of the emissions in construction alone (Prakash *et al*., 2019; Sundaresan; Ramamurthy; Meyappan, 2021). Among raw materials, only coal, petroleum oil and natural gas have a higher potential for GHGe (WBCSD, 2009).

One reflection that emerged in recent decades is the proposition of new cement formulations, by replacing clinker with alternative binders, named supplementary cementitious materials (SCMs), with similar characteristics, comprehending pozzolanic activities and contributing to improved hydration products. The reduction in cement manufacturing's carbon footprint and GHGe remains a challenge, with a strong appeal in the upcoming years.

On the optics of the SCMs assessment, when raw glass becomes waste, it is usually destined for landfill. It is not a sustainable approach once it does not decompose in the environment. The recovery of glass waste eliminates unnecessary landfill areas and can also reduce energy consumption. As a result, it is necessary to develop solutions more environmentally friendly. After the refinement of raw glass, it becomes glass powder (GP).

One of the proposed applications is the partial replacement of ordinary Portland cement (OPC), the most polluting component of concrete, by wastes and by-products, while keeping similar mechanical characteristics. Several industrial by-products have been successfully used as SCMs, including silica fume (SF), ground granulated blast furnace slag (GGBFS), and fly ash (FA) (Antoni; Chandra; Hardjito, 2015; Bani Ardalan; Joshaghani; Hooton, 2017; Shen *et al*., 2020). These materials' additions result in blended cements with the potential to improve concrete's durability, long-term strength, workability, costs and sustainability.

The GP studied in this paper, is highlighted as a feasible solution for manufacturing concretes with lower GHGe due to its pozzolanic properties (Paul; Šavija; Babafemi, 2018; Serpa *et al*., 2013; Shayan; Xu, 2004; Zidol; Tognonvi; Tagnit-Hamou, 2017).

Every year, millions of tons of glass waste are generated worldwide (Bouchikhi *et al*., 2019; Ling; Poon; Wong, 2013). In addition to reducing the amount of cement in

concrete, this waste can be recycled with that intention. This could be an important step toward sustainable development (Bouchikhi *et al*., 2019; Du *et al*., 2021).

Furthermore, GP provides an additional performance in terms of workability (Yin *et al*., 2021), microstructure properties (Gołek *et al*., 2020; Petrella *et al*., 2022), mechanical strength and performance in the long term (Gołek, 2019; Szydłowski; Szudek; Gołek, 2021), durability (De Castro; De Brito, 2013), and hygrothermal performance (Boukhelf *et al*., 2021; Chand; Happy; Ram, 2021; Du *et al*., 2021).

In the context of sustainable applications of by-products in environmentally friendly cementitious binders, life cycle analysis (LCA) is a suitable tool for quantifying the environmental impacts of those solutions and supply chains (Boesch *et al*., 2014).

Assessing the literature on LCA for concrete and cementitious materials, it is seen that the major pollutant component is the OPC, due to the clinker manufacturing process. Indeed, there are three main steps for OPC manufacturing: (i) the pre-processing, involving the transformation of the raw materials into a fine powder to enter the preheater; (ii) the calcination, with the clinker formation at temperatures higher than 1450 °C, and finally (iii) the gypsum addition and final grinding to transform them into a fine powder. Figure 1 describes this entire process over LCA inputs and outputs evaluation.

Figure 1 - Basic process, "cradle-to-gate" scope and system limits

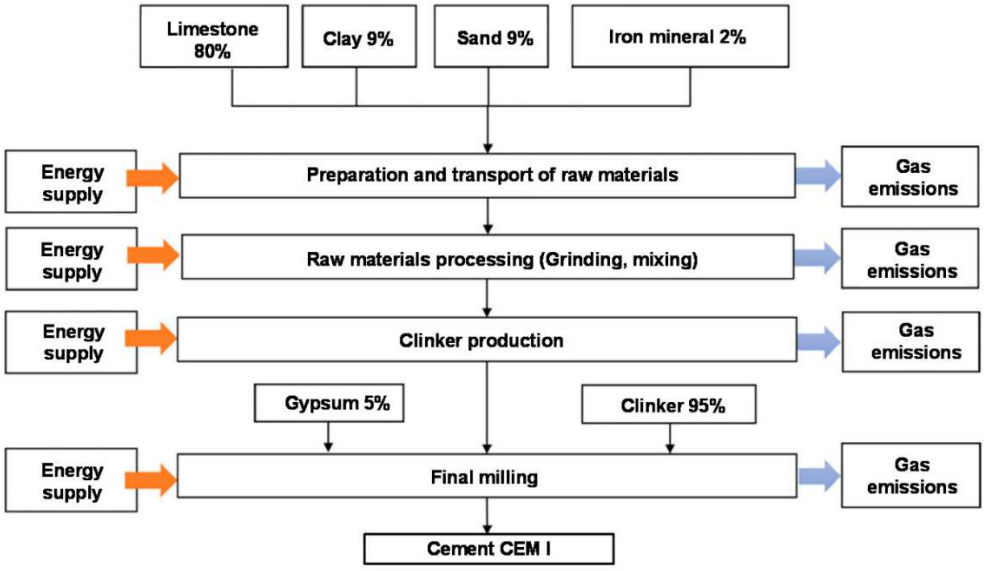

Source: Sánchez *et al*. (2021).

The main steps of the LCA are (i) the determination of the scope and boundaries of the OPC manufacturing process and its partial replacement by SCMs, (ii) the selection of the input and output data to compose the life cycle inventory (LCI) based on the literature data

(Chen *et al*., 2010; Crossin, 2015; Guignone *et al*., 2022; Huntzinger; Eatmon, 2009; Sánchez *et al*., 2021; Valderrama *et al*., 2012; Zulkarnain *et al*., 2021), (iii) the computing of the mix proportions and SCM additions to quantify environmental impact of the formulation proposed in this study, and (iv) finally, to present the results assessing the variations in GHG emissions, and energy and raw material consumption.

The regulatory parameters of the cements used are presented in Table 1, including the two types of cement used in this study (CEM I and CEM III).

Table 1 - Cement regulations following European Standard EN 197-1

Class	Mineral Content		Mineral Components/Inorganic Process Additions	Market Share
	Allowable	Average		
Ordinary Portland cement (CEM I)	≤5%	2.5%	Inorganic process addiction	30%
Portland Composite Cement (CEM II)	6–35%	20.5%	GGBFS, Silica Fume, Pozzolan, Fly Ash, Burnt Shale	57%
Blast Furnace Cement (CEM III)	36–95%	65.5%	GGBFS	5%
Pozzolanic Cement (CEM IV)	11–55%	33%	Silica Fume, Pozzolan, Fly Ash	6%
Composite Cement (CEM V)	36–80%	58%	GGBFS, Pozzolan, Fly Ash	3%

Source: Sánchez *et al*. (2021).

Indeed, the usual mineral addition for CEM I is gypsum ($CaSO_4$ $2H_2O$) with a maximum content of 5% to control the cement setting time. Regarding CEM III, it mainly contains ground granulated blast-furnace slag (GGBFS) with content between 36% and 95%. The current LCA assessment will be divided specifically into the assessment of these main three materials (i.e., Portland Clinker, GGBFS, and GP) with the resulting formulations.

To investigate the hydration kinetics of these alternative binders, several models have been proposed in the literature over recent decades. The heat of hydration models are dependent on several variables, some of which are difficult to foresee or account for. Finding a credible model that accurately describes the heat of hydration remains an endeavor.

Based on the literature, the simulation methods are classified into three categories: (i) linear regression models (Qin; Gong; Xie, 2021), (ii) physical models (Tahersima; Tikalsky, 2017), and (iii) intelligent computing models. Linear regression models are constructed based on the least-squares methods, fitting the model to the experimental data under the assumption that there are linear (or nonlinear) and independent correlations between heat of hydration and its influencing factors (i.e., hydration age, cement fineness and

compositions). The literature reports a non-assumptive linear regression method to predict the heat of hydration of OPC (Qin; Gong; Xie, 2021).

Concerning the physical models, several models have been proposed in the literature for modeling heat of hydration. Tahersima and Tikalsky (2017) used a finite element model to predict the heat of hydration in a concrete slab-on-grade floor with limestone cement. The results showed that the prediction accuracy of finite element results is about 15% more for the maximum temperature rise and 30% more for the peak time.

However, the main difficulty of these models lies in the accurate determination of their thermal properties to back-feed the simulation parameters and the calculation demands high computational processing. Kondo (1968) proposed a single-particle model that considers the circular-shaped layered growth of a uniform thickness of hydrates on a spherical single-reaction cement particle to characterize the hydration kinetics of alite (C3S). Pommersheim and Clifton (1979, 1982) suggested an integrated single-particle reaction-diffusion model for the hydration of C3S.

The hydration was modeled by using a classical approach to deal with reactions and diffusion at phase boundaries. Recently, He *et al*. (2020) developed a numerical method to describe the OPC heat of hydration under steam curing conditions. It has been employed with an iterative algorithm and validated by experimental results.

More recently, Nguyen *et al*. (2021) investigated the effects of cement particle size distribution (PSD) on hydration using a three-dimensional computer simulation. The simulation used a model based on the CEMHYD3D code and a random distribution method, which requires a lower computing demand in generating a pre-hydrated model than the correlation function method.

In the work of Chu *et al*. (2022a) the CEMHYD3D code was also used to numerically model the hydration of cement paste by following the evolution of all phases and predicting the properties of hydrated cements.

Furthermore, Zhao *et al*. (2022) studied the early-age hydration of blended cement and modeled its hydration kinetics by measuring the heat of hydration. Within this paper, the classification of hydration modes was discussed based on the Krstulovic–Dabic model (Dabić; Krstulović; Rušić, 2000; Krstulović; Dabić, 2000), which was built on the data from the hydration rate. The limitations of the numerical methods listed indicate that there is a knowledge gap to be addressed, making feasible the use of machine learning techniques to assess this phenomenon.

Indeed, machine learning models often encompass artificial neural networks (ANN) which are versatile models, able to assess and model different datasets having diverse complexity levels (Chen *et al*., 2019; Hong *et al*., 2020; Lin *et al*., 2020; Xu *et al*., 2022). Nevertheless, a knowledge lack on ANN applications to predict hydration was addressed.

Based on the literature, there was a scarcity of investigation on heat of hydration thermal analysis using machine-learning techniques. In addition, only two studies highlight the use of ANN models to investigate the OPC heat of hydration (Cook *et al*., 2021; Subasi; Yilmaz; Binici, 2009).

Subasi et al. used an approach based on an adaptive neuro-fuzzy inference system (ANFIS) (Subasi; Yilmaz; Binici, 2009). Cook *et al.* (2021) used a random forest (RF) model to achieve high-accuracy predictions of time-dependent thermal hydration kinetics of OPC. Indeed, the largest drawback of RF is that it can become too slow and ineffective for real-time forecasts when there is a large learning architecture.

In general, these algorithms are fast to be fitted, but take a longer time to predict after training. Additionally, ANFIS has a significant processing cost due to its complex data structure and learning gradient. This is a drawback for applications with a large dataset (Salleh; Talpur; Hussain, 2017).

Due to this wide range of factors influencing the performance of cement hydration, the dynamic simulation of the hydration is a difficult task. Several variables may influence the heat of hydration, being occasionally difficult or complex to account for. It makes difficult the proposition of models that accurately describe the hydration behavior.

Indeed, this is a complex and non-linear system also influenced by environmental aspects. However, the identification of the thermal parameters to back-feed the model is the main challenge of the physical models. For this reason, in this paper, it was employed an ANN model to analyze the hydration process and identify the cement hydration modes, based on the heat of hydration experimental data.

The paper aims to address a literature gap by presenting a numerical and ANN model that can overcome the mentioned obstacles, providing a feasible explanation of heat of hydration, with fewer inputs and faster calculations. To contribute on that matter, the specific objective of this current paper can be addressed as, (i) to assess the environmental impact of proposed binders, highlighting the potential of GP as an SCM, improving the cement's GHGe, (ii) to investigate the effect of GP on the heat of hydration, microstructure and mechanical properties of mortars, in addition to the thermogravimetric analysis (TGA) (iii) to propose a numerical approach to identify and classify the hydration modes of the cement hydration.

For this last intent, a multilayer perceptron (MLP) regressor was used to generate a numerical discrete model, which is adjusted to the thermal hydration experimental data. This method provides a model with less noise and interference. This noise refers to both fluctuations in the thermal readings and even inaccuracy or low precision of the testing method. Once validated, the generated model was assessed by a numerical approach to identify the hydration transition modes. This numerical analysis is based on continuous local maxima and minima identification through the continuous (Kolani *et al.*, 2012; Riding *et al.*, 2012; Luo; Wei, 2022; Meinhard; Lackner, 2008). This method allows the development of a reliable model that can efficiently assess the cement heat of hydration for different formulations (Wang, 2021).

2.2 Methodological Procedure – Part I

Following the approach presented in Figure 2, the methodology employed in this paper was divided into experimental and numerical procedures. The initial step concerns the materials' characterizations and their LCA assessment. The second step focuses on data processing to assess the heat of hydration of the proposed mortars.

Figure 2 - Conceptual study plan

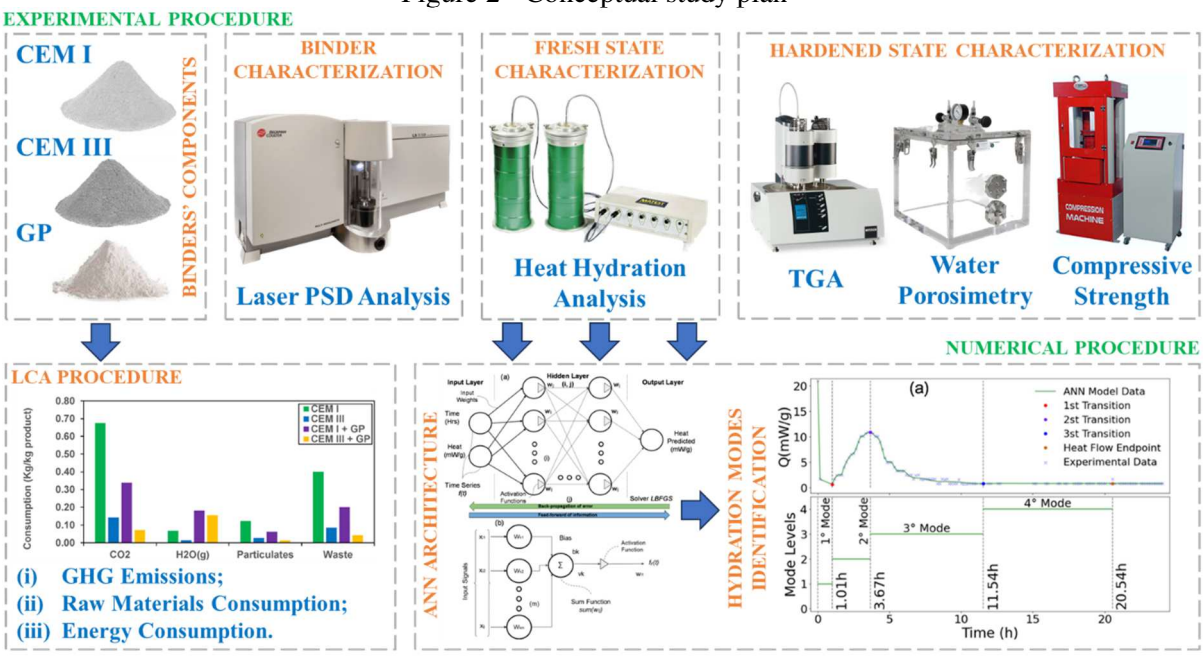

Source: Author (2023).

2.2.1 Experimental Procedure

Experiments were carried out to investigate the effect of the OPC replacement on the proposed binders. It can lead to significant improvements in GHGe, by incorporating alternative SCMs as GP. The GP addition can affect the workability, heat of hydration, and mechanical properties. In the first part of the methodology, a characterization of the cements' constituents was performed through PSD and density analysis. Afterward, mortars with OPC (CEM I 52.5 N), blast furnace cement (CEM III 32.5 N), and GP were mixed. In this study, the OPC replacement ratio was addressed in a fixed mass ratio of 50% by GP.

Zeybek *et al*. (2022) conducted a series of compressive, splitting tensile and flexural strength tests to investigate the effect of waste GP on concrete mechanical properties. In their study, GP was used in a mass replace ratio of up to 50% of OPC. The study conducted by Kalakada, Doh and Zi (2020) showed a decrease in compressive strength at high OPC replacement ratios. The concrete compressive strength was reduced by 65% having a 50% of OPC mass replacement by GP.

In this study, it was chosen the mass replacement ratio of 50% based on literature findings with high replacement rates. However, it is important to notice that the current focus is given to assessing the feasibility and validation of the proposed ANN model, assessing materials with low heat of hydration, which is expected from OPC formulations with high replacement rates, of up to 50%.

The mortars' microstructure characterization was conducted with an isothermal calorimeter assessment, water porosity tests and a TG analysis. In addition, the workability and mechanical strength were also evaluated and compared to reference mortars with CEM I and CEM III. To explain the mechanical strength improvement and the decrease in the porosity in the long term, the TG analysis was performed after 90 days.

2.2.1.1 Raw Materials

Two types of cement were used in this study, CEM I 52.5 N and CEM III 32.5 N in compliance with EN 197-1 (CEN, 2012a). GP was used as an SCM in the cement mass replacement. The raw glass was recovered from demolition glass waste, provided by a waste disposal plant in Caen metropolitan region (Normandy, France). The binders' density was determined using a helium pycnometer and the PSD was assessed by a laser PSD analyzer in the wet process in compliance with the NF EN 933-1 (CEN, 2012b).

Figure 3 shows the PSD of the binders' components. The results show that the studied CEM I and CEM III were almost the same size as the literature result (Kheir *et al.*, 2021) which is attributed to the clinker refinement control of the OPC manufacturing. Oppositely, GP presented a consistent coarse aspect, an influence of the adopted refinement process.

Figure 3 - PSD of the OPCs and GP employed

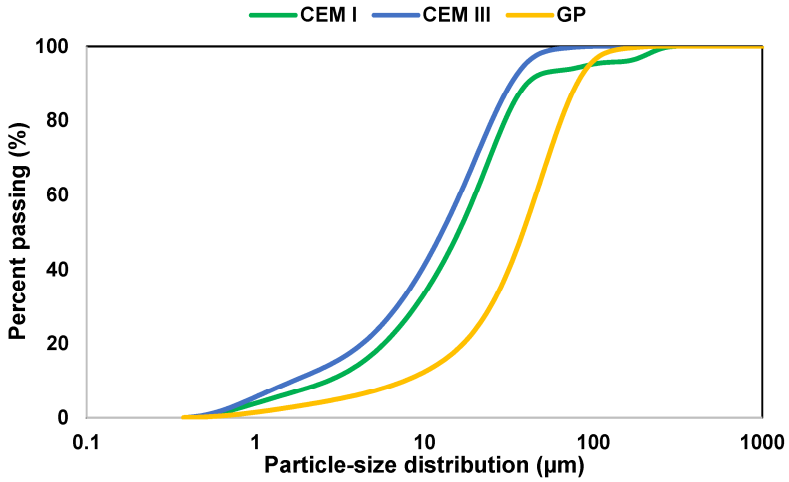

Source: Author (2023).

Furthermore, Table 2 presents the particle size percentile results, including max diameters and the density results assessed by the pycnometer methodology.

Table 2 - PSD percentile result and density of binders' components

	CEM I	**CEM III**	**GP**
d_{10} (µm)	3	1.5	8
d_{50} (µm)	16	13	40
d_{90} (µm)	40	32	80
d_{max} (µm)	300	70	120
Density (kg/m^3)	3150	2880	2510

Source: Author (2023).

Indeed, by assessing the PSD percentiles, the D_{50} were 16 µm, 13 µm, and 40 µm respectively. Studies have proven that a higher GP fineness, finer than 75 µm, results in pozzolanic activity instead of alkali-silica reaction (ASR) (Idir; Cyr; Tagnit-Hamou, 2010, 2011). Concerning density, CEM I presented the higher density, being a direct influence of the high clinker content of the formulation.

2.2.1.2 Mix Design and Experimental Protocol

The mortars were fabricated using the mix design method described by Equations 1 to Equation 4 (Bordy *et al*., 2017).

$$V_S + V_C + V_{GP} + V_W \approx 1m^3 \quad (1)$$

$$\frac{W}{GP + C} = 0.5 \quad (2)$$

$$\frac{GP}{C + GP} = 0.5 \quad (3)$$

$$\frac{S}{GP + C} = 0.3 \quad (4)$$

The V_S, V_C, V_{GP}, and V_W (units in m³) are the sand, cement, GP, and water volumes, respectively. S, W, GP, and C (kg) are the sand, effective water, GP, and cement contents per cubic meter of mortar, respectively. The water-to-binder ratio (W/B) was 0.5 (Equation 2).

The values of paste volume and W/B were chosen to obtain a homogeneous mortar mixture by limiting bleeding and segregation while ensuring workability (Bordy *et al*., 2017). Moreover, the W/B was adopted high enough to mitigate the self-desiccation phenomenon due to cement hydration (Jensen, 1995; Persson, 1997). The cement replacement ratio was fixed at 0.5 (Equation 3) to maintain the GP as equal to the C. The V_S was fixed to obtain a total mortar volume of 1 m³. The mortar mix designs are given in Table 3.

Table 3 - Mix proportions of mortar (kg/m3)

	CEM I	**CEM III**	**CEM I + GP**	**CEM III + GP**
Sand 0/4	1795	1638	1761	1685
CEM I	500	0	250	0
CEM III	0	500	0	250
GP	0	0	250	250
Water	250	250	250	250
Superplasticizer	1.8	1.5	1.4	1.2
Flow (cm)	12	13	17	21

Source: Author (2023).

A superplasticizer polycarboxylate was added to all mixtures to obtain a comparable consistency. Indeed, due to the low superplasticizer content, compared to the mortar constituents, its content was almost neglected. The superplasticizer/cement ratio varied between 0.36% and 0.54%. The slump at the fresh state varied between 12 and 21 mm.

In the fresh state, the workability of mortars was assessed using a flow table test according to the ASTM C230/230M (ASTM, 2014). This test was performed by placing mortar in a mini mortar cone in two layers on a vibrating table. Then, 15 vibrations are applied with a speed of 1 vibration/second. At the end of this test, the flow is measured. In the hardened state, the porosity, and compressive and tensile strengths were assessed.

Complying the NF EN 933-1, it was cast prismatic mortars with geometries of 4 cm × 4 cm × 16 cm (CEN, 2012b). The specimens were cured at the standard conditions (i.e., for 24 h at 20 ± 1 °C and relative humidity no less than 60%). Then, the specimens were unmolded and cured in water for different test ages (3, 14, 28, and 90 days) at 22 ± 1 °C.

The water porosity tests consisted of placing the specimens in saturation benches until the complete water saturation which was additionally ensured by a vacuum pump (LABORATOIRE MATÉRIAUX ET DURABILITÉ DES CONSTRUCTIONS, 2009). Following 24 hours of saturation the specimens were collected, wiped and their wet and underwater weights were measured. After that, the specimens were placed in an oven, at 105 °C, for 24 h having a second weight measurement in dry conditions (LABORATOIRE MATÉRIAUX ET DURABILITÉ DES CONSTRUCTIONS, 2009).

For the compressive and flexural strength test parameters, the loading rates were 2.4 ± 0.2 kN/s and 50 ± 10 kN/s, respectively. The TG analysis was carried out to monitor the solid phase formations and the pozzolanic content (portlandite—CH, calcite—CC, etc.). The device used was the NETZSCH® instrument (STA 449 F5 Jupiter, Selb, Germany). It consists of a sealed chamber for atmosphere control of the sample by injection of helium gas, an oven to manage the temperature, a weighing module (microbalance), a thermocouple to measure the temperature, and a computer for data acquisition.

During the test, the temperature is increased from the temperature room up to 1200 °C with a constant rate of 10 °C/min. This increasing rate is used in the literature, and it is recommended by the French standard (LABORATOIRE MATÉRIAUX ET DURABILITÉ DES CONSTRUCTIONS, 2009). The obtained TG results were used to calculate the portlandite rate ($\%CH$) and the chemically bonded water ($\%w_b$) by Equations 5 and 6 (Kalpokaitė-Dičkuvienė *et al*., 2022).

$$\%CH = \frac{m_{410} - m_{490}}{m_{490}} \times \frac{M_{Ca(OH)2}}{M_{H2O}} \times 100\% \quad (5)$$

$$\%w_b = \frac{m_{40} - m_{490}}{m_{490}} \times 100\% \quad (6)$$

The m_{40}, m_{410}, and m_{490} are the sample weights at 40 °C, 410 °C, and 490 °C, respectively. $M_{Ca(OH)2}$ and M_{H2O} are the molecular masses of portlandite ($\%CH$) and water ($\%w_b$), respectively. To compare the results, the $\%CH$ rate and $\%w_b$ were normalized to 100 g of anhydrous material.

2.2.2 Numerical Approach for Heat of Hydration Analysis

This section introduces a novel method for analyzing temperature data in the time domain from the heat of hydration tests, with the goal of identifying transition times between cement hydration modes. The method begins with the use of an Artificial Neural Network (ANN) model creation to process the heat of hydration test data and convert it into a continuous temperature model in the time domain.

Specifically, a Multilayer Perceptron Regressor (MLP) was employed to transform the experimental data (temperature readings vs. time) into a time series regression. This technique was employed to reduce the fluctuations in the thermal readings, both attributed to eventual inaccuracies of the testing method or insufficient reading precisions.

Subsequently, a numerical analysis of this time series model was performed to identify hydration modes based on the local maxima and minima values, allowing for the classification and differentiation of the modes. These steps are summarized in Figure 4.

Figure 4 - Numerical for hydration process classification proposed model

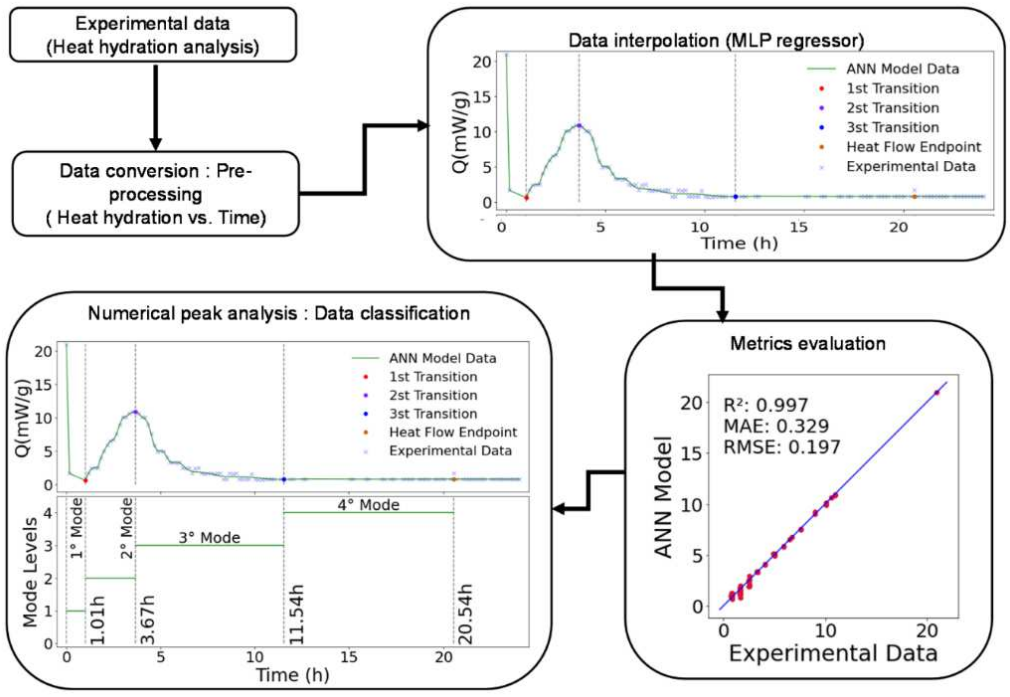

Source: Author (2023).

2.2.2.1 Artificial Neural Network Modeling

Assessing the literature on machine learning and civil engineering is often the use of ANN models for data-driven problems on diverse applications (Al-Swaidani *et al.*, 2022; Di Benedetto *et al.*, 2021; Shah; Pandit; Gaur, 2022), whereas diverse models have been developed over the years with varying characteristics.

An MLP is a class of ANN, that can be applied for both classification and regression problems, being a classical type of ANN, very flexible and can be used to map inputs to outputs among several other applications. In the field of study of machine learning, it is classified as supervised learning, using a backpropagation technique for training (cf., Figure 5).

The findings in the literature highlight good results in long short-term memory (LSTM) applications showing the MLP versatility in a multitude case of scenarios, for different applications (Abirami; Chitra, 2020; Davies, 2005; Gupta; Sinha, 2000; Menzies *et al.*, 2015). Figure 5 presents the illustration of the ANN model adopted and the illustration of the lower neuronal structure, highlighting the information feed-forward and error back-propagation flux, bias adjustment, network and all related aspects.

Figure 5 - Schematic of the ANN architecture adopted (a) and the neuronal structure (b)

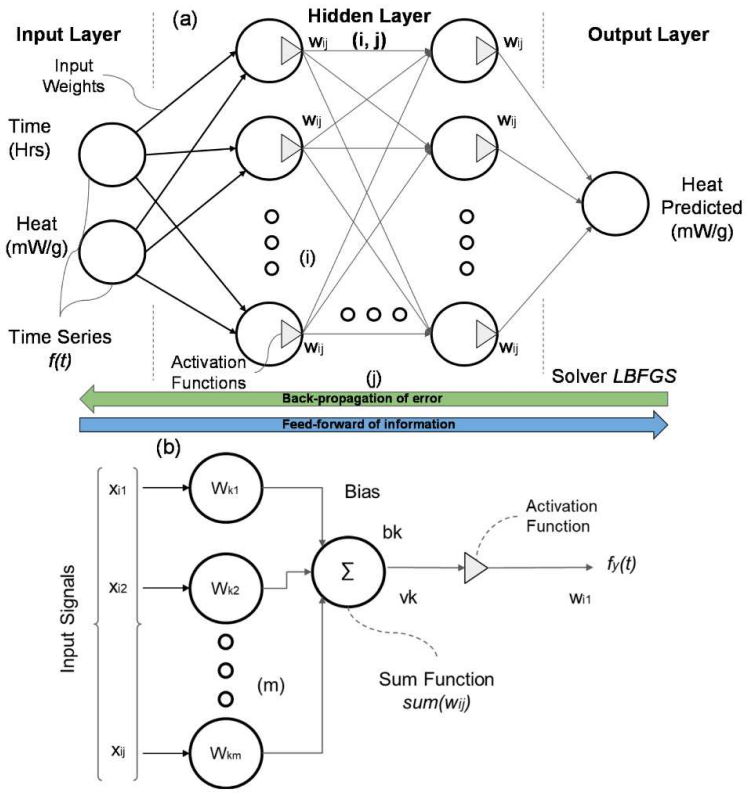

Source: Author (2023).

The adopted MLP architecture consists of three main components or nodes organized in the (i) input layer, (ii) hidden layers, and (iii) output layer. Excepting the input layer, all the other concepts apply non-linear activation functions, and the hidden layer size (number of hidden layers) can be best determined by hyperparametric optimization (Abirami; Chitra, 2020). The details of the inputs and internal weights are optimized depending on the problem addressed, the experimental dataset and the solver adopted.

As seen in Figure 5b, the neuronal structure is also composed of three elements, (i) the 'synapses' or connecting links, that are associated with the individual weights, (ii) the processing unit that handles the input signals weighted (summing junction) by the synaptic weight and adjusts them by adding a bias value (b_k), (iii) an activation function (φ) that limits the signal amplitude at the neuron's output (Hallinan, 2013; Yang; Yang, 2014).

Figure 5a demonstrates a neuronal structure applied to a hidden and output layer. The input layer differs from by the absence of the activation function and the single input, connected to the input data. The neuron k is described mathematically by Equations 7 and 8.

$$u_k = \sum_{j=1}^{m} x_j \times w_{kj} \tag{7}$$

$$v_k = u_k + b_k \tag{8}$$

The u_k is the linear combiner of the input signal and v_k is the weighted sum of the input values adjusted by the b_k. The activation function is a set of mathematical equations that define the output signal of the neuron k. These are divided into four distinct groups (Rajaoarisoa, 2020), as described in the following Equations.

Equation 9 represents the threshold function, which is equivalent to a Heaviside function. Equation 10 is an identity function (linear function). Equation 11 describes a logistic sigmoid function (having a sigmoidal nonlinearity as a slope parameter). Equation 12 is a hyperbolic tangent function, a variation of nonlinearity.

$$\varphi(v) = \begin{cases} 1 \text{ if } v > 0 \\ 0 \text{ if } v = 0 \\ -1 \text{ if } v < 0 \end{cases} \tag{9}$$

$$\varphi(v) = 1 \tag{10}$$

$$\varphi(v) = \log f(v) = \frac{1}{1 + e^{-\alpha v}} \tag{11}$$

$$\varphi(v) = \tanh(v) = \frac{2}{1 + e^{-\alpha v}} \tag{12}$$

The sum of the weighted and bias-corrected inputs passes through the activation function φ to obtain the final output signal (y_k), as shown in Equation 13.

$$y_k = \varphi\left(\sum_{j=1}^{m} x_j \times w_{kj} + b_k\right) \tag{13}$$

The implementation of the ANN model is summarized in three steps, (i) architecture definition, including the specification of layers' size, activation function and related parameters (ii) the training procedure or models' fitting, to adjust the neuronal weights to the expected outputs, and (iii) the testing and validation, by evaluating the comparison of predicted with the real data. Additionally, the solver (algorithm of weights optimization) has a crucial role in this wide scenario.

The LBFGS (Limited-Memory Broyden–Fletcher–Goldfarb–Shanno) is a widely used solver algorithm in machine learning applications, using a quasi-Newton method (Ali, 2021; Borhani, 2020; Erway; Marcia, 2017). The original LBFGS method uses an estimate of the inverse Hessian matrix, but in that case, in the most recent application, it stores only some chosen vectors to be able to represent the model with a required approximation, which implies a lower computing demand and reduced processing time.

2.2.2.2 Evaluation Metrics

To evaluate the models' performance several metrics can be adopted. Correlation coefficient (R^2), root mean square error (RMSE), and mean absolute error (MAE) are reported as the most common metrics for regression problems (Dung; Anh, 2019; Naser; Thai; Thai, 2021; Nguyen *et al*., 2020). The aim is to achieve a model that best fits the training data by evaluating the combined metrics. All these metrics are indicators used to evaluate the models' efficiency. These indicators are described in Equations 14 to 16, respectively.

$$R^2 = 1 - \frac{\sum_{i=1}^{n}(y_i - \hat{y}_i)^2}{\sum_{i=1}^{n}(y_i - \hat{y})^2} \tag{14}$$

$$RMSE = \sqrt{\frac{1}{n} \times \sum_{i=1}^{n}(\hat{y}_i - y_i)^2} \tag{15}$$

$$MAE = \sum_{i=1}^{n} \left| \frac{y_i - \hat{y}}{y_i} \right| \quad (16)$$

2.2.2.3 Hydration Modes Identification and Data Processing

Finally, after the ANN definition and the validation procedure, the heat of hydration temperature model in the time domain was submitted to a numerical analysis. This approach aims to find local maxima and minima through a continuous seek function in the time domain. This conceptual framework was built to describe and visualize the divergences in the hydration modes from different cement formulations (Chen *et al*., 2019; Dabić; Krstulović; Rušić, 2000; Hong *et al*., 2020; Lin *et al*., 2020; Xu *et al*., 2022; Zhao *et al*., 2022). Furthermore, the entire data processing procedure is summarized as follows:

- Data Collecting: the experimental data is composed of the temperature measures in the time domain from the cements' heat of hydration tests. Four datasets were obtained from CEM I, CEM III, CEM I + GP and CEM III + GP;
- ANN Model Definition: conceptualization of the ANN model, testing and hyperparameters optimizing, such as MLP hidden layers size, activation functions, and optimization algorithm (Al-Swaidani *et al*., 2022; Borhani, 2020; Nas□r; Thai; Thai, 2021; Shah; Pandit; Gaur, 2022) to generate models with high accuracy, on different metric parameters (R^2, RMSE, MAE) to proceed with the data classification (Dung; Anh, 2019; Nas□r; Thai; Thai, 2021);
- Hydration Mode's Identification: based on the generated model, the numerical approach is proceeded, with a local maxima and minima analysis to identify the hydration transition zones and, thus, the transition modes of cement hydration with time (Zhao *et al*., 2022).

As a result, the hydration modes are identified in the time domain, represented through a staircase levels plot, according to literature recommendations (Chen *et al*., 2019; Xu *et al*., 2022; Zhao *et al*., 2022). In addition to the formulations and chemical compositions of the cements, it is discussed the variations in hydration modes, which are directly altered by the addition of GP, which affect the hydration performance and resulting products.

2.3 Results and Discussion

2.3.1 Life Cycle Analysis (LCA)

Table 4, Table 5 and Table 6 present the LCI obtained after interpolations and considerations reported in the literature (Chen *et al*., 2010; Crossin, 2015; Guignone *et al*., 2022; Huntzinger; Eatmon, 2009; Sánchez *et al*., 2021; Valderrama *et al*., 2012; Zulkarnain *et al*., 2021).

Table 4 - Raw materials consumption inventory input calculations

Raw Materials	Units	CEM I (Clinker)	CEM III (GGBFS)	CEM I + GP	CEM III + GP
Limestone	kg/kg product	1.1737	0.4049	0.5868	0.2025
Clay	kg/kg product	0.3307	0.1141	0.1653	0.0570
Sand	kg/kg product	0.0503	0.0174	0.0252	0.0087
Iron ore	kg/kg product	0.0203	0.0070	0.0102	0.0035
Water	m³/kg product	0.0668	0.0230	0.0334	0.0115
GGBFS	kg/kg product	-	1.0316	-	0.5158
Raw glass	kg/kg product	-	-	0.6480	0.6480

Source: Author (2023).

The units given are in kg of raw material by kg of produced binder (kg/kg product). For raw materials in volume, such as water, units given are in m³ of raw material by kg of produced binder (m³/kg product). GGBFS is highlighted by the literature with a potential emission reduction of 78.84% in the production of CEM III (Bordy *et al*., 2017). Regarding GP and its manufacturing process, Table 4 is not on an industrial scale (Jensen, 1995).

The results show a significant reduction in mineral resource consumption which was replaced by a pronounced incorporation of wastes (GGBFS and GP). This also implies a reduction of landfills, a lower mineral resources extraction impact and environmental aspects.

Table 5 - Energy consumption inventory input and calculations

Energy	Units	CEM I (Clinker)	CEM III (GGBFS)	CEM I + GP	CEM III + GP
Electricity (kWh)	kWh/kg product	0.0687	0.0687	0.0403	0.0403
Petroleum coke	kg/kg product	0.0463	0.0463	0.0231	0.0231
Hard coal	kg/kg product	0.0559	0.0559	0.0280	0.0280
Diesel	kg/kg product	3.04×10^{-7}	3.04×10^{-7}	1.52×10^{-7}	1.52×10^{-7}
Fuel oil	kg/kg product	0.0117	0.0117	0.0058	0.0058
Natural Gas (MJ)	MJ/kg product	0.2777	0.2777	0.8768	0.8768
Light distribution	kg/kg product	0.0043	0.0043	0.0022	0.0022

Source: Author (2023).

For energy input, it is either given in terms of kWh of energy by kg of produced binder (kWh/kg product) or in kg of fuel source by kg of produced binder (kg/kg product) when applied to the context. And for the last, all emissions are summarized as a function of mass, as the mass of the emission by the mass of the resulting cement (kg/kg product).

Table 6 - General emissions inventory input and calculations

Emissions	Units	CEM I (Clinker)	CEM III (GGBFS)	CEM I + GP	CEM III + GP
CO_2	kg/kg product	0.0687	0.0687	0.0403	0.0403
NO_x	kg/kg product	0.0463	0.0463	0.0231	0.0231
SO_2	kg/kg product	0.0559	0.0559	0.0280	0.0280
$H_2O(g)$	kg/kg product	3.04×10^{-7}	3.04×10^{-7}	1.52×10^{-7}	1.52×10^{-7}
Particulates	kg/kg product	0.0117	0.0117	0.0058	0.0058
Waste	kg/kg product	0.2777	0.2777	0.8768	0.8768

Source: Author (2023).

Based on the LCI above, the LCA estimation can be presented as follows. Figure 6 shows the different raw materials consumption.

Figure 6 - Raw materials' consumption

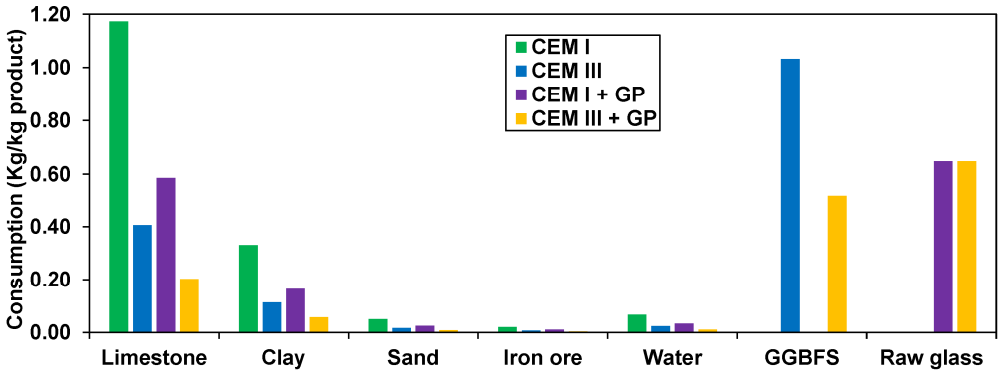

Source: Author (2023).

Figure 7 presents the results for the relevant energy demands. Apart from the electricity produced by different renewable resources (hydroelectric, wind, and thermoelectric), all other resources are derived from fossil origins.

Figure 7 - Fuels and Energy consumption

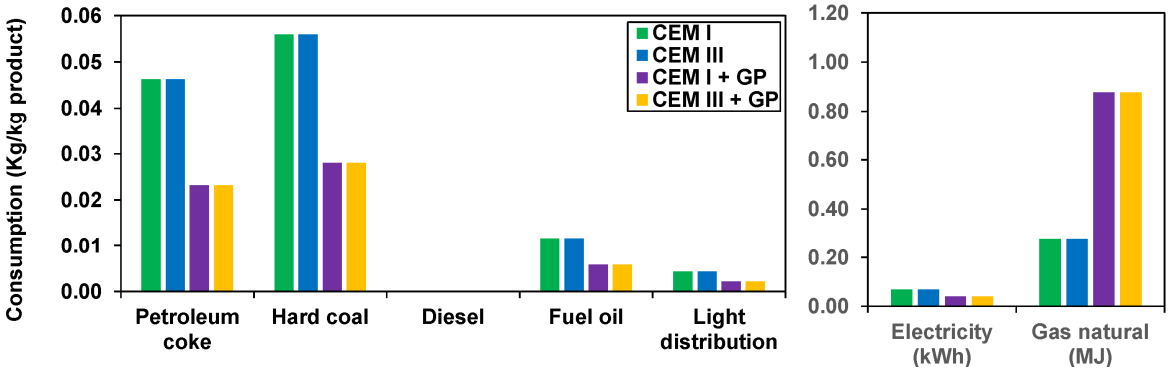

Source: Author (2023).

This parameter is a direct measure of the combustive materials used in the rotative oven for manufacturing clinker, converted into thermal energy, achieving an average temperature level of 1450 °C. Fossil fuels have the greatest impact on clinker production (petroleum coke, hard coal, and fuel oil).

The proposed formulations with 50% cement replacement contribute to a direct 50% reduction in fuel consumption once the clinker manufacturing process is directly addressed. Regarding the increase in natural gas, the GP LCA presented results not from an industrial scale, allowing an additional gap and possibly reducing further this consumption. Figure 8 shows the GHG emission results for the formulations studied.

Figure 8 - GHG Emissions results

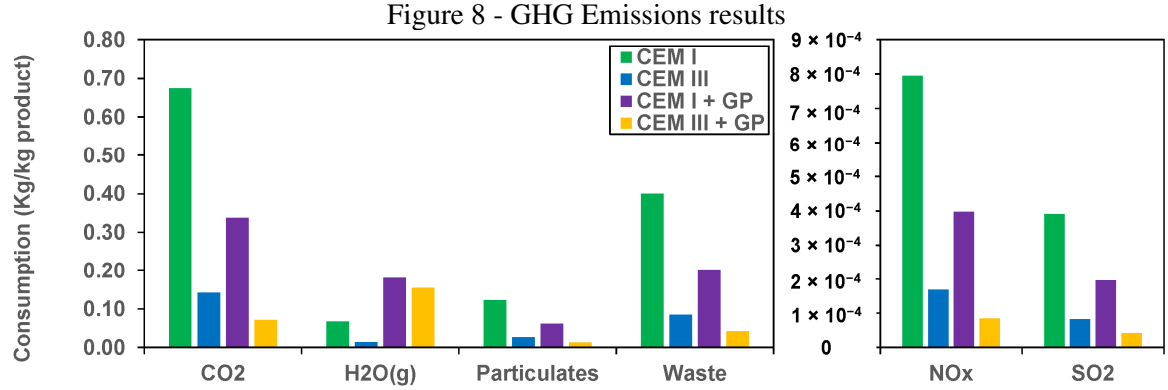

Source: Author (2023).

The results show a significant reduction in the GHG emission for the GP formulations. Regarding CO_2 emissions, CEM III + GP presented the lowest impact due to the 78.83% reduction of the CEM III formulation by GGBFS and an additional 50% by GP. The same profile is observed for hazardous gases. (i.e., nitrous oxide, NO_x, and sulfur dioxide, SO_2). According to the literature, NO_x is more detrimental to climate change with authors indicating it could be 300 times more detrimental compared to CO_2.

2.3.2 Experimental Results

Table 3 presents the findings of the flow tests of the assessed mortars. It was found results from 12 up to 21 mm, indicating a good range of consistency. Moreover, an improvement in workability is obtained of up to 41.6% and 23.5% for CEM I + GP and CEM III + GP compared to mortars with CEM I and CEM III, respectively. This result is attributed to the influence of GP content in the fresh state.

The OPC replacement with the GP addition decreases the water demand for hydration, i.e., by increasing the amount of free water and workability of the pastes (Boukhelf *et al*., 2021). Figure 9 presents the evolution of the porosity, and the compressive and the tensile strengths (from flexural tests) at several curing ages (3, 14, 28, and 90 days).

Figure 9 - Porosity, compressive, and tensile strengths for 3, 14, 28 and 90 days

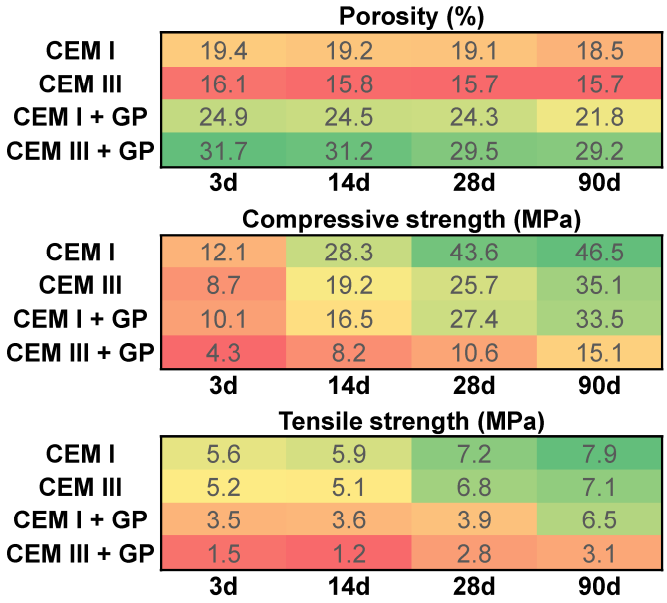

Source: Author (2023).

The CEM III mortar presented lower water porosity compared to CEM I. This is explained by the slag content in CEM III, leading to improved pores structures and creating other non-connected pores ranges (Cherif; Hamami; Aït-Mokhtar, 2020).

For 3 days of curing age, mortars containing GP presented high porosity compared to those with CEM I and CEM III only. This phenomenon is due to the coarse aspect of GP, changing the pore-size distribution (Bouchikhi *et al*., 2019; Boukhelf *et al*., 2021). A proportional decrease in porosity is observed with increasing age for all formulations.

At 90 days of curing age, this decrease was 4.6%, 2.5%, 12.4%, and 7.9% for CEM I, CEM III, CEM I + GP, and CEM III + GP respectively, compared to 3 days. This

result was in agreement with the found of literature (Bouchikhi *et al*., 2019; Boukhelf *et al*., 2021; Cook *et al*., 2021; Subasi; Yilmaz; Binici, 2009).

Concerning mechanical strength, there was an increase in all the results due to the continuous hydration of the cement and GP over time (Gołek *et al*., 2020). In addition, the OPC replacement also led to a systematic loss of mechanical strength in the short-term analysis. This was attributed to the clinker dilution effect, which is the immediate consequence of the replacement of a more reactive powder (cement) with a less reactive content (GP) in the short term (Zidol; Tognonvi; Tagnit-Hamou, 2017).

Nevertheless, the mechanical strength does not cease increasing (Bouchikhi *et al*., 2019; Boukhelf *et al*., 2021; Gołek, 2022). This phenomenon is due to continuous pozzolanic reactions between portlandite ($Ca(OH)_2$) and silica derived from GP (Kolani *et al*., 2012), in addition to the slag content in CEM III, corroborated by the TG analysis.

After 90 days of curing age, the CEM I + GP presented a decrease of about 28% in compressive strength and 17.7% in tensile strength compared to CEM I. For CEM III + GP, the decrease was about 57% and 56%, respectively, compared to CEM III. These results are in agreement with those reported by the literature (Adesina; Das, 2020). Nevertheless, these values of CEM I + GP remain adequate for use.

To investigate the GP pozzolanic reaction with portlandite ($\%CH$), the TG was conducted at 90 days. Figure 10 shows the results of mass loss in the temperature domain.

Figure 10 - TG and dTG analysis of the proposed formulations

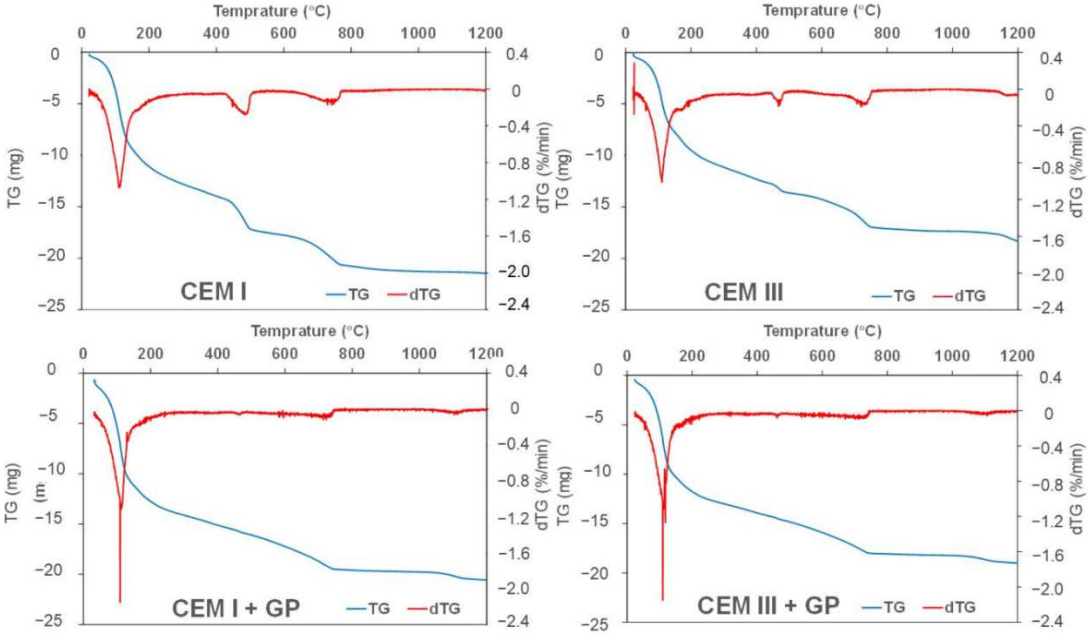

Source: Author (2023).

To ease the visualization, all the x-axis and y-axis were leveled. The mortar with CEM III resulted in lower portlandite and calcite content compared to CEM I by comparing the second and third drops in the respective dTG curves. This is attributed to the pozzolanic reaction of the blast furnace slag content in the CEM III formulation. In the GP mortars analysis, these two drops were even reduced, showing lower content of both hydration products justifying the strength reduction addressed previously (Boukhelf *et al*., 2021).

An increase in the first dTG drop was observed for the GP mortars, which is related to the water physically absorbed content of those materials. That behavior is in accordance with the literature (Stepkowska *et al*., 2004; Vance *et al*., 2013) whereas that parameter is directly influenced by the pores' structures and their exposure to the environment.

The first segment under 200 °C is attributed to the loss of free water as well as the dehydration of calcium silicate hydrate (CSH), ettringite, calcium monosulfo-aluminate, hemicarboaluminate, or calcium monocarboaluminate (summarized as AFm). The second peak around 400-500 °C is contributed to the dehydroxylation of portlandite (CH), while the decarbonization of calcium carbonates takes place at 700-800 °C.

From dTG patterns, those material phases are difficult to dissociate, as the corresponding bands are large, and the decomposition temperatures of these phases are narrow and overlay in some cases. Based on TG findings, the normalized amounts of $\%w_b$ and $\%CH$ are presented in Figure 11.

Figure 11 - $\%CH$ and $\%w_b$ of mortars studied

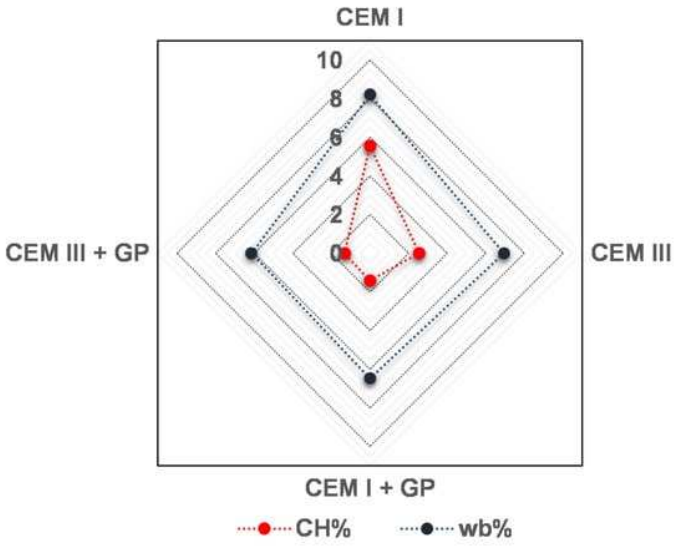

Source: Author (2023).

Indeed, the $\%w_b$ is indicative of the hydration product (CSH, AFm, and CH) formed during cement hydration, while normalized CH can be interpreted as an indication of changes in this direct product (CH consumption for the formation of additional CSH) as highlighted by the literature (Damidot *et al.*, 2011). Figure 11 shows that for the mortars containing low clinker content, the $\%w_b$ rate is lower than for the standard mortar with CEM I.

The increase in $\%w_b$ in the proposed formulations (CEM I + GP and CEM III + GP) is related to GP pozzolanic activity. Indeed, silica content reacts chemically with CH producing additional CSH. Due to that phenomenon, the normalized CH for GP mortars is lower than for the standard mortars (CEM I and CEM III). Furthermore, this behavior is in accordance with the literature (Lavergne *et al.*, 2018; Ni *et al.*, 2021), where $\%w_b$ and CH content for pure and siliceous blended pastes were addressed.

2.3.3 Data Processing/Numerical Results

Figure 12 shows the true vs. predicted plot of the generated ANN heat of hydration model. Indeed, the models were able to capture the hydration evolution of the assessed mortars having a good agreement with the experimental data.

Figure 12 - True vs. predicted plot and error metrics for (a) CEM I, (b) CEM I + GP, (c) CEM III, and (d) CEM III + GP

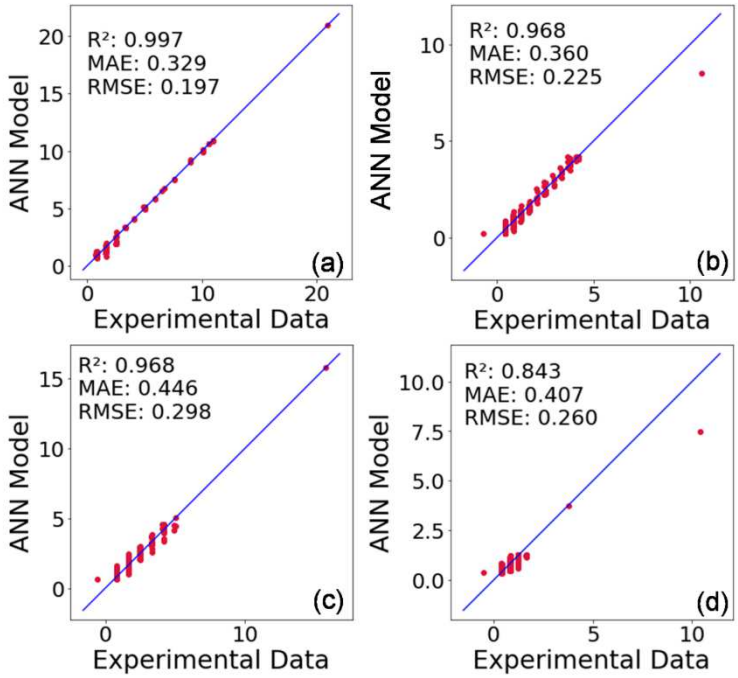

Source: Author (2023).

Assessing the error metrics, it was found a more pronounced variance in the MAE and RMSE metrics. For the RMSE, the lowest results are obtained with the CEM III + GP results with a 0.843 (R^2), with the further metrics in the same sense. The hydration modes identification of CEM I, CEM I + GP, CEM III, and CEM III + GP are shown in Figure 13a, Figure 13b and Figure 14a, Figure 14b, respectively.

Figure 13 - Heat of hydration experimental, ANN model and modes transitions identification for (a) CEM I and (b) CEM I + GP

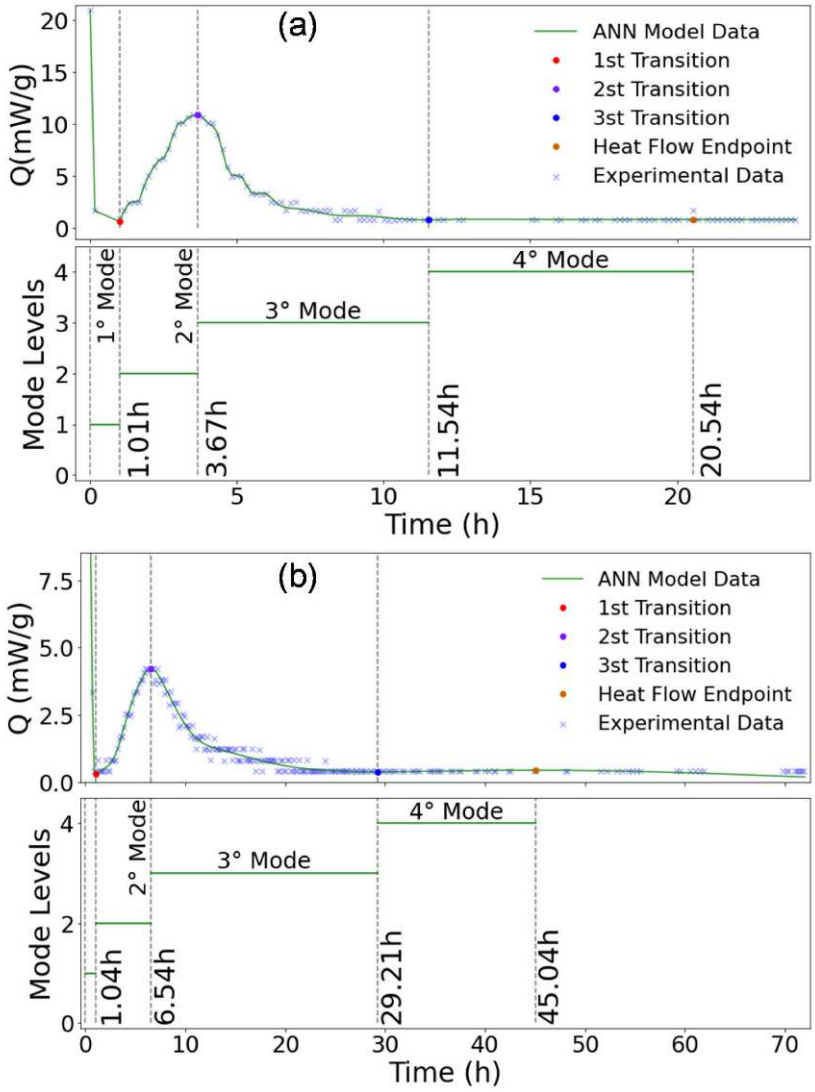

Source: Author (2023).

The proposed analysis identified in all cases four hydration modes, in agreement with the literature (Guignone *et al.*, 2022), which include (i) the initial reaction and slow reaction period (Mode 1), (ii) the acceleration period (Mode 2), (iii) the deceleration (Mode 3), and (iv) the stability or constant level (Mode 4).

Comparing these two initial results, the CEM I mortar had an earlier acceleration period than CEM I + GP, with a higher heat release. This mode corresponds to the induction phenomenon interpreted by the geochemistry dissolution theory. It corresponds to the primary mechanism controlling the kinetics up to the end of the induction period is the undersaturation of this surface layer (Scrivener; Juilland; Monteiro, 2015).

In addition, the tri-calcium aluminate (C3A) content reacts promptly with water, from an early age, to form calcium hydroaluminate (3CaO-Al2O3-Ca(OH)2-nH2O or hydroxy-AFm), as mentioned reported by the literature (Guignone *et al*., 2022).

Figure 14 - Heat of hydration experimental, ANN model and modes transitions identification for (a) CEM III and (b) CEM III + GP

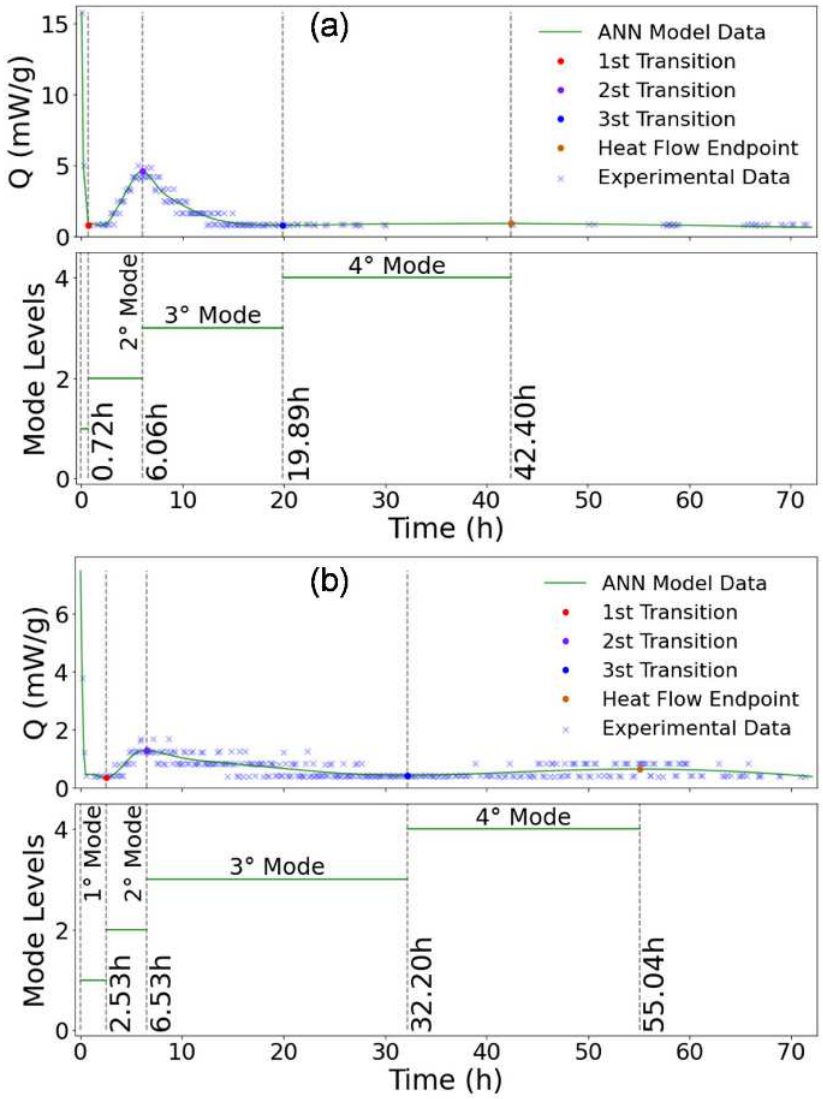

Source: Author (2023).

Comparing Figure 13b and Figure 14a, it was visualized a similar behavior for CEM I + GP and CEM III, assessing the thermal amplitude achieved in the second mode.

Nevertheless, these peaks were found at 6.54 h and 6.06 h respectively. This time delay can be explained by the slag content in the CEM III being more reactive than the GP.

In the second mode, the peak value decreases and shifts toward a longer hydration time when the CEM III and GP are combined. This phenomenon can be attributed to the consumption of C3S (Alite) which is consistent with the heat of hydration rate. It is known that the hydration rate of C3S is higher than that of C2S (Belite) due to the higher solubility and lower activation energy of C3S compared to C2S (Bentz, 1997).

Indeed, the solubility of C3S is between 5 and 8 times higher than C2S (Bentz, 1997). Therefore, it can be concluded that the second mode is strongly affected by the hydration of C3S being this stage is in agreement with the literature (Kishi; Maekawa, 1995).

At the end of the induction period, CSH and CH begin to have a fast development. There is still considerable controversy about the trigger for this increase in reaction rate. Indeed, in pastes, it seems possible to be the CH precipitation this trigger.

The third mode is most concerning the renewed dissolution of C3A with the formation of ettringite (AFt). Due to this C3A reaction retardation with sulfate, the main reaction of this phase should occur after the main peak, the alite reaction, in a sulfated Portland cement.

However, in CEM I, the AFt formation is continuous after the sulfate exhaustion in the solution (Bullard *et al.*, 2011). In conclusion, the ANN model makes it possible to determine when the initial hydration phase is completed, i.e., at 20.54 h, 45.04 h, 42.40 h, and 55.04 h respectively, evidencing the GP impact on the overall hydration behavior.

2.4 Final Comments

A novel ANN model approach is proposed to identify the different hydration modes of the proposed cement formulation using only the heat of hydration experimental data as an input parameter. This method was based on an MLP regressor, mapping the input signal and generating a heat of hydration temperature model in the time domain. Afterward, a numerical approach was proposed to identify hydration modes, addressing the transition zones.

Indeed, the ANN model detected four hydration modes in the experimental data assessed. In addition, the proposed approach achieved good error metrics results, indicating good heat of hydration models' accuracy. In addition to the mechanical strength levels, the 50% OPC replacement by GP was significantly positive for the LCA results. Indeed, the GHG emissions present the most significant results, by reducing up to 50% and 80% of the CO_2, NO_x and SO_2 emissions for the CEM I + GP and CEM III + GP formulations.

Additionally, it was revealed that GP can be employed as a partial replacement in mortars, being beneficial for GHG emissions of cementitious materials. The present study identified waste glass as a suitable SCM, accessible in large quantities, a local eco-material, and a feasible addition for concrete applications, considering both economic and environmental aspects. Nevertheless, when the use of GP as an SCM, the strength decrease should be accounted for by considering its influence on the dosage and mix designs.

To address this shortcoming, future research must focus on combining GP with other recycling fibers and SCMs. Moreover, the proposed ANN model succeeded in the cement hydration analysis, easily identifying the different modes of proposed cement formulation by assessing the heat of hydration as an input parameter.

3 COMPLEX MODULUS CHARACTERIZATION OF AN OPTIMIZED BINDER WITH SCMs: PROPOSITION OF AN ENHANCED CEMENT FORMULATION TO IMPROVE STIFFNESS BEHAVIOR AND DURABILITY OF MORTARS AND CONCRETES

The main content of this chapter is also available online at TARGINO; HOLANDA; MARTINEZ; FREITAS; BOUKHELF; EL MENDILI, (2023)*, published in the Journal of Building Pathology and Rehabilitation.*

ABSTRACT

Materials optimization is an aspect of continuous endeavor for civil engineering in many applications, especially in construction where the materials' durability and mechanical performance are crucial for structural integrity. Structures such as aerogenerators, both towers and foundations, are highly exposed to cyclic loads with a broad range of frequencies and levels. The improvement of the stiffness behavior can significantly enhance their fatigue resistance and consequently durability. This paper aims to evaluate the impact of a high-performance binder optimization, using supplementary cementitious materials (SCMs) to improve the mechanical behavior of mortars and concretes, by improving stiffness response under cyclic loadings, which is related to durability and fatigue life-service. Static tests (axial compressive and splitting tensile strengths) were conducted as well as cyclic stiffness tests that were proposed as a new methodology for these kinds of materials, which may better relate the mechanical behavior in field applications. The proposition consists of the evaluation of complex modulus, under sinusoidal loading in the frequency domain, either in pure compression and pure tension, adopting low (0.1-1 Hz) and mid-range (1-25 Hz) loading frequencies, comparing a proposed strain-enhanced cement formulation with ordinary Portland cement (OPC). The results show that the proposed formulation resulted in a superior material with up to 23% stiffer loading response and 13.8% more energy storage, with also inferences on improved durability, which is expected to delay pathological manifestations and extend fatigue life. The proposed testing protocol obtained results compatible with the literature and seems applicable for evaluating the dynamic behavior of cementitious materials.

Keywords: dynamic behavior; complex modulus; supplementary cementitious materials; ordinary portland cement; fatigue.

3.1 Introduction

The extension of the service life and the durability of cementitious materials is a continuous endeavor in materials science and civil construction. For this, the incorporation of supplementary cementitious materials (SCMs) has become increasingly popular in recent years due to their environmental appeal, with the potential to reduce greenhouse gas emissions (GHGe), and also due to their ability to improve the properties of cementitious composites.

These include alterations in the mechanical behavior (compressive and splitting tensile strengths, elasticity modulus, and Poisson's ratio), materials microstructure (pore sizes distribution, hydration products and interfacial transition zone), fresh state properties (workability, setting-time, and bleeding) as well as improve durability, reduce pathological manifestation and even enhance fatigue life-service (Baikerikar; Mudalgi; Ram, 2023; Boukhelf *et al*., 2023; Cândido *et al*., 2022; Fattouh; Elsayed, 2023; Hamad *et al*., 2021; Keerio *et al*., 2022; Li *et al*., 2019).

Over time, the incidence of repeated loads can result in cracks and mechanical degradation, leading to a gradual loss of supporting capacity and increasing the energy dissipation within cyclic loads (Jia *et al*., 2021; Yang *et al*., 2023). In addition, the measurement of strain can be used to assess the cracking and damage (degradation status) of cementitious materials under different loading conditions. Fatigue testing and structural modeling design require a thorough understanding of the frequency-dependent behavior of materials to accurately predict their long-term performance (Jia *et al*., 2021; Kuo; Zhuang, 2021; Medeiros *et al*., 2015; Myrtja *et al*., 2021; Saucedo *et al*., 2013; Yang *et al*., 2023).

In the renewable energy sector, the optimization of the structural materials used in the aerogenerators' towers and foundations (mostly concrete and grouts, which is a kind of mortar with improved fluidity and performance) is a strategic aspect to enhance efficiency in power generation (Bošnjaković *et al*., 2022; Chen *et al*., 2022; Kuo; Zhuang, 2021).

Such structures are crucial to ensuring the structural stability of the entire generation system, by resisting cyclic loads in different stress levels, temperatures and loading frequencies. Those structures must be able to resist a wide range of loading profiles, derived from high speeds winds, operational vibrations, seismic activity, alterations in the loading regimes (from compression to tension) and frequencies, their own structure weight and the mechanical system as well, sustaining the nacelle, rotors and blades (Bošnjaković *et al*., 2022; Jia *et al*., 2021; Kuo; Zhuang, 2021; Yang *et al*., 2023).

Studies have shown that the improvement of the modulus of cementitious materials used in aerogenerator towers and foundations can lead to improvements in durability (Chu *et al*., 2023a; Kuo; Zhuang, 2021; Liang *et al*., 2022b; Liu *et al*., 2023a).

Kuo and Zhuang also presented evaluations on high-performance concrete for aerogenerator foundations. It was found that a higher modulus of elasticity, compared to the usual values for normal-strength concrete, was more suitable for that application having an improved resistance to the mechanical and environmental incident loads from the aerogenerators' usual operation (Kuo; Zhuang, 2021). These findings emphasize the importance of enhancing mechanical behavior for those applications, especially concerning aerogenerators or other applications subjected to cyclic loading.

The complex modulus, which is a measurement of material stiffness for viscoelastic materials (and corresponds to the modulus of elasticity in perfect linear elasticity), is a crucial parameter to be accounted for, due to its ability to broader evaluate mechanical behavior (Brinson; Brinson, 2008; Liang *et al*., 2022b). It contains information on classical global stiffness and on the levels of dissipated energy during mechanical loading. Classical stiffness is evaluated from the absolute value of the complex modulus ($|E^*|$), also known in the literature as “dynamic modulus”, even if inertial effects are not present during tests.

Meanwhile, the proportion of dissipated and stored mechanical energy, during a load cycle, can be evaluated from measurements such as the phase angle (φ) of the complex modulus, the storage modulus (real part of the complex modulus) and the loss modulus (the imaginary part of the complex modulus) (Brinson; Brinson, 2008).

Complex modulus is also related to aspects of fatigue resistance, providing insights into aspects of pathological mechanisms and materials' durability (Kachkouch *et al*., 2022). A deeper understanding of the complex modulus and the fatigue behavior is necessary to develop more durable and sustainable structures, with more fatigue-resistant materials.

With respect to SCMs, silica fume (SF) and glass powder (GP) are considered by literature as two effective materials with the ability to improve several properties of cementitious materials. Their applications involve the addition or replacement of the cement content, also named ordinary Portland cement (OPC), with a significant focus on performance optimization and the sustainable incorporation of waste materials (Boukhelf *et al*., 2021; Fattouh; Elsayed, 2023; Singh; Mehta; Kumar, 2023).

The SF addition can improve the compressive strength, elastic modulus and result in improved durability (Fattouh; Elsayed, 2023; Fu *et al*., 2021; Hamad *et al*., 2021; Jahandari *et al*., 2021; Kachkouch *et al*., 2022; Keerio *et al*., 2022; Singh; Mehta; Kumar, 2023),

especially in harsh environments, reducing pores structures (Fattouh; Elsayed, 2023; Singh; Mehta; Kumar, 2023; Tripathi *et al*., 2020), improving durability in sulfate-rich and acid environments (Singh; Mehta; Kumar, 2023; Tripathi *et al*., 2020), and reducing microstructure permeability (Liu *et al*., 2023a; Singh; Mehta; Kumar, 2023; Tripathi *et al*., 2020). The SF incorporation in OPC for concrete and mortars has shown consistent results in enhancing performance and durability.

The GP addition has also shown high potential for improving similar properties (Baikerikar; Mudalgi; Ram, 2023; Bharathi; Adari; Pallepamula, 2022; Boukhelf *et al*., 2021, 2023; Fattouh; Elsayed, 2023; Jain; Sancheti; Gupta, 2020). It can enhance the compressive and flexural strength of concretes and reduce their permeability (Baikerikar; Mudalgi; Ram, 2023; Boukhelf *et al*., 2021) improve the workability and water retention (Fattouh; Elsayed, 2023) and increase the flexural and compressive strength at early ages (Boukhelf *et al*., 2023; Keerio *et al*., 2022; Schwarz; Cam; Neithalath, 2008). Moreover, GP has been found to be an effective SCM for enhancing the mechanical and fresh-state properties of cementitious materials, due to its inherent long-term effects (Boukhelf *et al*., 2021, 2023; Kachkouch *et al*., 2022; Schwarz; Cam; Neithalath, 2008).

Literature reports a wide range of optimizations for cementitious materials depending on the application. The increase in elastic modulus has been demonstrated as a valid approach resulting in improved durability, by reducing cracking and increasing stiffness (Chu *et al*., 2022b; Liang *et al*., 2022b). This is an important property of those materials that affect the strain response under different loading conditions, in which case its study is crucial for understanding the pathological manifestations mechanisms and fatigue life.

This paper aims to evaluate the influence of a cement optimization, achieved through the incorporation of SCMs, on the dynamic stiffness behavior of cementitious materials (concretes and mortars), which will be assessed by analyzing the complex modulus. To achieve this, the optimization adopted an approach with the addition of silica fume and glass powder, aiming to enhance stiffness, improve durability and delay pathological manifestations (modulus degradation and cracks). The binders were tested both in concrete and mortar using the same mix design derived from an in-site aerogenerator foundation. As a reference binder, a conventional OPC formulation was used (CEM I). The optimization involved the addition of GP and SF as a replacement for OPC. The experimental program comprised static tests, such as compressive strength and splitting tensile strengths, in addition to dynamic characterization, with complex modulus tests, under low (0.1-1 Hz) and mid-range (1-25 Hz) loading frequencies, in pure compression and pure tension.

By analyzing the mechanical behavior, this paper aims to provide better insights into the complex modulus properties with respect to cementitious materials' mechanical behavior. Ultimately, this research could lead to the development of more sustainable, efficient, and durable structures as it focuses on the mechanical behavior related to fatigue, which is a mechanism for pathological manifestations in structures subjected to cyclic or dynamic loads (De Domenico; Bernardo, 2022; Jahandari *et al*., 2021; Sanahuja; Dormieux; Chanvillard, 2007).

3.2 Methodological Procedure - Part Ii

The experimental program consists of three main stages: (i) the specimens' fabrication for characterization testing; (ii) the assembly and adjustment of the dynamic press setting for the splitting tensile testing and complex modulus analysis (CMA); and (iii) the testing procedures itself, comprising uniaxial compressive strength and splitting tensile strength, and CMA tests at different loading frequencies. All tests were conducted in a controlled temperature environment of 19 °C ± 0.50 temperature, with a minimum of 4 h allocated prior to the tests start to ensure temperature stabilization and heat flow equalization (Jiao *et al*., 2014; Shoukry *et al*., 2011).

3.2.1 Materials

The specimens were cast using two different cement formulations. The first was a commercial formulation of OPC to serve as a reference. The choice in this case was to adopt CEM I as the OPC, as it does not contain any SCMs in its manufacturing process, only the residual gypsum to control setting time. This avoided any undesired interaction within SCMs in the OPC manufacturing content.

The second cement formulation, the one proposed by this current methodology, was designed based on the best literature recommendations for optimizing durability, microstructure, fatigue life and modulus of elasticity (Boukhelf *et al*., 2021, 2023; Kachkouch *et al*., 2022). Table 7 provides the detailed cement formulations for the binders utilized in this study.

Table 7 - Proposed Binders Formulations

Binder Component	M1 (Reference)	M2 (Optimized)
Cement CEM I (%)	100	65
Glass Powder (GP) (%)	-	30
Silica Fume (SF) (%)	-	5
Clinker Ratio (%) (%)	95	62

Source: Author (2023).

The incorporation of GP and SF has usually a positive effect on the microstructure of cementitious materials, with the enhancement of those mechanical properties (Bharathi; Adari; Pallepamula, 2022; Boukhelf *et al*., 2021, 2023; Fattouh; Elsayed, 2023; Kachkouch *et al*., 2022; Shanmugasundaram; Praveenkumar, 2022). The proposed optimized formulation also had a low-carbon design, with a 33.25% clinker consumption reduction, which is also significant for sustainability aspects (Baikerikar; Mudalgi; Ram, 2023; Boukhelf *et al*., 2023).

The cement CEM I 52.5N employed complied with the European standard EN 197-1 (CEN, 2012a). The GP was obtained from demolition glass waste, of a waste disposal plant in Caen, France. The crushing and sieving process was repeated until achieving a diameter lower than 63 μm. The SF used complies with EN 13263-1 (CEN, 2005). It has a spherical aspect with an absolute density of 2.24 $g.cm^{-3}$ and a specific surface area of 225 m²/g with high purity (Si content higher than 95%). The normative requirements and related parameters are presented in Table 8.

Table 8 - Silica Fume Characterization according to EN 13263

Characteristics	Normative Requirements	Observed Values
SiO; Content (%)	≥ 85 %	96% ± 2
Elemental Si Content (%)	≤ 0.4 %	0.14% ± 0.05
$Na_2O_{eq.}$ Content (%)	≤ 1.0 %	0.50% ± 0.1
SO_3 Content (%)	≤ 2.0 %	0.27% ± 0.50
Activity index at 28 days (%)	≤ 0.4 %	≥ 101%
Loss on Ignition (%)	≥ 4.0 %	2% ± 0.5

Source: Author (2023).

The SF used in this study meets all EN 13263-1 and 2 (CEN, 2005) requirements. With 96% ± 2 of SiO_2 and 0.14% ± 0.05 of Si elemental, it is classified as highly pure and recommended for applications in cementitious materials. Na_2O eq. content of 0.50% ± 0.1 and

SO_3 content of 0.27% ± 0.50 are considered in an acceptable range, signifying the absence of harmful impurities to the performance.

The activity index at 28 days was higher than 101%, indicating high pozzolanic activity. Additionally, it was observed loss on ignition of 2% ± 0.5 indicating its good thermal stability. The fillers' density was determined using a helium pycnometer and the particle size distribution (PSD) was assessed by the wet process of EN 993-1 (CEN, 2018). The specific surface area was determined using the Brunauer-Emmett-Teller method (BET), based on the EN ISO 18757 (CEN ISO, 2003). These results are presented in Table 9.

Table 9 - Characterization of The Raw Powder Materials

Characteristics	**Cem 1 (OPC)**	**Glass Powder (GP)**	**Silica Fume (SF)**
Max Diameter (μm)	60	50	36
Specific Gravity (kg/m³)	3170	2710	2180
BET Surface Area (m²/kg)	6430	5650	22070

Source: Author (2023).

Comparing these results to the literature, the specific gravity values of the OPC and GP were within the usual range reported, with suitability for use as raw materials. However, the high BET surface area of SF was significantly higher and exceeded the conventional values, suggesting that the SF used is highly reactive and with a high level of fineness, which is beneficial to improving mechanical behavior and durability.

The importance of the fineness of cement and its constituents cannot be overstated, as it directly affects the microstructure and mechanical properties of the resulting concrete. Finer materials tend to improve the final density and porosity and usually have enhanced pozzolanic activity and pore-filling capability.

Therefore, it is crucial to consider not only the maximum diameter but also the entire particle size distribution (PSD) when selecting raw materials. The complete PSD curves, presented in Figure 15 provide a more comprehensive view that can aid in optimizing the mix design for improved performance.

Figure 15 - PSDs of the Cement, Glass Powder and Silica Fume

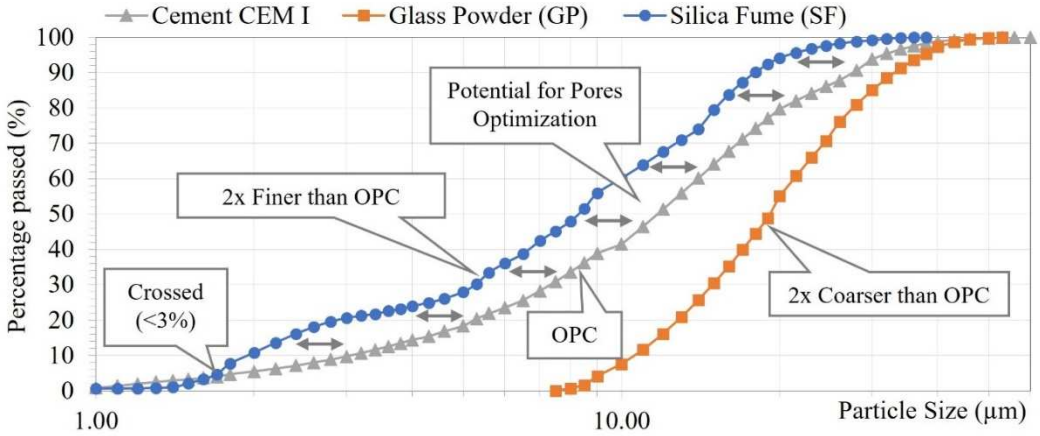

Source: Author (2023).

The results demonstrate a continuous distribution of the OPC, falling between those of the GP and SF. This observation suggests that the addition of GP may not have a significant effect on the porosity of the product, except for the influence of hydration reactions. In contrast, the addition of SF may lead to improvements in microstructure.

These findings may provide initial evidence of the potential benefits of SF incorporation. Further investigations are needed to fully understand the mechanisms behind these observations and to optimize these incorporations (Fattouh; Elsayed, 2023; Shanmugasundaram; Praveenkumar, 2022). Figure 16 presents the current methodology through the experimental procedure abstract.

Figure 16- Experimental Procedure Graphical Abstract

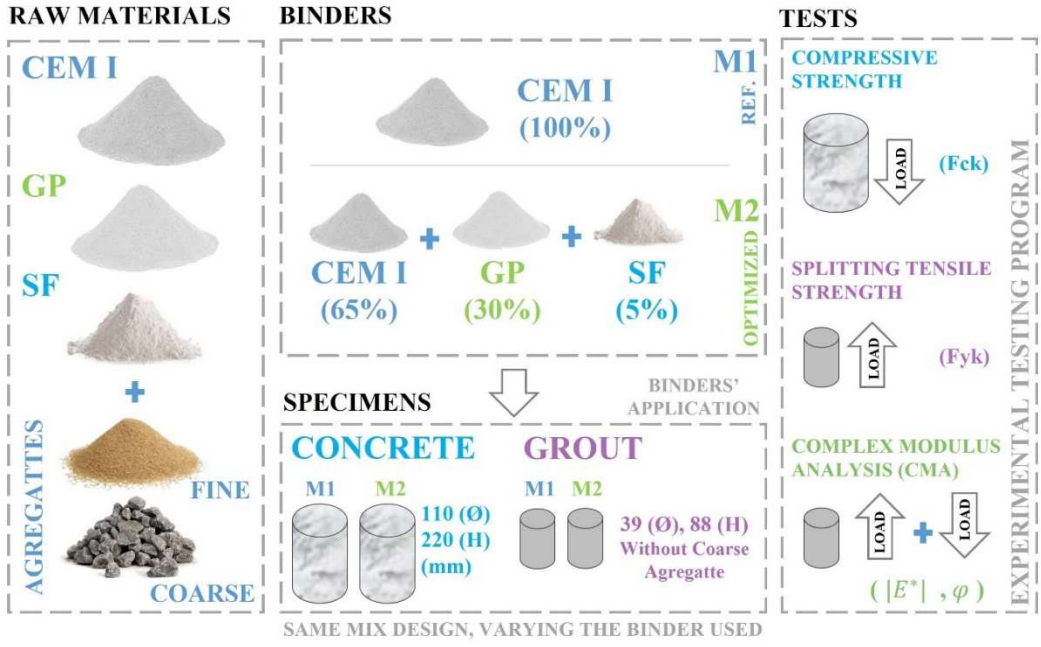

Source: Author (2023).

After the characterization of the raw materials, the concrete and grout specimens were cast and left to cure for 24 hours before being demolded. Then, they were placed in a humid chamber with a temperature of 22 °C and relative humidity of 50%, which is a common practice in the industry to simulate real-world conditions and avoid leaching of the material during curing (Jiao *et al*., 2014; Shoukry *et al*., 2011).

It is noteworthy that despite the differences in binders used in the specimens, both formulations maintained the same mix design and mixture procedures. This approach allowed for a more direct comparison of the effects of each binder on the mechanical properties of the specimens. The water/binder ratio (W/B) was kept constant at 0.45, with a binder consumption of 350 kg/m³. These details are summarized in Table 10.

Table 10 - Formulation Mix Design with Materials Consumption

Component	**Specific Gravity (kg/m³)**	**Concrete M1 (kg/m³)**	**Concrete M2 (kg/m³)**	**Mortar M1 (kg/m³)**	**Mortar M2 (kg/m³)**
Cement CEM I	3170	350	248.4	350	248.4
Glass Powder (GP)	2180	-	74.5	-	74.5
Silica Fume (SF)	2710	-	12.4	-	12.4
Clinker Ratio (%)	-	95	67	95	67
W/B Ratio	-	0.45	0.45	0.45	0.45
Water	1000	157.5	150.9	157.5	150.9
Sand (00/ 3.15)	2490	639	369	639	639
Gravel (3.15 / 12.5)	2310	1070	1070	-	-
Specimen Size (mm)	-	110 x 220	110 x 220	39 x 88	39 x 88

Source: Author (2023).

By keeping the same mix design, the study sought to isolate the effects of the cement formulations on the composite properties. In terms of geometry, two sizes of specimens were cast for this experimental program.

The first one was a (i) regular cylindrical size of 11 cm × 22 cm, used in regular compressive strength tests. The second one was a (ii) smaller cylindrical version, with 39 mm × 88 mm, required to obtain a specimen with a lower rupture loading, under 25 kN, due to the maximum loading limitations of the dynamic press. The regular-size specimens were meant for the compressive strength tests, while the smaller ones were used for the tensile strength and dynamic characterization tests.

For the last, to ensure that the cement formulations' mechanical properties were properly characterized, using the smaller specimens (39 × 88 mm), it was necessary to maintain the elementary representative volume (ERV). For this, it was excluded the coarse

aggregates from the mix design formulation, whereas its incorporation could result in size effects, overwhelming the mechanical behavior prior to the cementitious matrix influence.

Therefore, a minimum proportion of 1:10 between the maximum diameter of the fine aggregate and the diameter of the specimen was maintained, according to standard recommendations for size effects reduction, according to ASTM C192 (ASTM INTERNATIONAL, 2015). By adopting this approach, an ERV was achieved, and the smaller specimens could be used to evaluate the tensile strength and the complex modulus, under pure tension and compression loading conditions, with a high level of accuracy, highlighting the direct influence of the cements' formulations.

3.2.2 Static and Dynamic Press Sets

The experimental program comprised tests in two different laboratories. At first, it was conducted the static testing using a three-column compression testing machine, with a maximum load of 4000 kN, equipped with a digital control system, a load cell with ± 0.5% precision, an axial extensometer with ± 0.01 mm accuracy and a displacement rate of 0.01-100 mm/min. This testing set was meant for conducting compressive strength tests on the concrete specimens. Figure 17 shows the testing apparatus in the French laboratory.

Figure 17 - Three-Column Testing Machine (a), Digital Control System (b)

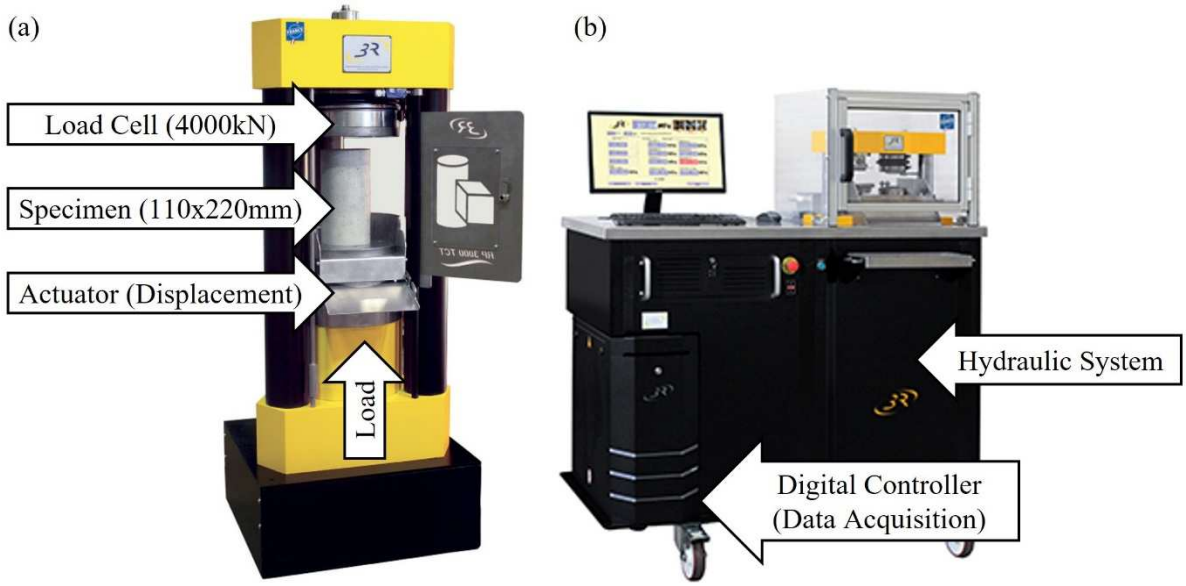

Source: Author (2023).

Secondly, it was used a Universal Testing Machine dynamic press (UTM-25), a servo-hydraulic equipped with a high-speed data acquisition system and real-time digital

control system, capable of measuring mechanical properties precisely under cyclic loading, with a maximum load capacity of 25 kN and displacement resolution of 0.1 μm.

This machine allowed for the accurate measurement of complex modulus and phase angle using a dynamic modulus analysis (DMA) testing routine, with the capability of applying sinusoidal loads up to a frequency of 100 Hz, facilitating the characterization of the viscoelastic behavior of cementitious materials, recording real-time data from stress and strain measures. This second testing set was meant for tensile strength tests and complex modulus assessment. Figure 18 presents the UTM-25 with the test apparatus in the Brazilian laboratory.

Figure 18 - Dynamic Press (a), testing set for Tensions and Compression (b) and LVDTs Assembly in detail (c)

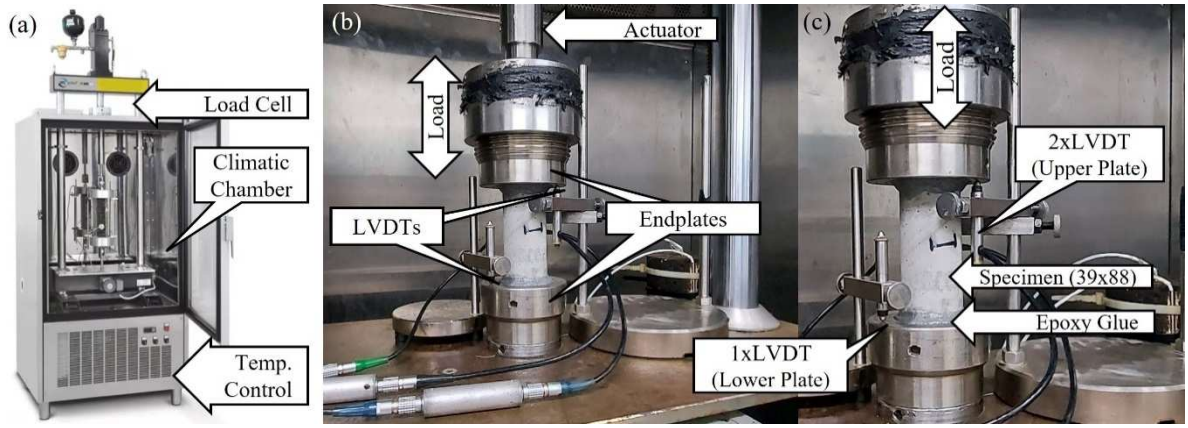

Source: Author (2023).

Concerning the connection between endplates and specimens, Figure 18c, both for compression and tension tests it was used a bicomponent epoxy structural adhesive to connect the upper and bottom endplates to the specimen surface. It was ensured to maintain a fine layer, by having a minimum applied load of 0.1 kN with the fresh glue positioned.

The positioning of the three Linear Variable Differential Transformers (LVDT) used to measure displacement was also modified. The first reading was taken at the bottom endplate to measure minor deformation throughout the tests, and the other two were in contact with the upper plate, to get their average position. The specimen deformation could then be assessed using Equation 17 and Equation 18, allowing for precise measurements of the specimens' strain response.

$$SpecimenStrain(t) = 1 - \frac{-P_1(t) + \frac{P_2(t)+P_3(t)}{2}}{InitialSpecimenHeight} \tag{17}$$

$$P(t) = CurrentPosition(t) - InitialPosition \tag{18}$$

The $P_i(t)$ variable represents the real-time position function of each LVDT recorded over the testing time, while the 'Initial Position' refers to the LVDTs' positions with a null load applied. The testing set was adapted to make possible the mechanical characterization through dynamic tests in the reduced specimens.

The precise deformation measurement was possible due to those modifications on the LVDTs' position and its position-capturing process as well. This new assembly has the potential to expand the testing possibilities being an innovative technique reducing the specimens' rupture loading, making feasible the use of smaller specimens and maintaining the ERV.

3.2.3 Complex Modulus Analysis (CMA): Concepts and Test Requirements

Cementitious materials can be considered complex viscoelastic materials whose mechanical properties are dependent on the complex modulus (Brinson; Brinson, 2008), which is a fundamental attribute to characterize responses to stress and deformation. The accurate determination of this parameter is critical for understanding the mechanical behavior and ensuring durability in practical applications (Brinson; Brinson, 2008; Evangelista Junior; Macedo; Farias, 2019).

Concrete and mortars have the ability to partially store and partially dissipate mechanical energy under cyclic loadings whereas the increase in this energy dissipation is a possible indicator of the degradation of the material (Kachkouch *et al*., 2022; Lee; Barr, 2004; Myrtja *et al*., 2021; Saucedo *et al*., 2013).

The phase angle, between other properties, is a direct measure of energy dissipation (Brinson; Brinson, 2008). Figure 19 demonstrates the modeling of a sinusoidal loading test and its corresponding strain response. By utilizing these modeling techniques, researchers can gain a better understanding of the viscoelastic behavior of concrete and optimize its mechanical properties for several applications, enhancing durability and performance.

Figure 19 - Complex Modulus Schematic (a) and Modeling in Time-Domain (b)

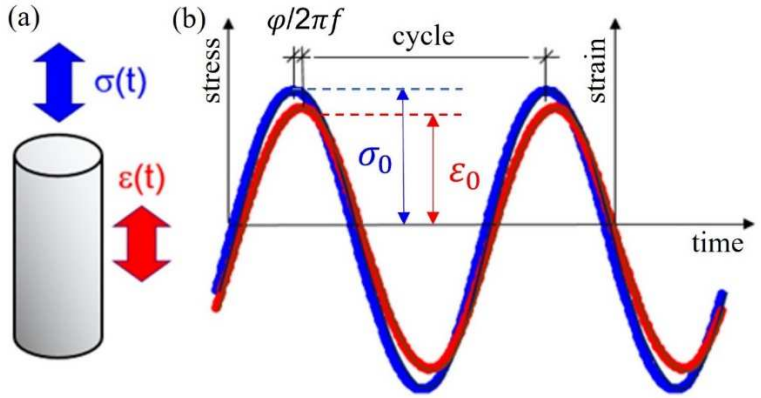

Source: Author (2023).

Figure 19a shows the stress applied to a specimen at a defined frequency (*f*) highlighted in blue, followed by its corresponding reading signal in Figure 19b (stress vs. time). Similarly, the red illustration portrays the strain response, specifically the axial strain, along with its respective readings (strain vs. time).

Equation 19 and Equation 20 describe the numerical function of the stress and strain signal, the time domain. Equation 21 presents the fundamental concept of the absolute value of complex modulus ($|E^*|$) and phase angle (φ), while Equation 22 provides the specific definitions for its components (the storage modulus and the loss modulus).

$$\sigma(t) = \sigma_0 sin\omega t \tag{19}$$

$$\varepsilon(t) = \varepsilon_0 \sin(\omega t - \varphi) \tag{20}$$

$$E^* = \frac{\sigma_0}{\varepsilon_0}[cos\varphi + i.sen\varphi] = E' + iE''; \qquad |E^*| = \sqrt{E'^2 + E''^2} \tag{21}$$

$$E' = |E^*|.cos\varphi; \quad E'' = |E^*|.sen\varphi \tag{22}$$

Whereas:

$\sigma(t)$ = stress function along the time; $\varepsilon(t)$ = strain function along the time;

σ_0 = stress amplitude, sinusoidal shape; ε_0 = strain amplitude, similarly;

φ = phase angle, the signals' delay; ω = angular velocity, with $\omega = 2.\pi.f$

f = loading frequency of the test, also named strain rate;

$|E^*|$ = absolute value of complex modulus;

E' = real part of complex modulus (storage modulus);

E'' = imaginary part (loss modulus).

The φ represents the angular lag between the stress and strain signals and is a fundamental characteristic of viscoelastic materials, which is closely related to the concept of

complex modulus. In the frequency domain, the complex modulus describes the behavior of the elastic modulus with respect to the strain and stress signals.

Equation 21 defines the relationship between the $|E^*|$, and their elastic and viscous component, the storage (E') and loss modulus (E") respectively. These equations have been extensively utilized in literature to model viscoelastic behavior. The $|E^*|$, also named dynamic modulus, is a measure of the material stiffness under dynamic loads. It is calculated from the real and imaginary parts of the complex modulus.

The real part, E', represents the material's ability to store energy elastically. The imaginary part, E'', corresponds to the material's characteristic to dissipate energy. It is important to note that despite being called the dynamic modulus, there are no inertial effects involved (Brinson; Brinson, 2008; Kuo; Zhuang, 2021; Saucedo *et al*., 2013).

Concerning the specifics of the CMA tests, the smaller specimens (39 mm × 88 mm) were fabricated to meet the reduced cylindrical geometry required to fit the maximum loading limitations of the servo-hydraulic universal testing machine (UTM-25), with a loading capability of 25 kN maximum.

For the experimental control, it was used of a dynamic mechanical analyzer controller (DMA) to record the load cell data and LVDTs' position under the loading conditions. The collected data was analyzed externally using an auditable interpolation routine to ensure the most accurate and precise results for the complex modulus ($|E^*|$ and φ).

To ensure the accuracy of the results, the interpolation routine utilizes more robust equations and numerical models to provide additional interpolation parameters and improve the fitting accuracy. This is particularly important since the tests may have imperfections in the loading control, strain records, testing assembly, and other factors that can potentially affect the accuracy of the results. Equation 23 and Equation 24 describe the mathematical functions used in those interpolation routines, while Equation 25 and Equation 26 demonstrate the calculation of the $|E^*|$ and φ results.

$$\sigma_{int}(t) = A_\sigma * \sin(\omega t) + \cos(\omega t) + C_\sigma * t + D_\sigma \tag{23}$$

$$\varepsilon_{int}(t) = A_\varepsilon * \sin(\omega t) + B_\varepsilon * \cos(\omega t) + C_\varepsilon * t + D_\varepsilon \tag{24}$$

$$|E^*| = \sum_{i=1}^{n} \frac{\sqrt{A_{\sigma i}^2 + B_{\sigma i}^2} \,/\, \sqrt{A_{\varepsilon i}^2 + B_{\varepsilon i}^2}}{n} \tag{25}$$

$$\varphi = \sum_{i=1}^{n} \frac{tan^{-1}\left(A_{\varepsilon i}/B_{\varepsilon i}\right) - tan^{-1}\left(A_{\sigma i}/B_{\sigma i}\right)}{n} \quad (26)$$

Whereas:

$\sigma_{int}(t)$ = stress interpolation function in the time domain;

$\varepsilon_{int}(t)$ = strain interpolation function in the time domain;

ω = angular velocity, in the frequency domain;

$|E^*|$ = absolute value of complex modulus;

φ = phase angle, the signals' delay;

n = number of cycles per sweep, for average;

A_σ and A_ε = in-phase amplitudes, for stress and strain;

B_σ and B_ε = out-of-phase amplitudes, for stress and strain;

C_σ and C_ε = linear component resulting from drift or damage;

D_σ and D_ε = stress and strain offset (mean values).

These definitions are widely used in literature, especially concerning signal processing and analysis (Brinson; Brinson, 2008; Evangelista Junior; Macedo; Farias, 2019). The CMA testing was conducted with loading control and sinusoidal loading shape, in agreement with the literature on this subject (Kachkouch *et al.,* 2022; Myrtja *et al*., 2021; Saucedo *et al*., 2013). A range of frequencies was assessed, varying from 0.1 up to 25 Hz.

The chosen frequency range encompassed both low and mid-frequency ranges, avoiding potential dynamic effects (frequencies higher than 25 Hz), as recommended by ASTM E1876 (ASTM, 2022). A careful selection of the frequency range is crucial to obtain reliable and accurate results for the viscoelastic characterization. Additional testing parameters are presented in Table 11.

Table 11 - CMA Testing Parameters

Characteristics	**Pure Compression**	**Pure Tension**
Frequencies (Hz)	0.1, 0.5, 1, 5, 10, 15, 20, 25	0.1, 0.5, 1, 5, 10, 15, 20, 25
Max Stress (kPa)	3000 (10% f_{ck})	0
Min Stress (kPa)	0	-300 (10% f_{yk})

Source: Author (2023).

The f_{ck} is the characteristic compressive strength for cylinder specimens and f_{yk} is the equivalent parameter for tensile strength, according to EN1992-1-1 (EUROCODE, 2004). The low-frequency range investigates the viscoelastic behavior under slow

deformations, usually implying a more pronounced viscous behavior, with more dissipation of mechanical energy. At the mid-range frequencies, the materials usually demonstrate behaviors closer to elasticity, with a reduction of φ and higher levels of $|E^*|$.

The frequency range selected for CMA is crucial for the accurate characterization, as it determines the degree of deformation, once the frequency range can have a significant impact on the complex modulus, especially concerning their phase angles (Brinson; Brinson, 2008; Evangelista Junior; Macedo; Farias, 2019; Kachkouch *et al*., 2022; Lee; Barr, 2004; Myrtja *et al*., 2021).

3.3 Results and Discussion

In sections 3.3.1 and 3.3.2, it is presented the results of the compressive and tensile strength of the concretes and mortars evaluated, discussing their findings in detail. Section 3.3.3 presents the results of the CMA characterization with insights into viscoelastic.

3.3.1 Compressive Strength results for Concrete formulations

The compressive strength results for 28 and 90 days are presented in Figure 20. Those results show the impact of the proposed formulation on that mechanical property.

Figure 20 - Compressive Strength results for 28 and 90 days

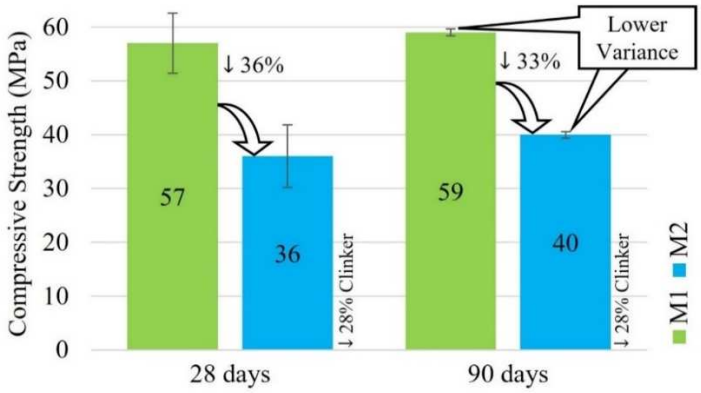

Source: Author (2023).

The proposed cement formulation with SF and GP demonstrated a significant effect on the compressive strength. M1 exhibited higher results at both 28 and 90 days. The standard deviations for both results were within an acceptable range, indicating consistency in the evaluation with lower variances at 90 days, with improved homogeneity.

The lower compressive strength of M2 was attributed to the 33.25% replacement of the clinker content, 35% on the total cement content, by GP (30%) and SF (5%), having a

dilution effect on the strength. It is noteworthy that the optimization aimed to improve the stiffness behavior and strain response, not necessarily the strength levels, being the case.

The assessment of the compressive strength is a crucial methodological parameter for the CMA tests. Despite the reduction observed, the focus remains on understanding the alteration in the viscoelastic behavior, with insight into fatigue behavior. It is noteworthy that the application of the M2 formulation remained suitable for the same purposes. Mix design techniques offer the potential to bring strength levels back to similar levels.

For the last, it is noteworthy that the strength increase from 28 to 90 days was more pronounced for the M2, with a 36% and 33% divergence respectively, which is attributed to the GP addition, reported by the literature as having a long-term effect (Baikerikar; Mudalgi; Ram, 2023; Fattouh; Elsayed, 2023; Keerio *et al*., 2022).

Therefore, the GP incorporation can still be considered suitable OPC replacement, leading to improved mechanical behavior and durability in the long term, having M2 a higher compressive strength increase (11.00%) compared to M1 (3.50%) from 28 to 90 days.

Several authors investigated the effect of GP on cementitious materials. It can lead to higher compressive strength and durability, reduced water absorption, lower chloride penetration and lower potential of carbonation, having significant effects even after 365 days.

It was found that its addition can result in improved resistance to chemical attacks, higher frost and thaw cycles fatigue resistance and lower potential of alkali-silica reactions (ASR), which are common causes of pathologies in structures and cementitious materials (Jain; Sancheti; Gupta, 2020; Schwarz; Cam; Neithalath, 2008).

The review also highlighted that the use of GP in concrete can contribute to more sustainable solutions, by reducing the waste disposal from glass manufacturing and decreasing the GHGe of the industry (Baikerikar; Mudalgi; Ram, 2023; Bharathi; Adari; Pallepamula, 2022; Boukhelf *et al*., 2023).

Furthermore, a synergic use of SF and GP has been shown to improve the resistance to pathological manifestations, such as sulfate attack, ASR and chloride penetration (Boukhelf *et al.,* 2021; Fattouh; Elsayed, 2023; Fu *et al*., 2021; Keerio *et al*., 2022), beyond the widely recognized improvements of the SF additions.

Thus, a comprehensive evaluation of the durability and resistance to pathological manifestations of M2 is necessary, to further the compressive strength. Despite the notable decrease in this parameter, with reductions of 36% and 33% for 28 and 90 days, respectively, it remains suitable for the same applications of M1. This is evident when considering the possibility of further assessing these mix designs to achieve similar strength levels.

3.3.2 Splitting Tensile Strength results of Mortars formulations

Figure 21 displays the results of the splitting tensile on mortar specimens at 90 days. The statistical analysis is also presented by the respective boxplots.

Figure 21 - Tensile Strength for 90 days (a) with boxplots for M1 (b) and M2 (c)

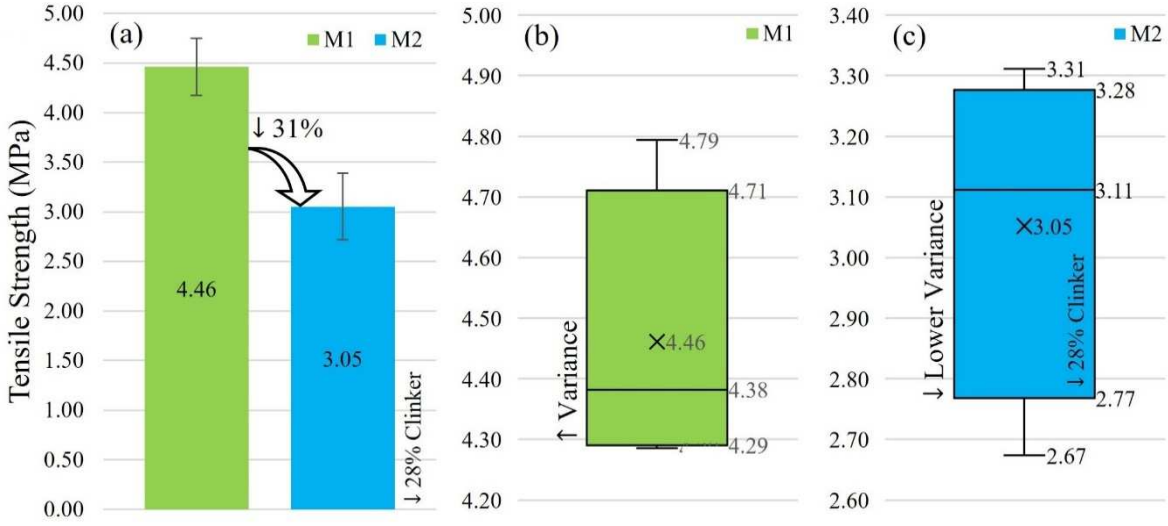

Source: Author (2023).

Similar to compression, in pure tension it was achieved proportional strength levels, concerning the effect of the clinker replacement. M1 exhibited higher results, followed by an average reduction of 31% for M2, noteworthy being a lower decrease compared to the reductions in compressive strength (36% and 33%).

The standard deviation for both formulations was within an acceptable range, indicating the tests' consistency. M2 presented a lower standard error, as visualized in Figure 21c, with narrow boxplot boundaries, indicating a more homogeneous material.

It is reported by literature a correlation between both parameters (compressive and tensile strength), ranging from 8% to 12%. The results visualized were consistent with this relationship, with M2 showing a higher proportion (8.47%) compared to M1 (7.81%). Furthermore, as discussed previously, the proposed formulation and the current main objective aimed to improve the stiffness behavior, not necessarily the strength levels.

3.3.3 Results for the Complex Modulus Characterization

3.3.3.1 Complex Modulus for Pure Compression (Compressive Stresses)

Figure 22 presents the results for the $|E^*|$ with its respective φ in pure compression. These are the average of the low (0.1 to 1 Hz) and mid-range (1 to 25 Hz) frequencies.

Figure 22 - Average $|E^*|$ (a) and φ (b) in pure compression in the frequency ranges

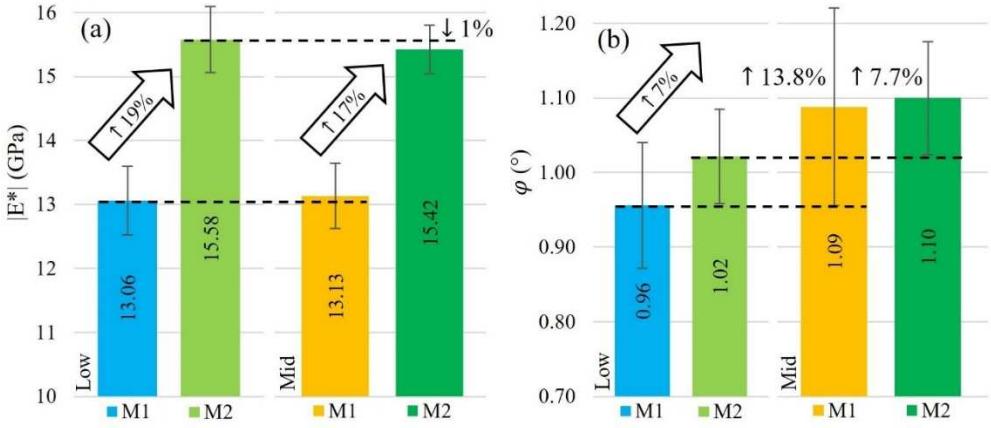

Source: Author (2023).

Regarding $|E^*|$, Figure 22a shows that M2 had a higher average compared to M1 consistently. Specifically, there was an 18% increase in $|E^*|$ and a 7% increase in φ comparing formulations. These findings suggest that the proposed formulation resulted a in stiffer material, which is a desirable outcome. A higher $|E^*|$ is considered advantageous on the material's durability and resistance to pathological manifestations (Chu *et al*., 2022b, 2023a; Liang *et al*., 2022b), being an indicative of the improved durability.

Assessing the $|E^*|$ variance, the M2 formulation exhibited a higher absolute standard error (0.52 GPa), compared to M1 (0.45 GPa), with a lower percentual deviation of 2.86% and 4.01% respectively. This implies that despite its absolute deviation, M2 had a higher homogeneity, being an influence of the proposed formulation, resulting in more consistent and homogeneous material. These findings comply with the literature on GP and SF addition assessing mechanical properties and durability (Baikerikar; Mudalgi; Ram, 2023; Fattouh; Elsayed, 2023; Jain; Sancheti; Gupta, 2020).

Regarding φ, M2 showed a more pronounced increase in the low-frequency range, suggesting a more energy-absorbing behavior, tending to dissipate more energy than lower φ in low frequencies (< 1 Hz), by 7%. The increase in stiffness observed in M2 is attributed to the optimization proposed, which is known to improve the strength and stiffness when added in appropriate proportions.

The alteration in the φ at low frequencies is aligned with the literature (Bažant; Jirásek, 2018; Mechtcherine; Slowik; Kabele, 2018) and it was more pronounced for the M2 formulation. It indicates that beyond the alterations in the φ average, the proposed formulation had impacts on the viscoelastic behavior of the composites.

These findings have important implications and future research may explore further enhancement in the formulations to achieve the desired balance between strength levels, stiffness and viscoelastic behavior, aligned with durability and resistance to pathological manifestations (Jain; Sancheti; Gupta, 2020; Schwarz; Cam; Neithalath, 2008). Figure 23 presents the $|E^*|$ results with its respective φ, in the frequency domain.

Figure 23 - Individual $|E^*|$ and φ in pure compression in the frequency domain

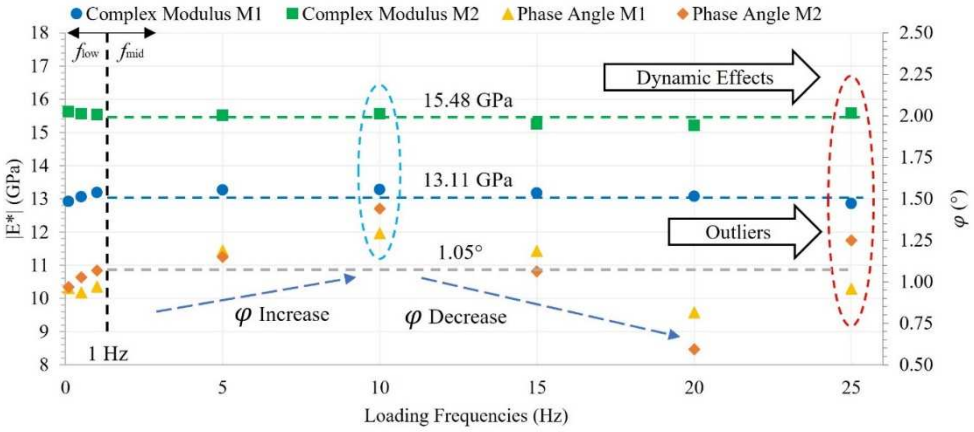

Source: Author (2023).

The complex modulus results in the frequency domain demonstrated that the proposed formulation, M2, exhibited a consistently higher $|E^*|$ across all sweep frequencies, with an average value of 15.48 GPa, with no convergence in those confidence intervals. This finding indicates that M2 has a higher stiffness, with the potential to improve durability and resistance to pathological manifestations such as cracking and modulus degradation (Kuo; Zhuang, 2021; Myrtja *et al.,* 2021).

There was an uptrend tendency in the low frequencies for M1$|E^*|$ results which is in agreement with the literature, with an increase in the concrete stiffness, closer to elasticity, as the frequency increases (Chen *et al*., 2022; Medeiros *et al*., 2015). However, for M2 it was divergent, with a downtrend in low-frequencies.

Upon analysis of the φ results, it was observed that M1 and M2 had similar readings with no significant difference, being feasible to represent them by an average of 1.05°. No statistical difference was found by ANOVA, comparing both φ series, even with a significance level of 99%.

Additionally, it was found that the loading frequency achieved a less pronounced peak in the φ for 10 Hz followed by the higher values of $|E^*|$. The φ is a direct function of the loss modulus whereas the higher results indicate a greater ability to dissipate energy, as presented by Equation 22. The M2 φ were mostly higher than M1, which suggests a less

pronounced improved ability to dissipate energy. These findings were consistent with literature findings (Fattouh; Elsayed, 2023), however, it should be taken caution, once there were no statistical divergences, as highlighted by the ANOVA results.

The increasing $|E^*|$ with frequency up to 1-10 Hz followed by a plateau, is a behavior reported by the literature on viscoelastic materials. It is explained by the alignment in the microstructure, where further changes in frequency do not significantly affect these properties (Chen *et al.*, 2022; Medeiros *et al.*, 2015; Sanahuja; Dormieux; Chanvillard, 2007), having a more ordered microstructure with the frequency increases.

Furthermore, it is noteworthy that there was variability in the results, as indicated by the standard deviations. This variability is attributed to several factors (measurement error, heterogeneity in the material and further experimental aspects) remaining feasible for improvements and further investigations.

Overall, these results suggest that the proposed formulation with OPC replacement led to improvements in the mechanical properties of M2. These improvements were frequency-dependent. For the last, at 10 Hz it was a less pronounced peak in both parameters and both formulations, indicating a greater energy dissipation ability (Jia *et al.*, 2021; Lee; Barr, 2004; Myrtja *et al.*, 2021).

3.3.3.2 Complex Modulus for Pure Tension (Tensile Stresses)

Figure 24 presents the results for $|E^*|$ with its respective φ for pure tension. The presented values correspond to the average of the different sweep frequencies, for low (0.1 - 1 Hz) and mid-ranges (1 - 25 Hz).

Figure 24 - Average of $|E^*|$ (a) and φ (b) in pure tension in the frequency ranges

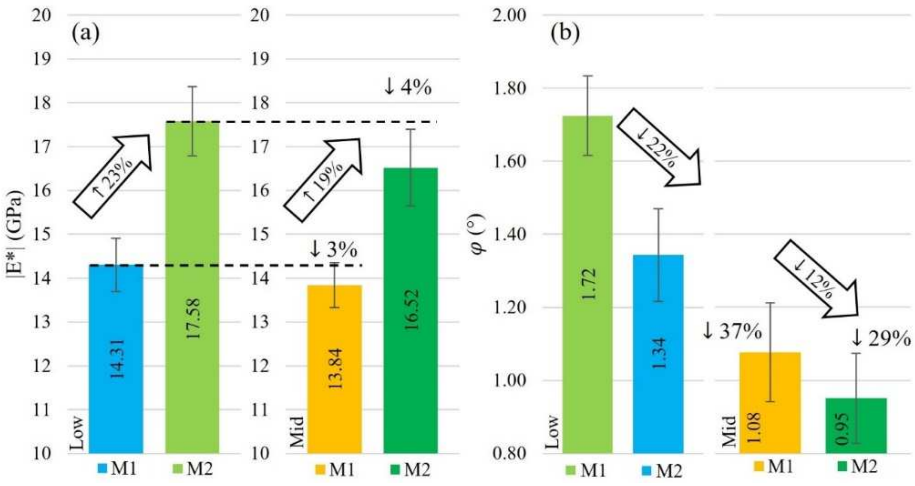

Source: Author (2023).

By comparing these averages, the $|E^*|$ of M2 was consistently higher (16.92 GPa) than M1 (14.01 GPa), similarly for compression results but with a larger difference. This stiffer material, even for tensile stress, can improve durability and reduce the susceptibility to pathological manifestations such as cracking. Furthermore, by comparing the variability of the results, M2 standard error (1.11 GPa / 6.3%) was higher than M1 (0.58 GPa / 4.09%). This can be possibly attributed to test alterations and misreading, not necessarily a higher variance of the material in pure tension, diverging from the higher uniformity so far.

The φ results exhibited a statistical divergence by the ANOVA test, indicating an influence of the formulation on those results. M1's average was 1.32° while M2's was 1.10°. This lower φ for M2 indicates that it is less prone to energy dissipation compared to M1 which has a behavior closer to elasticity, with insights into improved durability (Bažant; Jirásek, 2018; Mechtcherine; Slowik; Kabele, 2018).

The standard deviation for M2 (0.329°) was lower than M1 (0.355°), suggesting a more consistent and homogeneous behavior. Finally, the higher $|E^*|$ and lower φ of M2 could indicate a superior behavior of the M2 formulation in pure tension. Higher $|E^*|$ indicates a superior ability to resist mechanical loads with lower deformations or strains, The lower φ indicates a material with closer behavior to the elasticity, with low energy dissipation. This is highlighted by literature as an expected outcome in terms of improved durability of cementitious materials (Adil; Kevern; Mann, 2020; Bažant, 1970; Castro; Brito, 2013).

This behavior should be further assessed in order to assess its implications on durability and fatigue behavior once it contrasts with the compressive results. Figure 25 presents the individual results in the frequency domain.

Figure 25 - Individual $|E^*|$ and φ in pure tension in the frequency domain

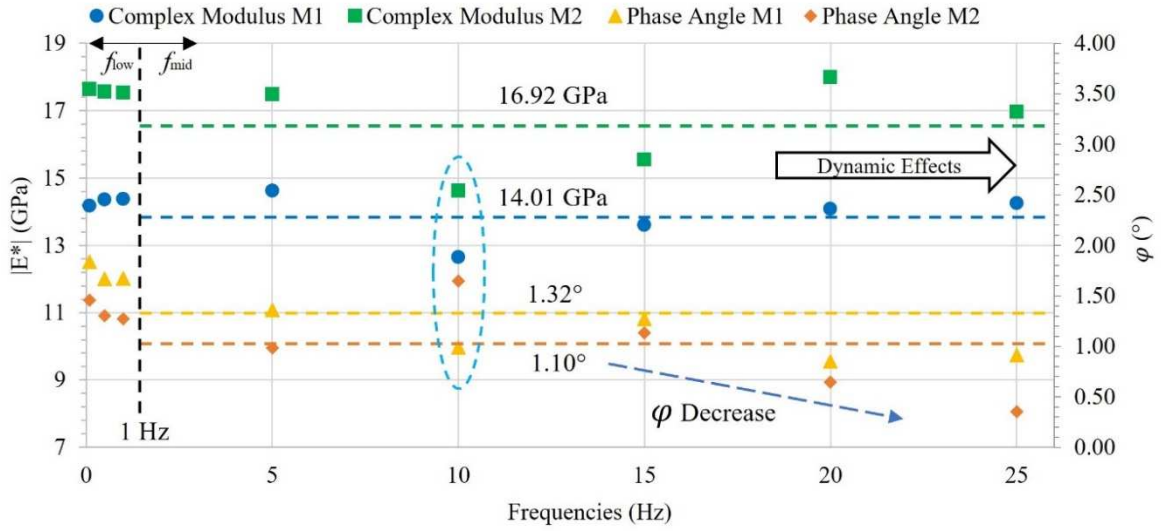

Source: Author (2023).

Similar to the previous results, M2 exhibited a consistently higher $|E^*|$ compared to M1 across all sweeping frequencies, and the 10 Hz frequency presented the lowest $|E^*|$ and highest φ. The results of $|E^*|$ showed a not clear trend within the frequency, varying around the average. The M2 average φ presented a more elastic behavior in pure tension compared to M1, with mostly lower values. It provides insights into the importance of understanding the materials' behavior under dynamic conditions, as it can impact their performance.

It was also observed that the φ increased with decreasing frequency for a low range, diverging from the previous results obtained for pure compression. This is more aligned with the expected behavior reported by the literature (Brinson; Brinson, 2008).

Also, it is suggested that mechanical behavior is dependent on the loading applied and the loading frequency is an important aspect of the resulting mechanical properties (Bažant, 1970; Bažant; Jirásek, 2018). The gradual increase in $|E^*|$ and decrease in φ after 10 Hz is consistent with similar mechanical behavior in pure compression, by the plateau effect reported by the literature (Chen *et al*., 2022; Sanahuja; Dormieux; Chanvillard, 2007).

The elevated variance in both results ($|E^*|$ and φ) indicates a significant variability in the results for pure tension. This variability can occur due to several factors, including variations in the specimens' strength levels, environmental and temperature conditions and eventually measurement errors.

The overall trends in the results are consistent with the expected behavior of viscoelastic materials, and it was found the $|E^*|$ and φ parameters are dependent on the frequency and temperature, as shown in previous studies on viscoelastic materials (Brinson; Brinson, 2008; Evangelista Junior; Macedo; Farias, 2019).

Furthermore, for pure tension results demonstrate that M1 exhibited a behavior closer to viscosity, while M2 showed a more elastic response, by comparing the average parameters of complex modulus. Both aspects imply fatigue behavior and durability. The findings of this paper were aligned with the literature for the importance of understanding the mechanical behavior of viscoelastic materials, at different frequencies and temperatures (Boukhelf *et al*., 2021; Fattouh; Elsayed, 2023; Jain; Sancheti; Gupta, 2020; Kachkouch *et al*., 2022; Medeiros *et al*., 2015; Myrtja *et al*., 2021).

Moreover, these results offer valuable insights into the viscoelastic behavior and complex modulus of cementitious materials. It can be beneficial for structural design and the development of more enhanced and stable materials, also with insight into durability and sustainability. This knowledge is particularly valuable in applications where increased stiffness and improved durability are desired, resisting cyclic loadings over time (context of

aerogenerators and pavement infrastructures). Additionally, the experimental insights and reliable data obtained can aid in accurate modeling and analysis.

3.4 Final Comments

This paper aimed to assess the impact of a proposed cement formulation on the dynamic stiffness behavior evaluating the complex modulus. The optimized binder was composed also of OPC, having additions of silica fume (SF) and glass powder (GP) as SCMs, aiming to enhance stiffness and durability. The binders were tested both in concretes and mortars using the same mix design derived from an in-site aerogenerator foundation. Also, it was proposed an adjusted method for complex modulus characterization of cementitious materials.

The results obtained demonstrate that the proposed cement formulation had a positive effect on the composites' mechanical properties compared to a regular OPC. In the static tests, it was observed that although there was a decrease in strength due to a reduction in clinker content, this effect was less significant for longer ages, specifically at 90 days (due to the GP long-term hydration effect). Nonetheless, all results for compressive and tensile strength remain suitable for structural applications.

The complex modulus showed M2 as a consistently stiffer material with an increase in the energy dissipation ability for compression and a decrease in tension. Also, it was presented a comprehensive overview of its implications on durability, pathological manifestation resistance and even fatigue life.

Indeed, the proposed characterization method and the materials characterization results (complex modulus) achieved experimental outcomes consistent with the literature. These findings have valuable insight for applications that require strain hardening, durability enhancement and fatigue resistance. The conclusions can be summarized as follows:

- The compressive and splitting tensile strengths decreased by an average of 33% and 31%, directly attributed to the OPC replacement (30% GP and 5% SF) and consequently to the clinker reduction (33.68% replacement). However, the proposed cement formulation achieved relevant strength levels, making it feasible to assess the mix design parameters to achieve similar strength levels for further formulations;
- By characterizing the $|E^*|$ and φ of M1 and M2, under pure compressive and tensile stresses, it was demonstrated that these materials can exhibit distinct results within frequencies, demonstrating a frequency-dependent behavior and depending on the loading regime.

These insights are crucial for developing more resistant and durable materials, on structural applications, and for further assessments and developments on the degradation mechanisms;

- The proposed formulation resulted in a higher $|E^*|$ for M2, stiffer than M1. It was also demonstrated that a higher $|E^*|$ is considered beneficial for improving the material's durability concerning its mechanical behavior;
- Aside from the modulus increase, the optimized formulation (M2) demonstrated a mostly higher φ in pure compression, implicating a higher loss modulus (more viscoelastic behavior), which is not a usual behavior in literature for improved durability. However, the results for pure tension were consistently lower, indicating a behavior closer to elasticity, addressing improved durability as well;
- The SCMs' addition proved to have a major effect on the mechanical response. It was seen an up to 37% variation in the complex modulus for the same loading regimes between the assessed materials (M1 and M2), with a 23% modulus increase of M2 in compression with lower φ in pure tension, with implications on durability.

These findings provided valuable insights into the modeling, design and engineering of concrete structures, as well as for the understanding and prediction of mechanical behavior and durability over time. The M2 binder, applied in mortar, showed better performance, with improved stiffness and durability. Also, with a focus on fatigue behavior, may indicate a possible improved performance in that same aspect. The complex modulus of M2 was consistently higher than M1 across all sweep frequencies and loading regimes, indicating that the optimization has resulted in a more stable and predictable stiffer material.

As a final contribution, to fully understanding the relationship between mechanical behavior and durability, further research may lead to further insights. For this, it is suggested research with a focus on (i) fatigue testing, to supplement the modulus characterization and to quantify degradation over time, (ii) modulus characterization over different loadings amplitudes (stress levels) and temperatures, providing insights into different stress levels and freeze-thaw cycles throughout years and seasons, for long-term effects, and (iii) durability tests, to substantiate the current claims of improved resistance to pathological manifestations. This future research can provide a more holistic assessment of the long-term structural performance and can help guide the development of materials with tailored properties while accounting for sustainability.

4 INFLUENCE OF MICROSTRUCTURE AND SCMs ON STIFFNESS AND TENSILE FATIGUE BEHAVIOR OF CEMENTITIOUS MATERIALS

The main content of this chapter is planned for submission to the International Journal of Fatigue.

ABSTRACT

Fatigue of cementitious materials is an ongoing research topic in engineering and construction, aiming at optimizing their performance and durability. The current paper addresses three research gaps identified through a bibliometric analysis of 31,198 papers and 89,059 patents worldwide. These gaps concern (i) the influence of the supplementary cementitious materials (SCMs), (ii) the influence of microstructural aspects on quasi-static and fatigue behavior, and (iii) fatigue investigations under pure tension loads. This paper aims to investigate the influence of the microstructure and supplementary cementitious materials on the stiffness and tensile fatigue behavior of cementitious materials. A fatigue-enhanced cement formulation was proposed and resulted in several microstructural improvements, with lower heat of hydration (by 32.15%), enhanced pore structure (with 43.42% lower diameters), and reduced porosity (up to 61.36%). Mechanical investigation revealed no significant variance in the modulus of elasticity (under tensile static loading), but there was a significant difference in the absolute value of the complex modulus (under quasi-static sinusoidal loading), up to 24.64% improvement. Lastly, concerning the fatigue experiments, the proposed formulation led to improved fatigue resistance, with a 19.80% higher endurance limit. The fatigue results were compared to standard codes involving fatigue of concrete structures, specifically the DNV (Norwegian), and EC2 and CEB-FIP (both Europeans). However, only the proposed formulation met the minimum criterion on them. The investigation demonstrated that a more in-depth fatigue analysis can be addressed by accounting for the microstructural parameters that impact fatigue. These findings contribute to the development of materials with improved fatigue-resistance and stiffness response. Those are capable of withstanding higher stress levels during cyclic load while contributing to sustainability.

Keywords: fatigue behavior; microstructure; cement; supplementary cementitious materials pure tension.

4.1 Introduction

Fatigue of cementitious materials is a mechanical degradation phenomenon characterized by a reduction in load-bearing capacity and loss of modulus of elasticity when subjected to cyclic loads, corrosion, and thermal fatigue, accumulating damage within time. It may happen on rendering facades mortars, concrete structural elements, such as aerogenerators' towers and foundations, pavements and bridges, and structural elements subjected to varying loads in general (Balbo *et al*., 2021; Kachkouch *et al*., 2022; Myrtja *et al*., 2021). These cyclic loads can encompass compression, tension, torsion, bending, or a combination of these stresses. The material experiences internal damage that gradually diminishes its load-bearing capability and modulus of elasticity, leading to structural failure or collapse (Huang *et al*., 2016).

The increased use of high-strength concretes in lightweight structures has highlighted the importance of addressing fatigue. Variable loads now constitute a more substantial proportion of the structural load distribution (Vicente *et al*., 2016). Structures like aerogenerators are subjected to a wide range of cyclic loads, with different frequencies and stress levels.

Enhancing the stiffness properties can potentially improve fatigue resistance and extend durability. Several factors, including stress levels, loading frequencies, admixtures, and fibers, can influence the strain response of those materials (Kachkouch *et al*., 2022; Oneschkow, 2016; Zhao; Chang; Yang, 2008). An understanding of these mechanisms is crucial for improving performance (Parant; Rossi; Boulay, 2007).

In recent years, there has been an increase in interest in the field of fatigue of cementitious materials, reflecting its recognized significance and the need for more durable and resistant structures (Jain; Sancheti; Gupta, 2020; Kachkouch *et al*., 2022; Wang; Duan; Zhu, 2021). This heightened attention is driven by the challenges faced by structures subjected to cyclic loads (bridges, pavements and wind turbines). As these structures increasingly require durable and environmentally friendly materials, the interest has grown stronger.

Before further detail, it is worth noting that despite its uptrend interest, several gaps remain to be further addressed. To overview this scenario, it was performed a systematic literature review (SLR) of the current state-of-the-art research over articles and patents (Cambia, 2023). Table 12 presents a database query designed for the current SLR research.

Table 12 – Design of the SLR query for the current research topic

Mandatory Words	Excluded Words	Excluded Fields
(Fatigue OR Modulus of Elasticity) AND (Cement OR Paste OR Grout OR Mortar OR Concrete)	Asphalt, Macadam, Bituminous, Soil, Geopolymer, Alkali-Activated	Mathematics, Biology, Thermodynamics, Physics, Bone cement, Dentistry, Mineralogy, Polymer, Geology, Metallurgy, Medicine, Geotechnics

Source: Autor (2023).

The results yielded 31,198 papers and 89,059 patents collected worldwide. Notably, there was a more pronounced increase in article publishing around 2010, with a decrease after 2020, probably influenced by the COVID pandemic that hindered the ability to produce experimental data in labs. China, the U.S., and the U.K. emerged as the top contributors by country. The provided data underscores the sustained interest and investment in this research field.

Figure **26** provides insights by presenting this document counts over the years, from 1950 to 2023. This visual representation of the data can help in understanding the evolution of research and the geographic distribution in the field of fatigue of cementitious materials.

Figur□26 – Arti□l□s and pat□nts □ounting ov□r th□y□ars (a) and worldwid□ distribution (b) from th□do□um□nts qu□ry

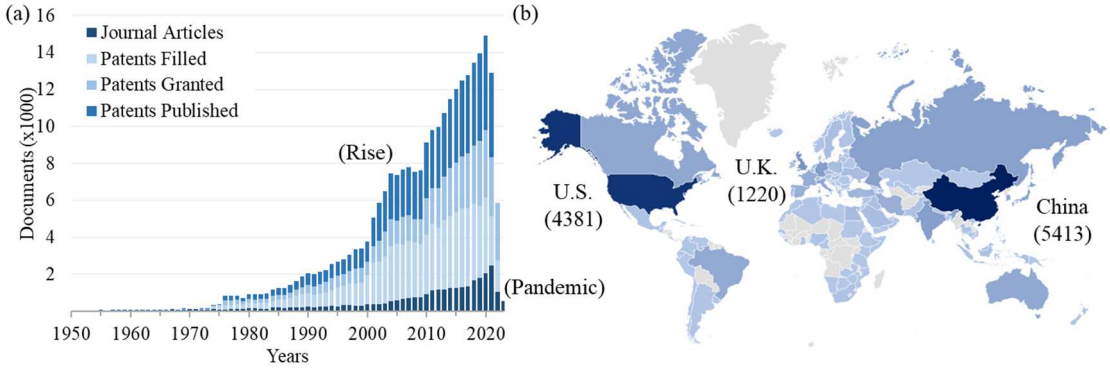

Sour□: Author (2023).

Recent research topics have shifted towards optimization strategies and the application of this knowledge in more resistant and durable materials (Abdelli; Mokrani; Kennouche, 2021; Jain; Sancheti; Gupta, 2020; Wang; Duan; Zhu, 2021). The usual experimental programs on fatigue behavior handle the strain evolution and the number of cycles to failure (*Nf*) for continuous stress sinusoidal loading repetitions (Hümme *et al*., 2016; Kachkouch *et al*., 2022; Liang; Li, 2015; Viswanath; Lafave; Kuchma, 2021).

The investigations on the fatigue behavior of cementitious focus on the understanding of their degradation mechanisms and the material stress-strain response under repeated loads. Also, it provides a further understanding of parameters to improve their resistance under cyclic loads (Hümme *et al*., 2016; Kachkouch *et al*., 2022; Liang; Li, 2015; Vicente *et al*., 2016;

Viswanath; Lafave; Kuchma, 2021). The SLR results underwent a bibliometric analysis. The results and two visual plots are presented in Figure 27 organized by thematic clusters (keywords and groups of keywords, Figure 27a) and by chronological evolution (with the colors indicating the time scale, Figure 27b).

Figure 27 - Sub-themes network clusters (a) with their chronological evolution (b)

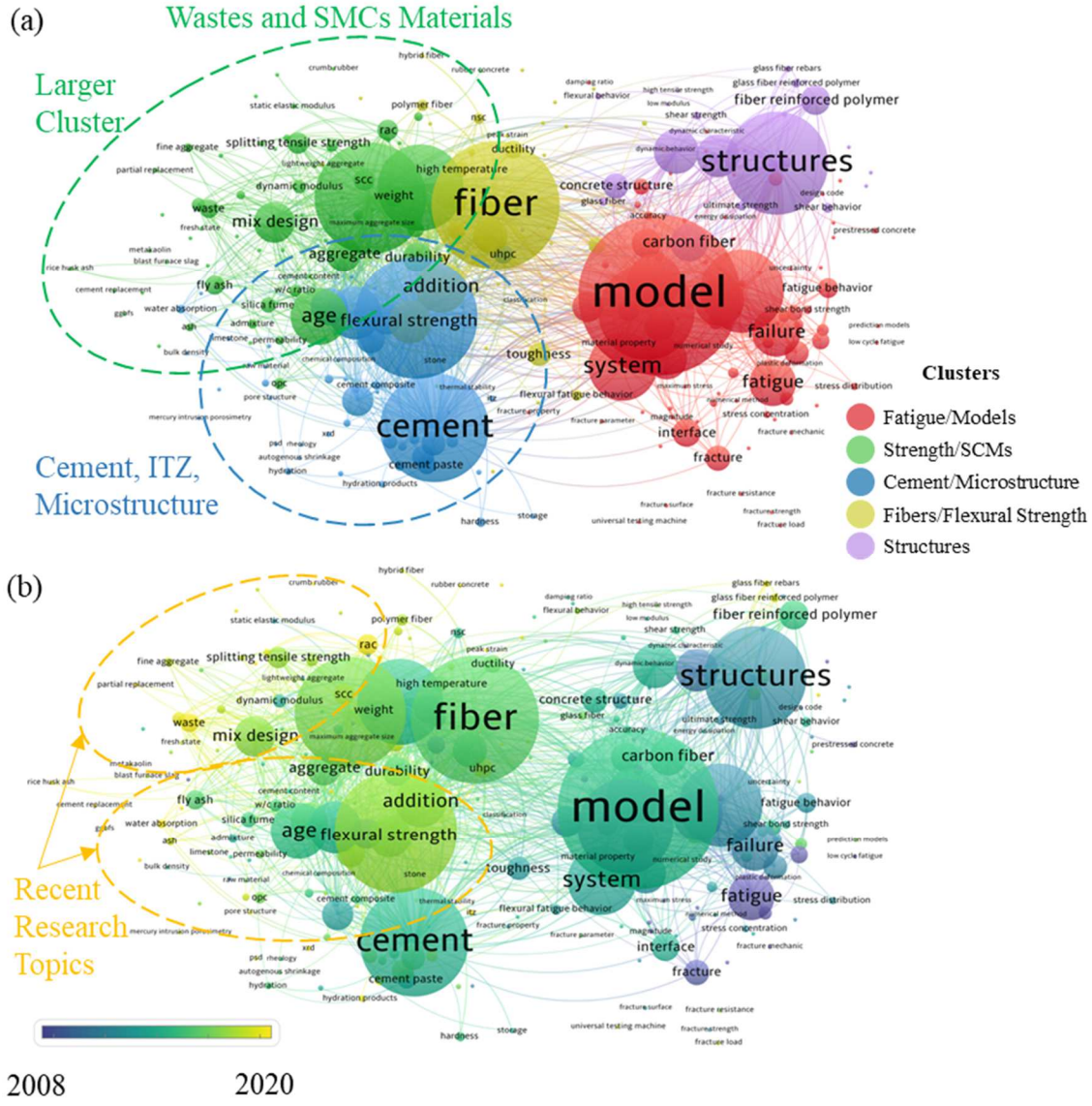

Source: Author (2023).

Upon examination, it is possible to identify gaps that need addressing. The cluster of characteristic strengths addressed SCMs such as fly ash, metakaolin, and slags. However, there were no connections with other clusters, particularly with fatigue (red cluster). Such observation indicates that it is still poorly known what effects SCMs have on fatigue of concrete.

Secondly, the cement cluster addressed microstructural aspects such as particle size, porosity, morphology, ITZ, and nanomaterials in the most recent trend (Chaudhary; Sinha,

2020; Fattouh; Elsayed, 2023; Uzbas; Aydin, 2020). These factors impact cement hydration and strength development, possibly enhancing mechanical properties. Exploring the interplay between those can be strategic for the development of the field.

SCMs offer the potential to partially replace ordinary Portland cement (OPC), creating more sustainable solutions with reduced carbon emissions. The literature highlights different suitable materials for enhancing properties. When integrated and accounting for fatigue, these materials have the potential to offer solutions for enhancing resistance and improving durability (Abdelli; Mokrani; Kennouche, 2021; Jain; Sancheti; Gupta, 2020; Kachkouch *et al*., 2022; Vicente *et al*., 2016).

Silica fume (SF) is recognized as an effective SCM, improving mechanical, microstructural, and durability properties (Adil; Kevern; Mann, 2020; Chaudhary; Sinha, 2020; Ni *et al*., 2021; Singh; Mehta; Kumar, 2023; Tripathi *et al*., 2020). However, its effect specifically on fatigue has not been thoroughly investigated. Given its ability to enhance the ITZ and reduce crack formation, it is plausible to hypothesize that SF positively effects the fatigue resistance of cementitious materials (Kachkouch *et al*., 2022). The SF addition enhances the ability to restrain damage (Ozaki; Sugata, 1992), resulting in better mechanical performance, which is also expected in fatigue resistance (Yan; Sun; Chen, 1999). It improves the ITZ, by reducing the cracks' incidence and their size (Boukhelf *et al*., 2021; Chung, 2002; Liu *et al*., 2023b).

Glass powder (GP) is also a potential SCM that has not been extensively investigated, especially concerning fatigue. The literature demonstrates several positive effects on strength, porosity, workability, and modulus of elasticity (Boukhelf *et al*., 2023; Chang *et al*., 2015; Kalakada; Doh; Zi, 2020; Omran *et al*., 2017; Pappa *et al*., 2018). These aspects are highly related to fatigue, but there is still not enough evidence on that.

Lastly, several studies have examined the fatigue behavior of concrete under compressive, bending, or flexural loading conditions (Kachkouch *et al*., 2022; Myrtja *et al*., 2021; Oneschkow, 2016). However, there remains a scarcity of contributions focusing on other loading regimes, such as pure tensile or torsional/shear loadings. This understanding is crucial for generating accurate design models and predicting service life.

The current paper aims to investigate the influence of the microstructure and SCMs on the stiffness and tensile fatigue behavior of cementitious materials, with a special focus on GP and SF as SCM additions. The proposed cement formulation derives from Chapter 3 (Targino *et al*., 2023), having the same comparison with regular OPC, in this case, CEM I. In this chapter, these same formulations were subjected to further analyses and mechanically tested over a longer period, from 90 to 120 days. Those were applied to concretes, grouts, and

paste, depending on the tests and analyses addressed. The outcomes hold the potential to drive the development of more fatigue-resistant, durable, and sustainable materials, especially for those exposed to cyclic loads.

4.2 Methodological Procedure - Part III

The experimental program was divided into four sections: (i) analysis of the microstructure and physical aspects, (ii) compressive and tensile strength tests, (iii) quasi-static characterization, and (iv) data analysis and software development. The first three sections involve experimental procedures and materials characterization, and the fourth is dedicated to data analysis and software development for data processing complex modulus and fatigue test results.

In section 4.2.1, the focus was the influence of microstructure and physical parameters on fatigue, providing additional analysis beyond the usual mechanical parameters. These investigations aimed to provide an understanding of these influences on fatigue.

Section 4.2.2. aimed to characterize the static mechanical properties, including compressive and tensile strength, with the determination of the static modulus by the stress-strain curves. Their accurate assessment is crucial for the fatigue testing procedures, especially concerning the determination of the stress level.

Section 4.2.3. presented the quasi-static characterization, in low deformations zones, and in the frequency domain, with the fatigue tests for different stress levels in pure tension. First, it is presented a comparison between the static and quasi-static methods, and second, the fatigue resistance and S-N curves are investigated. Also, it is presented the interlinks between the microstructure and the mechanical characterization results.

Lastly, accurate data processing is crucial for the correct determination and evaluation of complex modulus and fatigue properties. To drive, manage, and verify the entire process the current methodology proposes the development and validation of analysis routines. Section 4.2.4 describes this methodology with a numerical approach to sinusoidal data analysis, which involved the development of two analysis software routines, for complex modulus analysis (CMA) and fatigue test analysis (FTA). The results were validated and evaluated for their accuracy, by comparing with a built-in analysis software from a dynamic press (UTM-25).

4.2.1 Microstructure and Physical Aspects

4.2.1.1 Cement Formulations and Concrete Mix Design

The refinement of the microstructure is recurrently addressed by literature on cementitious materials (Chaudhary; Sinha, 2020; Fattouh; Elsayed, 2023; Petrella *et al*., 2022; Singh; Mehta; Kumar, 2023). The proposed cement formulation was conceived aiming to improve microstructure, whereas the SF and GP demonstrated feasible potential to achieve that.

It was adopted a 5% OPC replacement rate for the proposed formulation, due to its high fineness and better capacity to address micropores (Boukhelf *et al*., 2021; Chaudhary; Sinha, 2020; Kravtsova *et al*., 2020). On the GP, it was found positive results for the microstructure with the 30% replacement ratio (Adil; Kevern; Mann, 2020; Boukhelf *et al*., 2021).

For the reference OPC (M1), it was adopted a (i) CEM I 52.5N. The proposed formulation (M2) was composed of the same OPC, with a partial mass replacement by (ii) GP, undertaken at a ratio of 30%, and (iii) SF, incorporated at 5%. These cement formulations were applied to pastes, grouts and concrete for the following analysis. Figure 28 presents a graphical abstract of the binders' compositions.

Figure 28 - Graphical abstract of the cement formulations proposed.

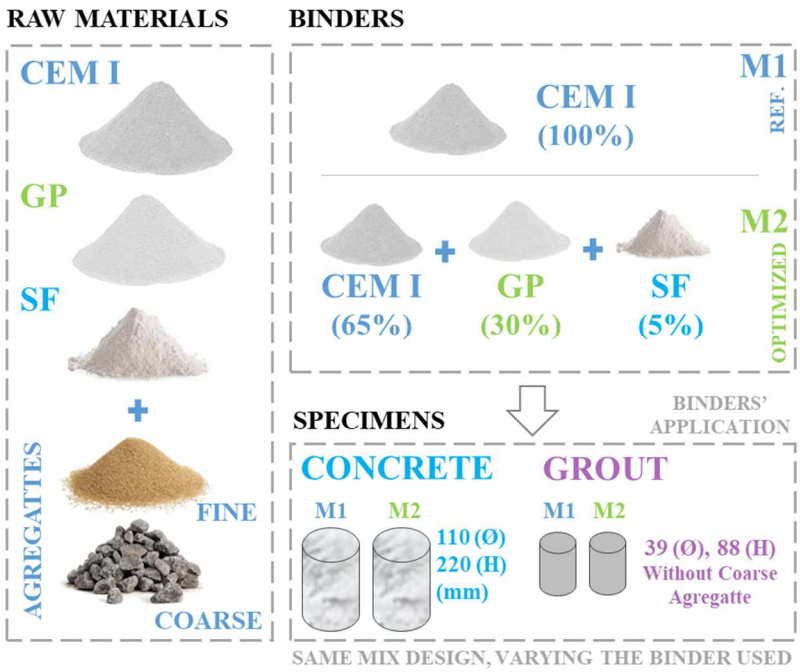

Source: Author (2023).

The concrete mix design was derived from an on-site aerogenerator foundation mix design from a French-Brazilian collaborative research project that evaluated an aerogenerator's foundation in France. The corresponding grout was adapted by excluding the coarse aggregate

from the mix formulation and keeping all remainder proportions. This adjustment allowed for the fabrication of specimens with a scaled-down geometry, which also meets the stress levels requirement of the quasi-static tests while preserving adequate elementary representative volume (ERV) for testing. Table 13 summarizes the mix designs for the binders and composites.

The cement CEM I 52.5N conformed to the European Standard EN 197-1 (2012). The GP was obtained from glass waste demolition at a disposal plant in Caen (Normandy, France). The crushing process was repeated to obtain a diameter smaller than 63 μm. The SF complied with EN 13263-1 (CEN, 2005), with 96% of silica content (high purity).

Table 13 - Cement formulations, and the grout and concrete mix designs

Component	**Density (kg/m³)**	**Cement M1 (%)**	**Cement M2 (%)**	**Grout M1 (kg/m³)**	**Grout M2 (kg/m³)**	**Conc. M1 (kg/m³)**	**Conc. M2 (kg/m³)**
Cement CEM I	3170	100	65	350	248,40	350	248,40
Glass Powder (GP)	2180	-	30	-	74,50	-	74,50
Silica Fume (SF)	2710	-	5	-	12,40	-	12,40
Clinker Content	-	95	63	-	-	-	-
W/B Ratio	-	-	-	0,45	0,45	0,45	0,45
Water	1000	-	-	157,50	150,90	157,50	150,90
Fine Aggregate - Sand (0/3,15 mm)	2490	-	-	639	639	639	639
Coarse Aggregate - Gravel (3,15/12.5 mm)	2310	-	-	-	-	1070	1070
Specimens Size (mm)	-	-	-	39x88	39x88	110x220	110x220

Source: Author (2023).

The density of fillers was determined using a helium pycnometer. All grouts and concrete mixtures maintained the same water/binder ratio (W/B) of 0.45 with a cement consumption of 350 kg/m³. The same W/B ratio was used in the composition of the pastes for the heat of hydration analysis. After molded, the specimens were placed in a humid chamber with 50% RH at 22 °C. After 24 hours, they were demolded and kept under ambient conditions up to the respective testing ages.

The particle size distribution (PSD) of the powder materials (CEM I, GP, and SF) was determined using a dry method analyzer (CEN, 2012b). Those specific surfaces were assessed using the BET method, based on Brunauer, Emmett, and Teller's theory, in compliance with EN ISO 18757 (CEN, 2003). Figure 29 presents these respective results.

Figure 29 - Percentage passed, fraction retained and specific surface of raw materials.

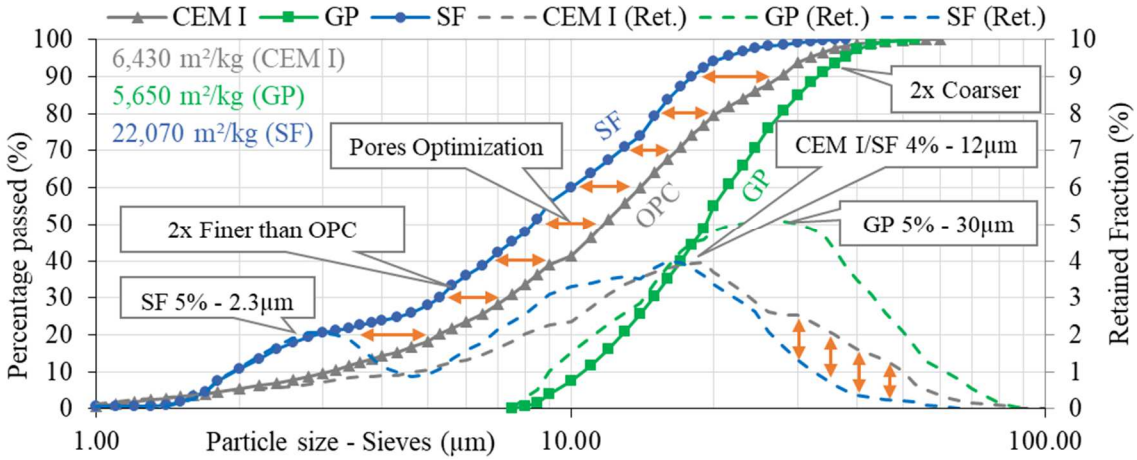

Source: Author (2023).

All the materials exhibited a continuous curve distribution. The CEM I settled between both SCMs indicating a promising potential for pore optimization concerning the SF incorporation. The GP curve consistently demonstrated a coarser aspect. The results align with the findings in the literature (Boukhelf *et al.*, 2021; Omran *et al.*, 2017; Pappa *et al.*, 2018). Nevertheless, there is potential for improvements in the microstructure and pore size distribution due to the GP influence on hydration and long-term effects.

4.2.1.2 Heat of hydration Analysis

The cement paste formulations were applied to pastes with the same W/B as the grouts and concretes (0.45). After mixing in the fresh state, they were tested in compliance with ASTM C1702 (ASTM, 2017). The heat flow was recorded over a period of 25 hours, and isothermal conditions were maintained at 20°C ± 0.02°C within the measuring cells. This method provides insights into the heat evolution and reactivity of the cementitious system, shedding light onto the influence of GP and SF on early-age hydration (Al-Hasani *et al.*, 2023; Lavagna; Nisticò, 2022; Li *et al.*, 2023).

4.2.1.3 Concrete Slump Tests

The Abrams cone slump test, following NF EN 12350-2 (2019), is a widely employed monotonic technique to evaluate concrete workability (CEN, 2019).

4.2.1.4 Scanning Electron Microscopy (SEM) Images

SEM images were obtained both for the raw materials (CEM I, GP and SF) and the concrete sections (M1 and M2). The SEM analysis was performed using an FEI Quanta 200

ESEM FEG, equipped with a FEG Field-Effect GUN electron emitter and a Large Field Detector (LFD) of Secondary Electrons (SE). The testing was conducted at a water vapor pressure of 1.5 mbar and a voltage of 20 kV. The concrete specimens were sectioned using a precision saw. These surfaces were then polished to remove any saw-induced damage and to expose an unaltered cross-section of the material's microstructure. Tests were carried out for 28 aging days.

4.2.1.5 Water (WIP) and Mercury Intrusion Porosimetry (MIP)

Porosimetry is a widely used technique for assessing microstructure, particularly in relation to the influence of the pore structure. Two employed methods are water intrusion porosimetry (WIP) and mercury intrusion porosimetry (MIP). The WIP tests were conducted in triplicate according to AFPC-AFREM (LABORATOIRE MATÉRIAUX ET DURABILITÉ DES CONSTRUCTIONS, 2009). The MIP tests were performed on specimens with a size of 3 cm³, in compliance with ASTM D4404-18 (ASTM, 2018) with injection pressure of up to 400 MPa. All tests were carried out at 90 days.

4.2.1.6 Thermogravimetric (TG) Analysis

Thermogravimetry is an analytical technique employed to measure variations in sample mass in the temperature domain. This method is useful for monitoring processes such as solid-phase transformations, moisture content, water bonding, and the estimation of the content of hydration products, such as portlandite. During the test, the temperature was increased from the ambient up to 1000 ◦C at a rate of 10°C/min.

The obtained TG results can be used to calculate (i) the physically adsorbed water ($\%w_{pa}$), (ii) the chemically bonded water ($\%w_b$), (iii) the carbon oxides content ($\%CO_x$), including CO_2 and CO resulting from carbonaceous molecules degradation, (iv) the portlandite content ($\%CH$) and (v) the calcite content ($\%Calcite$). Equations 27 to 31 establish the content estimation for different components, based on the mass loss (Boukhelf *et al*., 2021; Idir; Cyr; Tagnit-Hamou, 2011; Issaadi *et al*., 2017; Vogler *et al*., 2022).

$$\%w_{pa} = \frac{m_{40} - m_{200}}{m_{200}} \times 100\% \quad (27)$$

$$\%w_b = \frac{m_{400} - m_{500}}{m_{500}} \times 100\% \quad (28)$$

$$\%CO_x = \frac{m_{600} - m_{800}}{m_{800}} \times 100\% \quad (29)$$

$$\%CH\ [Ca(OH)_2] = \frac{m_{410} - m_{490}}{m_{490}} \times \frac{M_{Ca(OH)_2}}{M_{H_2O}} \times 100\% \quad (30)$$

$$\%Calcite\ (CaCO_3) = \frac{m_{500} - m_{900}}{m_{900}} \times \frac{M_{CaCO_3}}{M_{CO_2}} \times 100\% \quad (31)$$

Whereas:

$\%w_{pa}$, $\%w_b$ = water physically and chemically absorbed, in percentage [%];

$\%CO_x$ = estimation of carbonaceous materials mass content, in percentage [%];

$\%CH\ [Ca(OH)_2]$ = estimation of portlandite mass content, in percentage [%];

$\%Calcite\ (CaCO_3)$ = estimation of calcite mass content, in percentage [%];

$m_{\text{temperature}}$ = sample weights at a specific temperature in °C [g];

$M_{Ca(OH)_2}$, M_{H_2O} , M_{CaCO_3} , M_{CO_2} = chemical component molar mass [g/mol].

4.2.1.7 Life Cycle Analysis (LCA)

LCA is a technique employed to assess the environmental repercussions of processes, products, or services. The current LCA extracted data from the literature concerning CEM I, GP, and SF. This data encompasses (i) raw material consumption, (ii) energy demand, and (iii) greenhouse gas emissions (GHGe) (Chen *et al*., 2010; Crossin, 2015; Guignone *et al*., 2022; Huntzinger; Eatmon, 2009; Sánchez *et al*., 2021; Valderrama *et al*., 2012; Zulkarnain *et al*., 2021). Based on that, it was established the life cycle inventory (LCI), incorporating the average of these findings. The LCA estimated the environmental impact of the proposed formulation with the effect of the chosen SCM additions in comparison to the OPC formulation of CEM I.

4.2.2 Compressive and Tensile Strength, and Tensile Static Modulus

Characteristic strengths have a major influence on fatigue. Enhanced compressive strength has the potential to increase fatigue resistance (Huang *et al*., 2017), load-bearing capacity, and reduce crack propagation (Magalhães *et al*., 1996). The compressive strength tests were conducted on the concrete formulations using cylindrical specimens of 110 mm diameter x 220 mm height, at 28 and 90 days, in compliance with EN 12390-3 (CEN, 2019).

The tensile strength tests were performed on the grout formulations using cylindrical specimens of 39 mm diameter x 88 mm height, at 90 days after casting. Tests were conducted in a Universal Testing Machine dynamic press (UTM-25) measuring the strain response during the tests. The loading regime was in pure tension with loading control, with a 10% loading rate for compressive tests (ABNT, 2007; ASTM, 2020; CEN, 2019). The load cell had a

maximum capacity of 25 kN with a 0.001 kN resolution. Also, the static modulus was determined from the slope of the stress-strain curves up to 30% of the stress-strain levels.

4.2.3 Quasi-static Characterization

The modulus of elasticity is a widely used parameter for assessing concrete stress-strain. A higher modulus can improve fatigue resistance (Huang *et al*., 2017), and reduce the risk of failure (Magalhães *et al*., 1996). Cementitious materials exhibit a signal delay between stress and strain (Bažant, 1970; Bažant; Jirásek, 2018; Brinson; Brinson, 2008; Evangelista Junior; Macedo; Farias, 2019; Zhao *et al*., 2013), a parameter named phase angle (φ), influenced by parameters such as loading frequency, and stress levels (Liu *et al*., 2019). This is a common material property studied in many viscoelastic materials, but still rare in cementitious materials, usually considered perfectly elastic for modulus characterization.

The complex modulus is a measurement of material stiffness for viscoelastic materials being a useful parameter, due to its ability to broader evaluate mechanical behavior (Brinson; Brinson, 2008; Liang *et al*., 2022b), containing information on the stiffness and dissipated energy during mechanical loadings.

The complex modulus (CM) quantifies the storage modulus (E', the real part of the complex modulus and related to the ability of the material to store and give back, instantly, mechanical energy, then considered elastic) and the loss modulus (E'', the imaginary part of the complex modulus, related to the ability of the material to dissipate mechanical energy, then considered viscous). In perfect elasticity ($\varphi \approx 0$), the absolute value of the CM ($|E^*|$) coincides with the modulus of elasticity. Equation 32 describes those relationships.

$$E^* = \frac{\sigma_0}{\varepsilon_0}[cos\varphi + i.sen\varphi] = E' + i.E''; \qquad |E^*| = \sqrt{E'^2 + E''^2} \tag{32}$$

Whereas:

φ = Phase Angle, the signals' delay;

$|E^*|$ = Absolute value of Complex Modulus;

E' = Real part of Complex Modulus (Storage Modulus) with $E' = |E^*|.cos\varphi$;

E'' = Imaginary part of Complex Modulus (Loss Modulus) with $E'' = |E^*|.sen\varphi$.

The literature on cementitious materials usually determines the CM using stress-controlled tests (Chen *et al*., 2022; Evangelista Junior; Macedo; Farias, 2019; Yan; Sun; Chen, 1999). Figure 30 illustrates the experimental data and the numerical interpretation of the test to determine the absolute value of complex modulus and phase angle.

Figure 30 - Experimental vs. modeled data for Complex Modulus

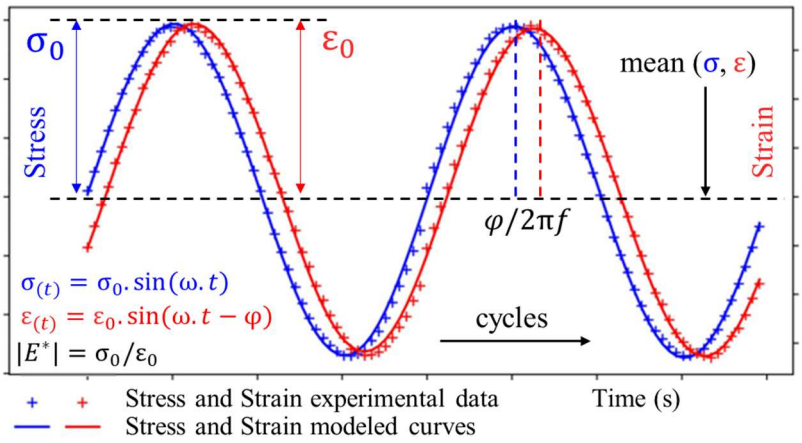

Source: Author (2023).

Equations 33 and 34 describe the numerical models to represent general stress and strain signals with a sinusoidal part, respectively. Equations 35 and 36 illustrate the numerical calculation of the $|E^*|$ and φ results. Those equations describe stress and strain interpolation functions over time, denoted as $\sigma_{int}(t)$ and $\varepsilon_{int}(t)$ respectively, necessary for signal processing during complex modulus and fatigue tests.

$$\sigma_{int}(t) = A_\sigma * sen(\omega t) + B_\sigma * \cos(\omega t) + C_\sigma * t + D_\sigma \tag{33}$$

$$\varepsilon_{int}(t) = A_\varepsilon * sen(\omega t) + B_\varepsilon * \cos(\omega t) + C_\varepsilon * t + D_\varepsilon \tag{34}$$

$$|E^*| = \sum_{i=1}^{n} \frac{\sqrt{A_{\sigma i}^2 + B_{\sigma i}^2} \Big/ \sqrt{A_{\varepsilon i}^2 + B_{\varepsilon i}^2}}{N} \tag{35}$$

$$\varphi = \sum_{i=1}^{n} \frac{\tan^{-1}\left({}^{A_{\varepsilon i}}/_{B_{\varepsilon i}}\right) - \tan^{-1}\left({}^{A_{\sigma i}}/_{B_{\sigma i}}\right)}{N} \tag{36}$$

Whereas:

$\sigma(t)$, $\varepsilon(t)$ = stress and strain function in the time domain;

ω = angular velocity, in the frequency domain, with $\omega = 2\pi f$;

N = number of cycles for the average calculation, adopting the total of the loading cycles for the CM tests and 1 for the individual cycle calculation of fatigue tests;

A_σ and A_ε = wave amplitude in phase, for stress and strain, respectively, while the index i denotes the cycle for which the parameter is obtained;

B_σ and B_ε = wave amplitude out of phase, for stress and strain, respectively;

C_σ and C_ε = linear component resulting from drift or damage, for stress and strain, respectively;

D_σ and D_ε = stress and strain offset (mainly due to the application of non-centered loading signals), for stress and strain, respectively, also named as its respective mean values.

Both CM and fatigue tests are stress-controlled and conducted with varying stress levels ($S_{level} = \sigma_{applied}/\sigma_{max}$), being defined as the minimum (S_{min}) and maximum (S_{max}) parameters of the sinusoidal loading amplitude. Also, the loading frequency (f) is defined. Equations 33 and 34 are applied to each loading cycle individually.

For the CM tests, the outcome is the average of the $|E^*|$ and φ, calculated individually for each loading cycle. Those averages are summarized for each loading frequency test. For fatigue, the results of $|E^*|$ and φ are presented individually for each loading cycle. In both cases, it is employed Equations 33 to 36, with a difference in the N adopted for each case.

These tests were performed at UTM 25 dynamic press under different loading conditions. The recorded data was analyzed externally by analysis software (CMA and FTA). Figure 31 presents the test apparatus.

Figure 31 - Dynamic Press (a), testing set apparatus with LVDTs in detail (b)

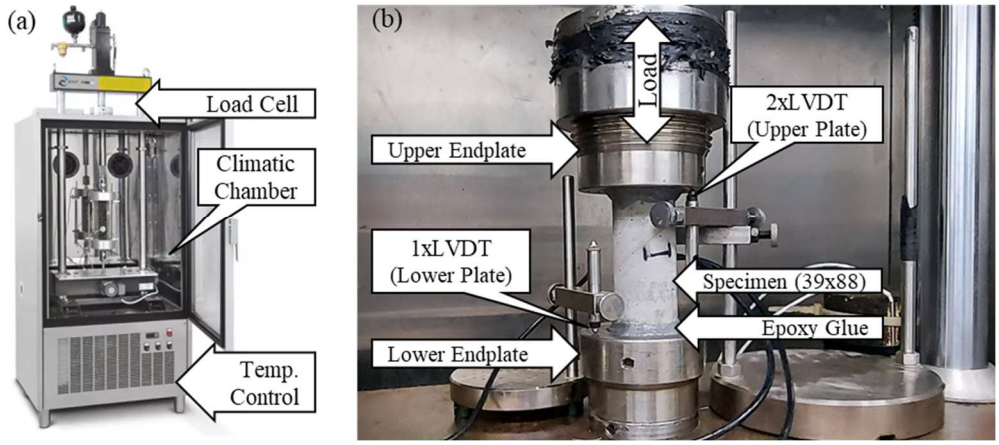

Source: Author (2023).

As presented in Figure 31, the LVDTs' position' is not usual, being necessary to explain the strain measurement procedure. Equation 37 and 38 presents the LVDT position calculation as a time function ($P(t)$) and the specimen strain ($SpecimenStrain(t)$).

$$P(t) = CurrentPosition(t) - InitialPosition \tag{37}$$

$$SpecimenStrain(t) = 1 - \frac{-P_1(t) + \frac{P_2(t)+P_3(t)}{2}}{InitialSpecimenHeight} \tag{38}$$

The $P_1(t)$ refers to the LVDT positioned in the lower endplate, and $P_2(t)$ and $P_3(t)$ are placed in contact with the upper. The $InitialPosition$ and $InitialSpecimenHeight$ are measured on the start of the testing procedure.

The tests were performed on grout formulations (Grout M1 and M2) using cylindrical specimens of 39 mm diameter and 88 mm height. The specimen sizes' reduction was necessary to accommodate the press load limits (maximum static load of 25 kN). It corresponds in such reduced geometry to a compressive strength limit of 20.9 MPa, while it would have given a 2.63 MPa on a 110-mm diameter, limiting the possibility of investigating stiffness both for compressive and tensile tests and making impractical the fatigue tests. The expected compressive and tensile strength was 50 MPa and 5 MPa, respectively.

4.2.3.1 Complex Modulus Analysis (CMA) in Pure Compression and Pure Tension

This characterization was conducted with low-stress levels estimated from the specimens' strength levels under monotonic loading (for compressive and tensile loading regimes), to ensure that it poses no risk of damage to the integrity of the materials. The goal was to assess the behavior of the complex modulus ($|E^*|$ and φ) at low stress and strain levels.

This procedure was repeated for different loading frequencies, which is also named "frequency sweep" in the literature. The selected frequency range covered up to the mid-range (lower than 25 Hz) avoiding dynamic/inertial effects, which would need to be addressed with other techniques, complying with ASTM E1876 (ASTM, 2022).

All tests were carried out with temperature control ensured by a climatic chamber, with a range of 19 °C ± 0.50. CM tests were both in pure compression and pure tension, ranging from low (0.1 - 1 Hz) to mid-range (1 - 25 Hz) frequencies. The maximum and minimum stress levels are percentages based on the compressive and tensile strength levels. Table 14 provides the specifics of the frequency sweep tests.

Table 14 - Testing Parameters of the Complex Modulus Tests

Testing Group	**PCLF**	**PCMF**	**PTLF**	**PTMD**
Loading Regime	Compressive	Compressive	Tensile	Tensile
Frequencies Range (Hz)	0.1 - 1 (+0.1)	1 - 25 (+1)	0.1 - 1 (+0.1)	1 - 25 (+1)
Number of Cycles (N)	10	100	10	100
Maximum Stress	10%	10%	0	0
Minimum Stress	0	0	10%	10%

Source: Author (2023).

4.2.3.2 Pure Tension Fatigue characterization

The fatigue tests follow a similar methodology with the application of sinusoidal loading and measuring the strain responses over time. For this case, the loading frequency was set at 10 Hz. As outcomes, it is measured (i) the stress and strain response, and (ii) the number of cycles (N) up to (iii) the number of cycles at failure (Nf) providing the necessary data for the calculation of the complex modulus parameters. For each cycle is calculated its respective $|E^*|$ and φ, focusing not on their average, but on their variation through fatigue cycles.

The Nf indicates how long the material can endure cyclic loading before collapse, while the modulus degradation (ΔE) is a measure of the material's stiffness loss due to damage accumulation. The fatigue model refers to the numerical modeling of the experimental findings to predict fatigue life. Also, it determines the endurance limits (ELs), a stress level that a material can withstand for an infinite number of cycles without fatigue failure.

Those stress levels are higher (about 60% to 100% of the static strength) than in CM tests (about 10% of static strength). Fatigue damage curves consist of the modulus degradation and loss of stiffness that the material evolves with repeated cycles. In damage mechanics models, it is a percent change of the initial modulus, related to the loss of cross-sectional resistant area (Kachanov, 1958; Kattan; Voyiadjis, 2002; Lemaitre; Sermage; Desmorat, 1999; Lemaitre; Chaboche, 1990).

Lastly, there is an aging effect on the fatigue behavior of cementitious materials. Early-age concretes develop hygrothermal cracks and deformations (Wei, 2012). It may exhibit stiffness evolution, thermal strains, and viscoelastic effects, leading to an initial degradation due to internal stresses (Massoud *et al*., 2008). Fatigue resistance increases with age (Galloway; Harding; Raithby, 1979). The current tests were carried out from 90 to 120 aging days. Furthermore, the SEM analysis can address the mentioned phenomena described.

The numerical data processing used was the same as those described in Equations 33 to 36. Table 15 presents a summary of the parameters.

Table 15 - Testing Parameters of the Fatigue Tests

Testing Group	**Grout M1**	**Grout M2**
Loading Regime	Tensile	Tensile
Loading Frequency (Hz)	10	10
Stop Criteria (Cycles)	10^6 or failure	10^6 or failure
Max Stress ($\sigma_{applied}/\sigma_{max}$)	60% - 100% (5% increments)	80% - 100% (+5% increments)
Min Stress ($\sigma_{applied}/\sigma_{max}$)	10% of σ_{max}	10% of σ_{max}

Source: Author (2023).

To avoid uncontrolled loading rates in the initial loading, it was adopted a loading ramp program. This program led the measurement in the load cell from zero to the planned average stress between the maximum and minimum stress levels of the cyclic sinusoidal loadings. This loading rate complied with the standards (ABNT, 2007; ASTM, 2020; CEN, 2019).

4.2.4 Data Analysis: Software development and validation

The literature review highlighted a lack of solutions for data processing of complex modulus and fatigue tests. To address this gap, two software routines were developed, named (i) Complex Modulus Analyzer (CMA) and (ii) Fatigue Test Analyzer (FTA). Figure 32 presents an overview of the data workflow for both tools.

Figure 32 - CMA and FTA data-processing Flowchart

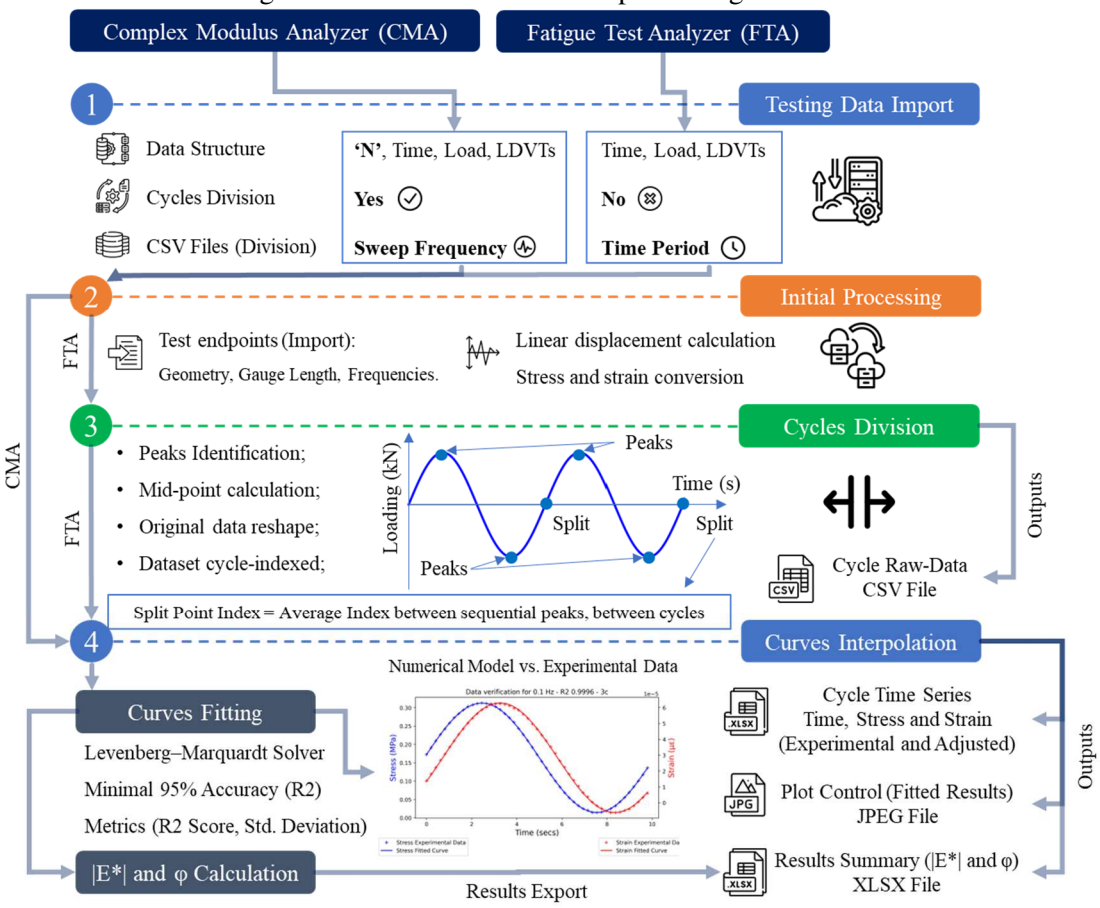

Source: Author (2023).

CMA provides the average values of $|E^*|$ and φ, for a number of cycles (N) and varying the testing frequencies (f). The $|E^*|$ and φ are calculated for each loading cycle individually and proceed with the average calculation. The materials are meant to be tested at a non-damage stress level. For FTA, the results of $|E^*|$ and φ for each cycle are presented in the function of the cycles, to assess the material's degradation over cycles up to a Nf.

To develop the referred tools, a validation process was conducted. This process is described following, which is used to interpret results from CM and fatigue tests in the paper. To evaluate the results' accuracy, two metrics were adopted: (i) the R^2 Score (a global quality measure) and (ii) the Standard Error (a linear measure of the difference between results).

For the validation, a comparative analysis was conducted between the current analysis method (CMA) and the built-in analyzer from the UTM 25 dynamic press, comparing the results of $|E^*|$ and φ, and the mean standard error (MSE). The tests were performed using samples of asphalt concrete, cementitious concrete and steel. In total, 49 results were compared. Figure 33 presents an illustration of the validation process used for this analysis.

Figure 33 - Software validation, comparison with the UTM 25 analysis software.

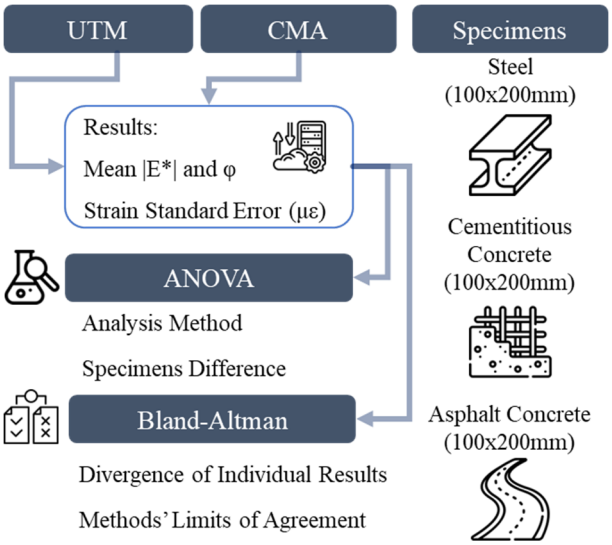

Source: Author (2023).

To investigate the variance of the results, it was employed a two-way ANOVA, and a Bland-Altman Analysis, to assess the individual differences and the limits of agreement (LoA). The validation results are presented as follows.

Regarding the comparison of the MSE, the UTM method obtained an average of 4.02 ± 1.45 με, while for CMA was 0.15 ± 0.02 με. It indicates a significant improvement in the accuracy of the CMA method, with a 27-factor reduction in the MSE average and standard error (from 36.06% to 13.33%). Moreover, it is emphasized that the average modulus by the CMA method was 215.42 GPa for steel, 37.50 GPa for cementitious concrete, and 15.84 GPa for asphalt concrete. The ANOVA results are presented in Table 16.

Table 16 - Two-way ANOVA results for the complex modulus results

	$\|E^*\|$	Steel	Cementitious Concrete	Asphalt Concrete	φ	Steel	Cementitious Concrete	Asphalt Concrete
p-Value		0.394	0.842	0.993		0.460	0.066	0.896
Fcalc./Fcrit.		0.178	0.009	1.560×10^{-5}		0.133	0.970	0.016

Source: Author (2023).

All the p-values were above the minimum threshold of 0.05, indicating that there is no statistically significant difference between the results of both analysis methods. The F parameters also supported the consistency of the results. Bland-Altman is presented in Figure 34.

Figure 34 - Bland-Altman results for individual divergences

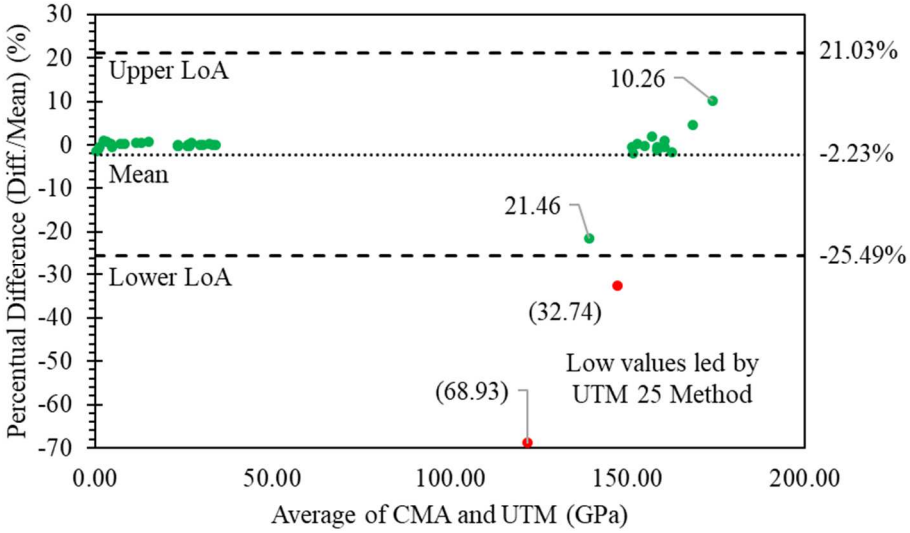

Source: Author (2023).

The analysis compared the CMA results with those obtained from the UTM 25. The mean difference was -2.23%, indicating that on average the CMA results were higher than those of UTM 25. From all 49 observations, only two were labeled as outliers, in red.

By examining these two outliers, it was found that the lower percentage difference was led by the UTM method. Assessing these individual results, no evidence was found for that decrease of the modulus in the literature, with a drop in the results of steel samples by 68.93% and 32.74%. These findings were inconsistent with the literature, attributed to a processing error, on the amplitudes' adjustment. The expected values for these cases were close to the CMA results, and aligned with the literature (Liang *et al.*, 2022a; Zhao *et al.*, 2013).

Furthermore, excepting these two outlier values, there was no statistically significant difference between these two methods. The Bland-Altman plots show that most data points fall between the LoAs, indicating agreement for the methods.

Summarizing the validation, by comparing all three parameters adopted ($|E^*|$, φ and MSE) it was concluded that both analysis methods were consistent with the expected results and specifically the CMA results were more accurate.

The outliers, led by the UTM-25 data processing, do not reflect the literature behavior, once these results (118.01 and 132.07 GPa) are lower than the usual range of 190 to 215 GPa for the modulus of elasticity of steel. Additionally, both occurrences were at the same loading frequency of 0.5 Hz, corroborating the hypothesis of error, due to a possible wrong adjustment of the amplitudes, frequency, or similar parameters by the UTM software.

The ANOVA and Bland-Altman analyses support the effectiveness of the CMA method in processing the results. This consistency highlights the reliability of the methods developed in correctly processing the results. The agreement between the two methods enhances the confidence in the reliability of the proposed approach.

4.3 Results and Discussion

4.3.1 Microstructure and Physical Aspects

4.3.1.1 Heat of hydration Analysis

The delayed ettringite formation (DEF), and thermal and early-age cracks are related to the energy released during hydration. It impacts fatigue resistance (Maruyama; Teramoto; Igarashi, 2014). Figure 35 presents the heat of hydration results.

Figure 35 - Heat of hydration of the assessed cement formulations

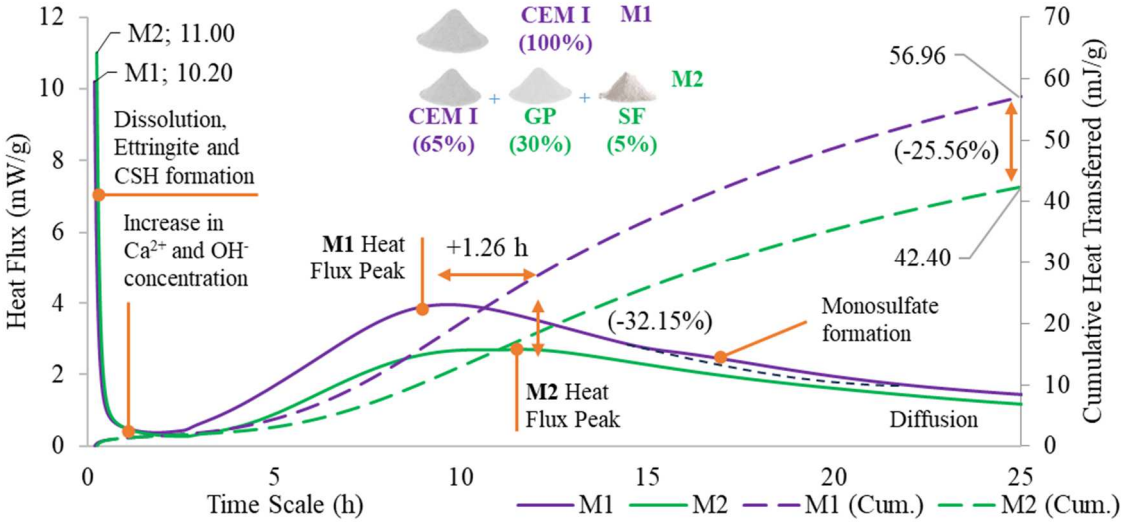

Source: Author (2023).

Assessing the amplitude peak (a measure of the maximum thermal energy release rate, defined in Figure 35) it was observed a reduction of 32.15% and a delay of 1.26 h by comparing both results. On the cumulative energy, there was a reduction of 25.56%.

The reduction in heat of hydration is beneficial for the microstructure and fatigue resistance, with low-heat cements preferred for those applications (Maruyama; Teramoto; Igarashi, 2014), with a lower potential for cracks' formation, enhanced hydration products, and reduced incidence of large pores. The SF and GP addition is found to reduce the released energy at early ages (Tavares *et al.*, 2020).

On the influence of the SCMs' mass replacement, the peak reduction (32.15%) had a similar range as the clinker replacement, and the GP and SF content demonstrated quasi-zero heat contribution. The obtained results point to a lower susceptibility to thermal and early-age cracks, improving the mechanical behavior and possibly fatigue resistance, with a focus on degradation mechanisms (cracks formations and coalescence) of the fatigue phenomenon. This hypothesis can be further confirmed by the SEM and Fatigue results.

4.3.1.2 Concrete Slump Tests

The slump test assesses the adequacy of the use, influencing the strength and microstructure. Figure 36 presents the results (CEN, 2019).

Figure 36 - Concrete workability test results

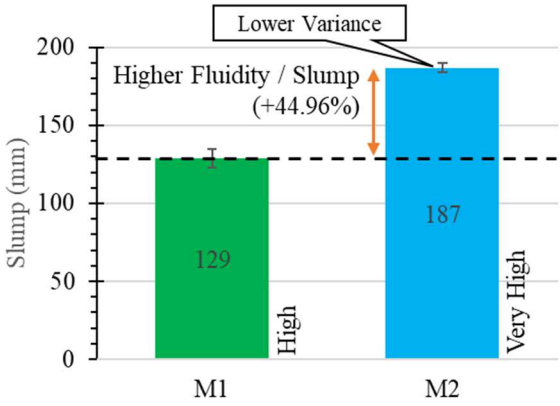

Source: Author (2023).

The proposed formulation yielded a very high fluidity (187 mm) compared to the reference formulation (129 mm). The presented outcome has a direct implication on the water content and mix design. The increase in fluidity indicates a lower water demand, which could have promoted a reduction in the W/B ratio, resulting in improvements in microstructure and strength levels.

This outcome is influenced by the SCM additions, specifically on the GP. Literature reports its particles with a smooth superficial aspect, with a lower grain friction, improving mechanically the fluidity. It improves the flow (Singh; Talwar, 2020), increases workability (Akçaoğlu; Çubukçuoğlu; Tarassoly, 2020; Gokulnath; Ramesh; Priyadharsan, 2020; Singh; Talwar, 2020), and its sole addition only improves the freezing-thawing fatigue resistance (Grinys *et al*., 2021).

On the other hand, the SF with a 5% addition results in an increase in paste consistency. It results in a higher viscosity by 3 % and a yield stress by 18% (Adil; Kevern; Mann, 2020). Despite the increase in consistency, the 5% replacement is highlighted as the better replacement ratio (Chaudhary; Sinha, 2020).

Finally, the improved fluidity (+44.96%) encompasses both an improved flow led by GP, with higher consistency led by SF. Overall, the potential reduction in water demand is a positive aspect for those applications. Reduced W/B ratios have a positive effect on ITZ bonding strength, composite durability, and higher compressive and tensile strength levels (Kachkouch *et al*., 2022; Paul; Šavija; Babafemi, 2018).

4.3.1.3 Scanning Electron Microscopy (SEM) Images

Figure 37 presents the SEM results of the raw materials. The general observation of shapes and geometries agreed was consistent with similar investigations of CEM I, GP, and SF (Chaudhary; Sinha, 2020; Fattouh; Elsayed, 2023; Muller *et al*., 2015; Petrella *et al*., 2022; Uzbas; Aydin, 2020).

Figure 37 - SEM images of (a) CEM I, (b) GP and (c) SF on a 50µm scale

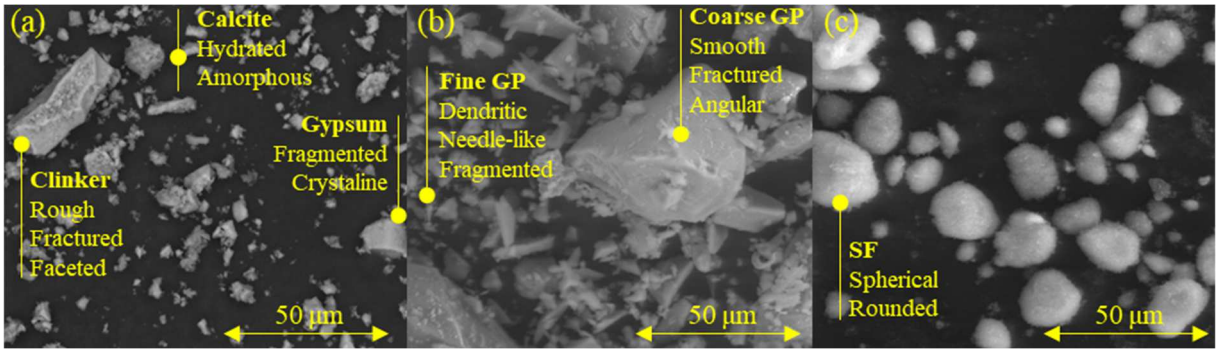

Source: Author (2023).

Figure 37a presents mostly particles with a fractured aspect, resulting from the clinker refinement. Figure 37b presents the GP aspect. The particles mainly encompass two types, (i) a coarse smooth shape (Coarse GP) and (ii) finer dendritic fragments (Fine GP). The

visualized shape formats corroborate the hypothesis in the workability section, attributing the improved fluidity to the GP influence, also aligned with the evidence presented.

Figure 37c presents the SF aspect, in agreement with the literature. Those particles directly address pores fulfillment, resulting in a denser matrix (Santos *et al*., 2021), and improved microstructure (Boukhelf *et al*., 2021, 2023). All these aspects are beneficial to fatigue resistance, by the lower W/B ratio potential, denser cement matrix, and better pores fulfillment, which can be confirmed in the SEM of the resulting microstructure. Figure 38 presents the concrete SEM results.

Figure 38 - SEM images of the concretes (a) M1 and (b) M2 on a 250μm scale

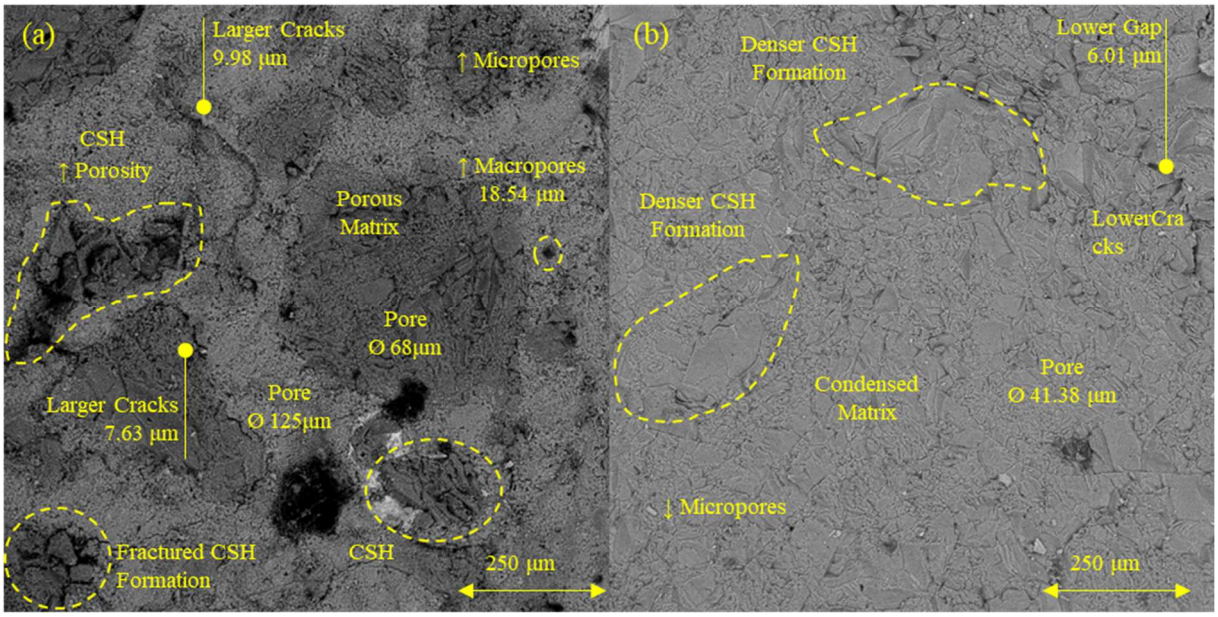

Source: Author (2023).

The concretes' SEM images of the proposed formulation demonstrated an improved microstructure. The Calcium Silicate Hydrate (CSH), the main product of cement hydration, is primarily responsible for the strength (Zhan *et al*., 2018). M1 demonstrated CSH structures with larger gaps, ranging from 5 to 15 μm, with a non-cohesive aspect. M2 was denser and more cohesive. Thinner gaps result in a lower potential for crack formation and coalescence.

The second overview is on the cracks' incidence, due to early-age phenomena (cracks due to internal effects) and heat of hydration. For M1, the cracks were more evident, with large gap widths (up to 10 μm). M2 had a narrower range (up to 6 μm).

Additionally, there were diverging pore structures. For M1, the macropore diameters range from 68 up to 125 μm. The M2 presented smaller pores, up to 41.38 μm. Lower pores structure and diameters lead to improved fatigue resistance and mechanical behavior (Kachkouch *et al*., 2022; Myrtja *et al*., 2021; Zhao; Chang; Yang, 2008). Moreover, aligned

with the heat analysis, the low heat observation resulted in a more intact and less damaged microstructure, possibly leading to improved fatigue resistance.

4.3.1.4 Water (WIP) and Mercury Intrusion Porosimetry (MIP)

Figure 39 displays the average porosimetry from both the WIP and MIP methods. The proposed formulation resulted in a lower average porosity of 7.20% and 0.75% by the WIP and MIP methods.

Figure 39 - Water and Mercury porosimetry results

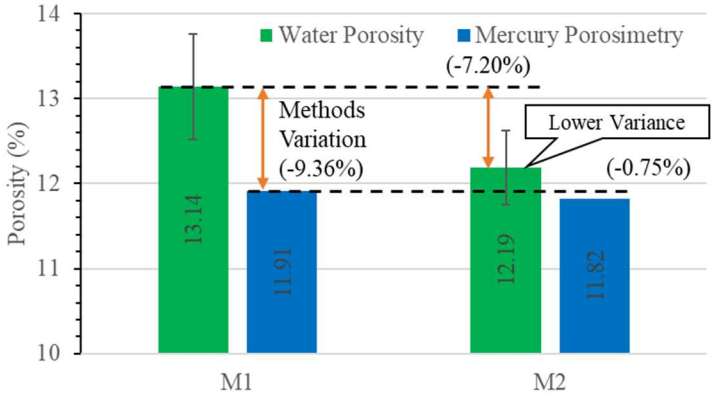

Source: Author (2023).

The addition of GP leads to a more refined microstructure (Serelis *et al.*, 2021) increasing the hydration degree (Tremiño *et al.*, 2021). The SF addition addresses the pores sizes lower than OPC capabilities (gel pores and mesopores ranges as follows), also improving hydration (Kravtsova *et al.*, 2020). In further detail, Figure 40 presents the pores' incidence in the pores' diameter domain.

Figure 40 – Distribution of pore diameters within the diameter range

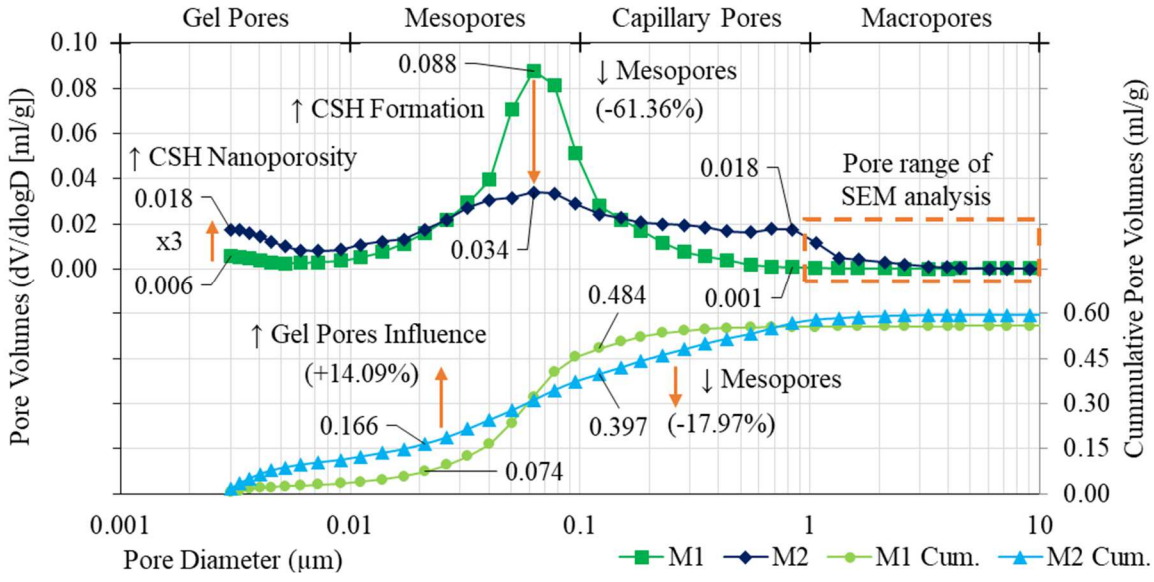

Source: Author (2023).

The gel pores and mesopores ranges are influenced by the cement hydration products. The more pronounced alteration, with a 61.36% decrease in the mesopores followed by an increase in the gel pores range suggests an improvement in the CSH formation. The mesopores range is mainly composed of CSH clusters (Muller *et al.*, 2015). Literature reports CSH with an inherent nano-porosity of about 26% (Liu *et al.*, 2021), increasing the porosity in this range, as a consequence of the higher CSH formation.

In this way, a higher CSH content can reduce the void content in the mesopores and increase the gel pores range, similar to the effect visualized (Gao *et al.*, 2015). In summary, lower porosity, higher CSH content, and improved pore structure are all beneficial for fatigue resistance and mechanical behavior (Kachkouch *et al.*, 2022).

4.3.1.5 Thermogravimetric (TG) Analysis

Figure 41a presents the results of the TG and dTG results in the temperature domain. Based on Equations 27 to 31 the mass content estimations are presented in Figure 41b.

Figure 41 - Results for TG and dTG analysis (a) and contents estimation (b)

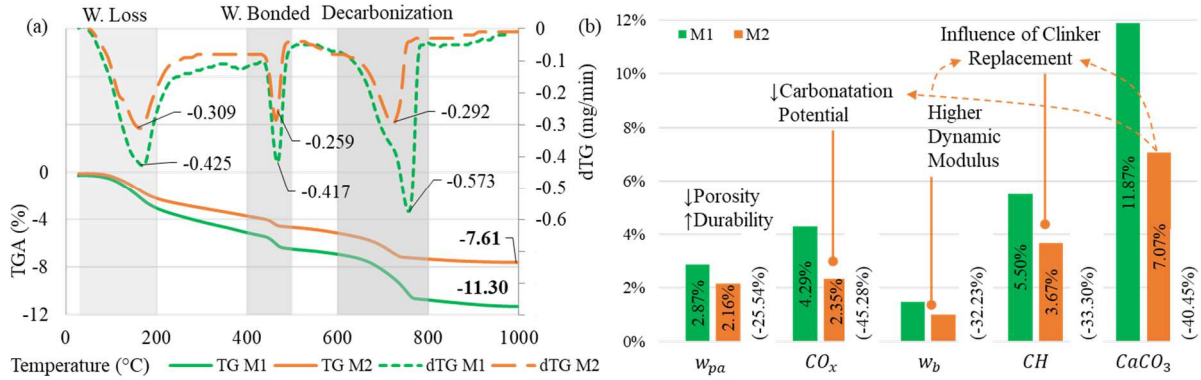

Source: Author (2023).

M2 had a greater thermal stability through these results (-32.65% loss of mass). The GP is reported with the potential to improve thermal stability and freezing-thawing fatigue resistance (Grinys *et al.*, 2021), and SF as well (Chung, 2002).

On the parameter of water physically absorbed ($\%w_{pa}$), lower results are beneficial for the composites' properties, improving durability, and reducing autogeneous shrinkage (Ding *et al.*, 2020; Huang *et al.*, 2020; Yamashita; Yoshida; Hirashima, 2017).

For the carbon oxides content ($\%CO_x$), it is a measure of the carbonaceous content. Lower $\%CO_x$ implies an improved freezing-thawing fatigue resistance (Grinys *et al.*, 2021), and lower carbonatation potential. There were improvements in both parameters.

Lastly, the lower portilandite ($\%CH$) and calcite ($\%CaCO_3$) contents reaffirm the higher CSH formation (Abzaev *et al.*, 2022; Lu *et al.*, 2023). Both contents are consumed for the CSH formation. The observed results presented an additional effect on the clinker replacement confirming the initial insights.

The water chemically bonded ($\%w_b$) influences mechanical properties (Zhang; Li; Li, 2019). Also, the elastic modulus can be affected by this same parameter (Miller *et al.*, 2016). Based on the 32.23% reduction, it is possible to a possible a higher elasticity modulus, also as an influence of that parameter (Kazmierczak *et al.*, 2019).

4.3.1.6 Life cycle analysis (LCA)

Assessing the LCA results, Figure 42 presents the estimations for raw materials and GHGe. The overall reduction was a direct influence of the clinker replacement, the most pollutant constituent of the cement industry. On the GHGe, Figure 42b and Figure 42c, the same overall was observed.

Figure 42 - LCA of (a) raw materials, (b) GHG emissions and (c) hazardous emissions

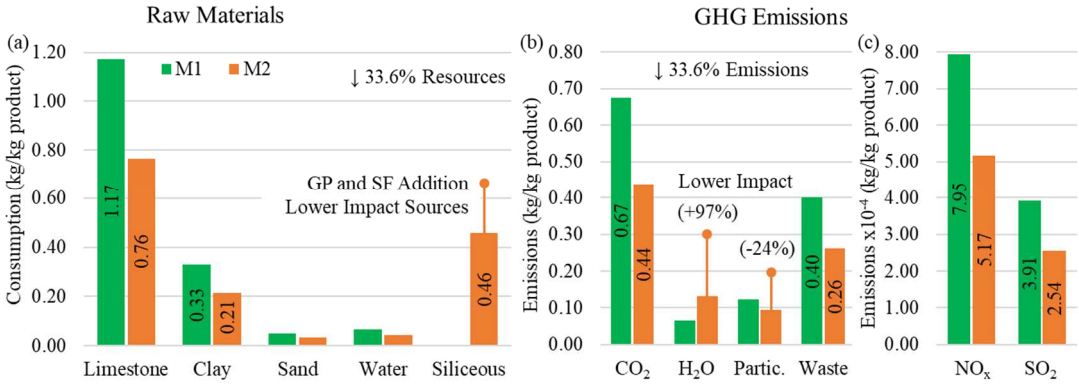

Source: Author (2023).

The addition of SCMs led to additional changes in the particulate emissions, reduced by only 24.14%, and gaseous H_2O, increased by 97.83%. The first case is influenced by the SF obtaining process (high particulate emission) as well as the GP, due to a non-industrial scale obtaining process (Guignone *et al.*, 2022; Orouji; Zahrai; Najaf, 2021).

Lastly, when evaluating trade-offs between different environmental impacts, these emissions constitute a more local problem, when compared to the global concern of CO_2 and GHGe. Lastly, Figure 43 presents energy consumption.

Figure 43 - LCA results from energy consumption

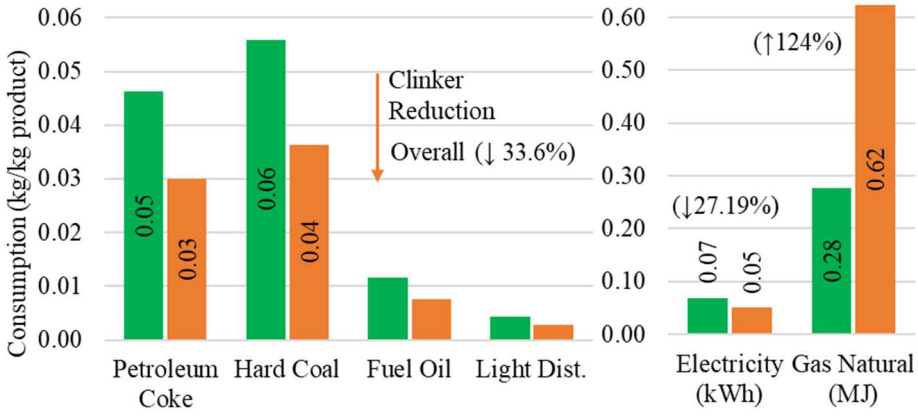

Source: Author (2023).

Natural gas is a cleaner-burning fossil fuel compared to coal and oil, producing fewer air pollutants, such as SO_2 and NO_x, leading to improvements in local air quality. Also, shifting from fossil fuels to electricity has benefitted LCA. Electricity generation produces lower local air pollutants and GHGe.

In general, the results show improvements in (i) lower demand for mineral resources, (ii) incorporation of waste materials, (iii) lower GHGe, and (iv) use of more clean energy. All these aspects are positive for LCA and the environment and demonstrate the potential of the proposed formulation both in the fatigue performance and environment.

4.3.2 Compressive and Tensile Strength, and Tensile Static Modulus

Figure 44 presents both strength results for 28 and 90 days. The strength reduction (32% to 36%) was mainly attributed to the clinker replacement (33.68%).

Figure 44 - Concretes' compressive strength at 28 and 90 days (a) and grouts' tensile strength at 90 days (b)

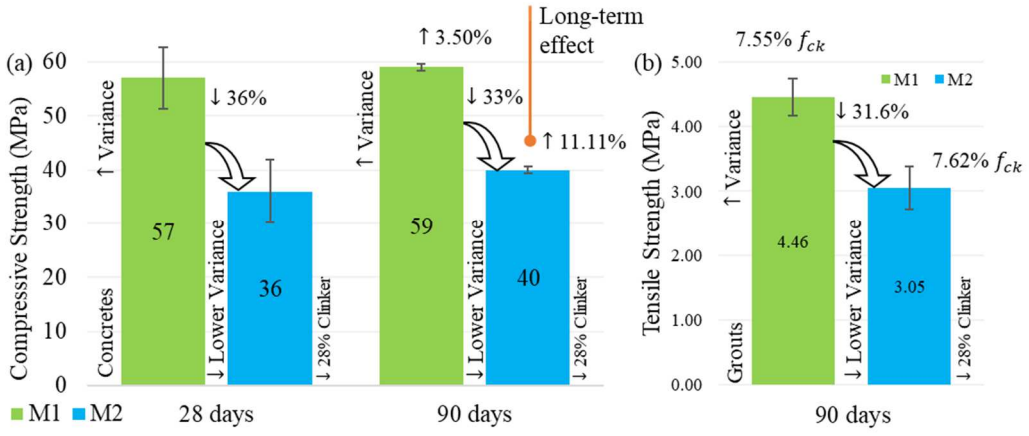

Source: Author (2023).

On the strength evolution, M2 had a higher strength increase (11.11%), compared to M1 (3.50%). This was attributed to the long-term influence of GP (Gołek, 2019; Omran *et al.*, 2017) and SF (Saurabh; Darji, 2016; Sealey *et al.*, 2017).

Lastly, the lower water demand of the proposed formulation also has an impact on this outcome. As expressed by the workability analysis, with improved fluidity, there was more free water due to the GP addition and its coarse particle fineness. This fact could have been used to reduce the water consumption in the concrete, and therefore reduce W/B and increase strength. However, for this paper, it was decided to maintain W/B fixed for all formulations, evidencing the influence of the cement formulation and its respective fatigue behavior.

Additionally, the lower variability (higher homogeneity) is also positive for the fatigue behavior, providing an improved strength levels' prediction. Furthermore, the stress-strain curves of the tensile strength test can provide additional results on the mechanical characterization. Figure 45 presents the stress-strain curves for the tensile strength tests. The strain is presented in x-axis and stress in y-axis.

Figure 45 - Stress-strain experimental results for grouts (a) M1 and (b) M2 at 90 days

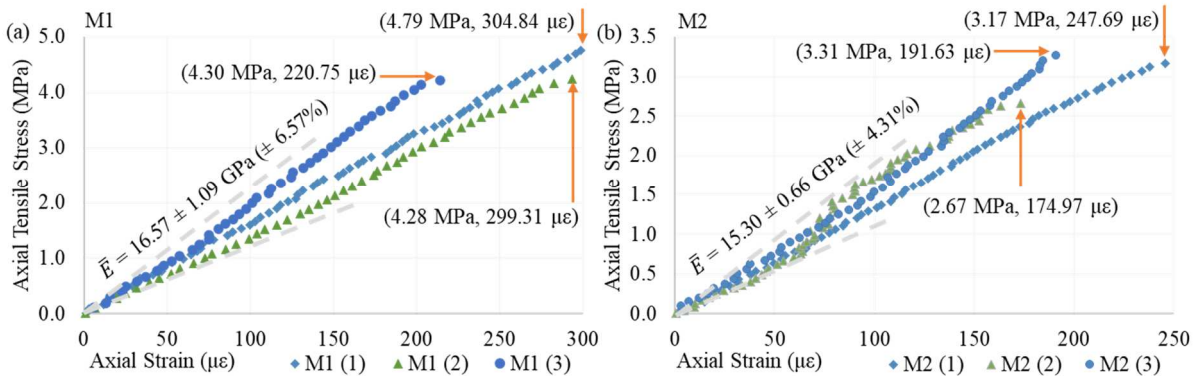

Source: Author (2023).

Despite the small difference in average value (16,6 GPa for grout M1 and 15,3 for grout M2), it was observed that there is no significant difference in slope between formulations, indicating a similar modulus of elasticity in the static loading regime. The curves' shape format had a good adjustment to linear models, mainly for strains under 40-50% of the static strength, with R^2-scores above 0.995. The static modulus of elasticity was determined from the slope of the linear models for stress-strain from up to 30% of the maximum strain. The static modulus and the maximum strain levels (near rupture) are presented in Figure 46.

Figure 46 - Elasticity Modulus (a) and Maximum Strain (b) at 90 days

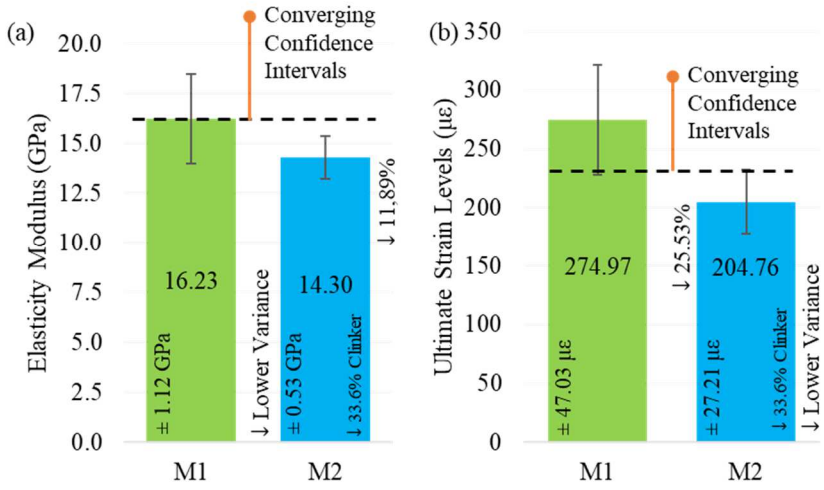

Source: Author (2023).

Similar to the stress-strain curves result, there was a superposition of the confidence intervals, indicating that the results have no significant difference, considering the margin of error. The M2 standard error was lower, which contributed to better prediction of stress levels for fatigue (Lei *et al*., 2017; Li; Ren, 2009), implying a lower variability for that formulation.

The same specimens addressed to the tensile strength tests were tested for the complex modulus which had been done before. The following is presented a comparison of the modulus of elasticity based on the stress-strain response of the static and quasi-static characterization methods, presented in Figure 47.

Figure 47 – Average linear model for static characterization and stress-strain curves for quasi-static method, for M1 (a) and M2 formulations (c) with the average adjustments for both (b, d)

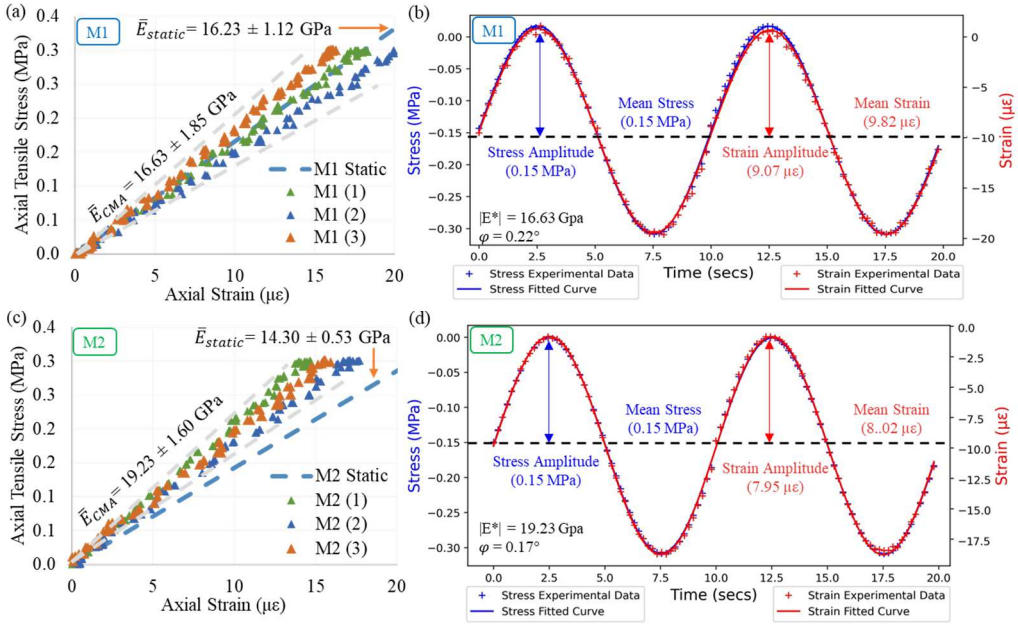

Source: Author (2023).

The previous curves are represented by the average adjustment on the linear models. By comparing both stress-strain curves, the M1 results were coincident, having both curves a modulus of elasticity near 16.23, with a 0.3% variation. On the other hand, the M2 had a 25.63% alteration in the average results, with the quasi-static results yielding higher values.

The expected difference should be near by ±10%. That discrepancy should be further assessed. In the literature, this may indicate an amplitude effect with a difference from the linear model proposed previously (Bažant; Jirásek, 2018; Brooks, 2015), or even can be attributed to possible damage.

Moreover, these findings provide an additional parameter for stiffness behavior. Lastly, it is concluded that the quasi-static characterization can provide additional parameters for the understanding of the stiffness, providing an initial determination of the materials' φ, being an initial step for fatigue assessment.

4.3.3 Quasi-static Characterization

4.3.3.1 Complex Modulus Analysis (CMA)

Figure 48 presents the complex modulus results in pure compression. The results showed a consistent higher $|E^*|$ for M2. The average standard error was also lower (0.33 GPa, 1.81%), indicating a lower variability (-0.93%).

Figure 48 - CMA in Pure Compression

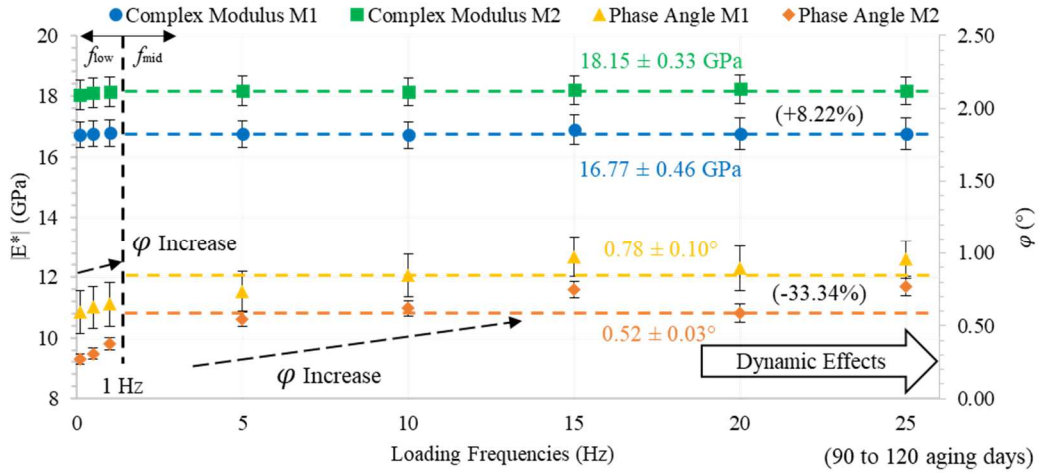

Source: Author (2023).

Microstructural parameters have an influence on this improvement (Wei; Liang; Kong, 2023). There are mainly three observations, from the microstructural analysis, that can be addressed on this outcome: (i) the lower $\%w_b$ content, which improves the elastic modulus of cementitious materials (Kazmierczak *et al.*, 2019), (ii) the higher CSH content and crystal

molecular formation, along with other hydration products, and (iii) the improved pores structure (Wei; Liang; Kong, 2023). Additionally, it can be suggested alterations in its Poisson ratio led by the improvements in the pore structures and denser cement matrix.

Moreover, the assessment of φ is not usual for the characterization of cementitious materials (Luo *et al.*, 2017). A lower φ, assessed by the complex modulus, indicates a reduced lag in stress-strain, resulting in a viscoelastic behavior closer to elasticity, with lower energy dissipation and reduced potential for cracks' formation. The results demonstrated that the incorporation of those SCMs resulted in a lower average of φ (-33.34%).

A similar interlink for microstructure and $|E^*|$ is observed for φ, being this case more focused on the denser cement matrix, improved hydration products, and lower incidence of pores with large diameters (Wei; Liang; Kong, 2023).

Additionally, by comparing the φ results with the findings of Chapter 3 (Targino *et al.*, 2023), it was found an aging effect on the φ. The results for 45 aging days indicated a higher φ compared to the reference formulation. This result was reversed by the age of 90 to 120 days, having a 33.34% drop in the same M2/M1 φ comparison. This is indicative of an aging effect, having the long-term ages a viscoelastic behavior closer to elasticity.

Lastly, due to the similarity of low amplitudes ($\varphi \approx 0{,}6°$), questions about the possibility of a systematic error may be raised. However, it is common to observe temperature increase during fatigue tests in concrete, on the order of 20°C for tests at 75% of stress levels (Kachkouch *et al.*, 2022; Myrtja *et al.*, 2021; Oneschkow, 2016), which could be explained by a viscoelastic character of the material with small phase angles. Figure 49 presents the CMA results for pure tension.

Figure 49 - CMA in Pure Tension

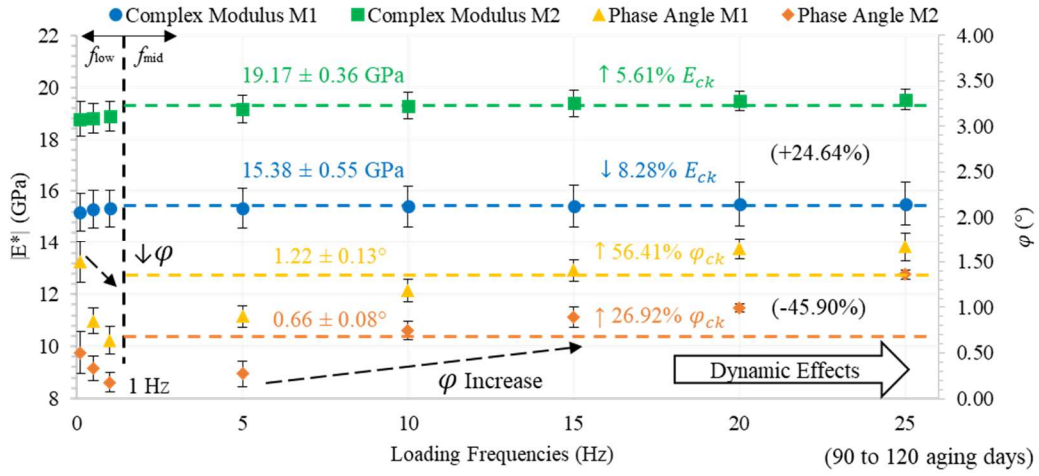

Source: Author (2023).

The overall improvement was 24.64% in $|E^*|$ and a drop of 0.56° in φ, implying a low viscous parcel on the viscoelastic behavior in pure tension. It was observed an aging effect, with increases of 9.85% and 13.29% respectively by comparing those results with 45 aging days of Chapter 3 (Targino *et al.*, 2023), reaffirming the SCMs' influence on the quasi-static behavior, especially on the long-term influence of GP.

The discrepancies by comparing with the CMA results in pure compression, of -8.28% and +5.61% respectively, evidences the bimodularity between the loading regimes and non-linearity of their strain behavior varying the loading regime.

Additionally, there was an evident variation in the φ results with respect to frequency, confirmed by the ANOVA, yielding lower values for 1 Hz. This behavior could reaffirm the possibility of systematic error. To assess those specific variations in φ in further detail, the current protocol was adjusted to closer step variations of frequency (0.1 Hz in low frequencies and 2 Hz at mid-frequencies). These results are presented in Figure 50.

Figure 50 - Results for short step investigation on φ, for (a, c) low and (b, d) mid-range frequencies, in (a, b) pure compression and (c, d) pure tension, at 90 to 120 days

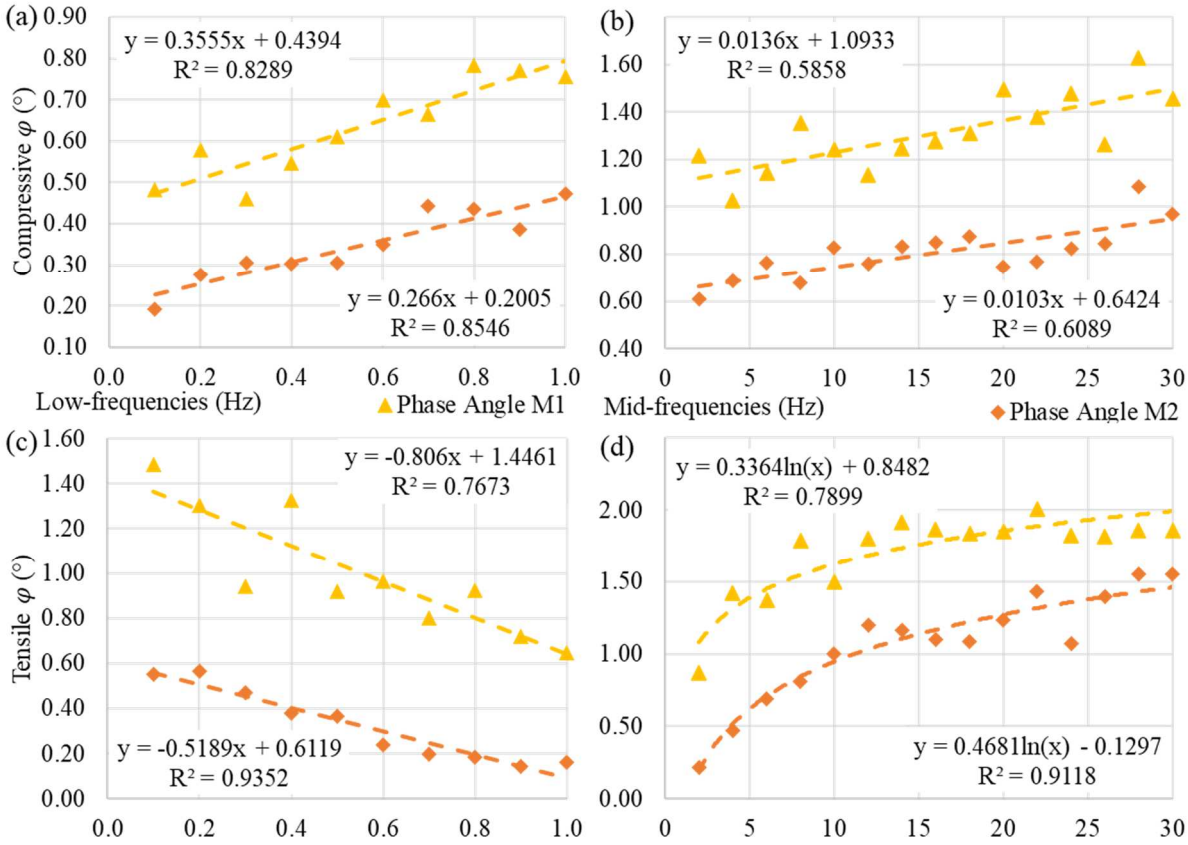

Source: Author (2023).

The φ behavior diverged from the literature in some cases, a trend that is currently under investigation. It is expected a reduction in the φ results when the frequency increases

(Bažant; Jirásek, 2018; Evangelista Junior; Macedo; Farias, 2019). In this way, only the results of φ in low frequencies and pure tension followed this behavior. It is worth noting that there could be a possibility of a systematic error influencing these trends. If present, these potential errors appear to be in an acceptable range.

By approaching the linear models to the y-axis (frequency tending to 0) we can also gain insights into the mechanical properties in quasi-static loading and the creep behavior. The higher φ, the higher the potential of creep effects under static loadings over time (Bažant, 1970; Bažant; Jirásek, 2018; Lemaitre; Chaboche, 1990). Further research is needed to understand these results and their implications on the material properties.

The current results present the M2 with a lower susceptibility to creep effects by accounting for the y-intercept approach. The average results were 0.76° and 0.99° for M1, and 0.42° and 0.24° for M2 (compression and tension respectively). Finally, it can be seen that M2 presented a lower viscous parcel and a lower potential for creep effects. It's also worth considering that these trends might be influenced by our measurement techniques rather than being solely due to the inherent properties of the materials.

Furthermore, it can be concluded that the quasi-static characterization can provide several insights for fatigue tests and characterization, providing (i) an estimation of the initial complex modulus to be expected, in terms of $|E^*|$ and φ, and with the phase angle as an important parameter that may be behind observations of temperature increase during fatigue tests in the literature (Konsta-Gdoutos; Danoglidis; Shah, 2019; Oneschkow, 2016; Zhao *et al.*, 2013), (ii) the investigation of the frequency influence, providing additional parameters for the loading frequency on the fatigue tests, and (iii) an initial investigation of the creep effects.

4.3.3.2 Pure Tension Fatigue characterization

The results of the fatigue in pure tension are presented, whereas Table 17 summarizes the specimen counting over the experiments.

Table 17 – Summary of the fatigue specimens' usage and rejection

Description	M1	M2
Specimens Tested	22	12
Specimens Rejected	12	3
Specimens Used	10	9

Source: Author, 2013

Early ruptures were observed during some of the initial loading ramps or even ruptures with significantly fewer cycles than expected for the tested stress level. It was necessary

to evaluate their conformity based on mechanical and visual aspects. Those criteria included (i) the initial estimation of Nf, based on the experimental data available in the literature and from the other obtained results, (ii) the verification of the conformity of the stress-strain levels, based on the average stress-strain results from previous specimens (after a minimum triplicate) and the stress-strain results from tensile strength tests, (iii) the visual inspection of uniformity and homogeneity of the rupture section, and (iv) rupture on the loading ramp.

Based on that verification, the lack of uniformity was the aspect most visualized/incident during the specimens' verification, with entrained air voids (EAV) and pores concentration in almost all rupture sections. Secondly, it was observed several early ruptures, with fewer cycles than excepted and even during the initial loading, which was attributed to variations in the strength levels. Those specimens with abnormalities had their results discarded. Figure 51 illustrates an example of this scenario.

Figure 51 - Ruptures for M1 (a) and M2 (b), with their section defects details (c)

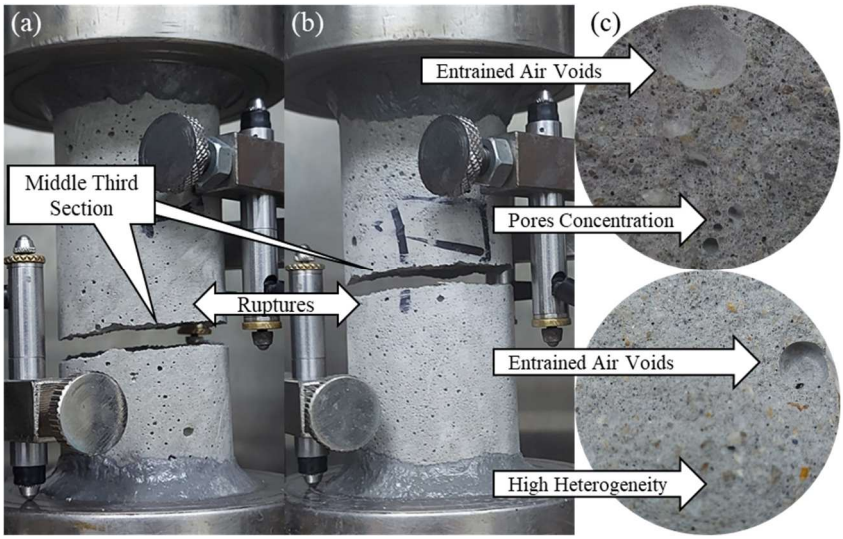

Source: Author (2023).

The fatigue test stop criterion encompassed two criteria: (i) the specimen collapse, with the number of cycles at failure, if lower than 10^6 cycles, and (ii) the test interruption at 10^6 cycles. During that period (28 hours of testing), there were no interruptions, with continuous loading application. The EL is the stress level under which the materials can withstand a theoretically indefinite number of cycles. It can be determined experimentally by using a fatigue model for the S-N curve and an adopted criterion of long-term cycles.

There are differences between methodologies and standard codes on EL (Beriha; Sahoo; Steyn, 2019; CEB, 1990; DNV, 2004; EUROCODE, 2004). However, the current EL was set to the stress level at which the number of cycles at failure is 10^7 cycles, being the most conservative criterion among those reviewed. Finally, Figure 52 presents the experimental data

of the fatigue tests in the form of an S-N curve for M1, with its respective candidate fatigue models assessed and determined ELs.

Figure 52 - Fatigue Results and Models for M1 formulation at 10 Hz

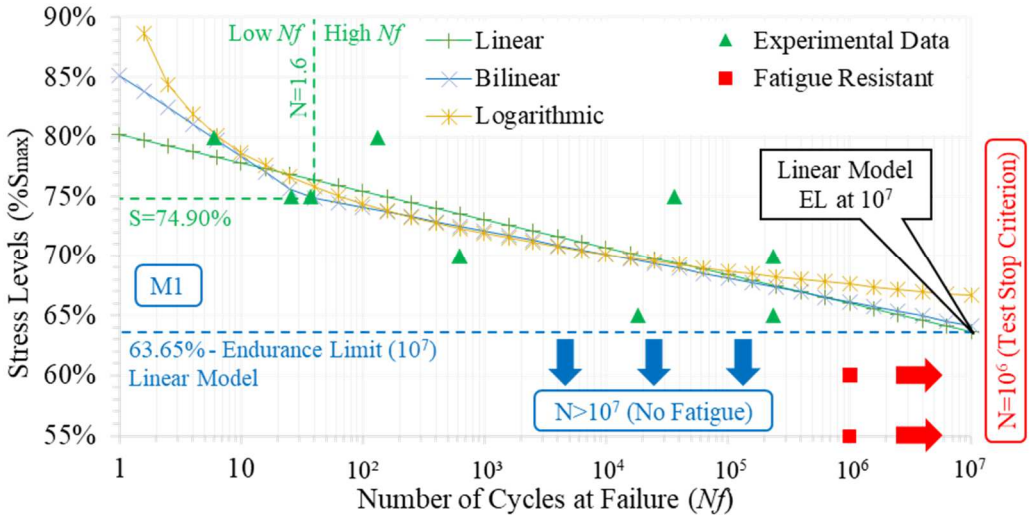

Source: Author (2023).

The axes consist of a log-linear base plot. The M1 experimental on the specimens' rupture ranged from 55% up to 80% of S_{max}. In the range of 85% to 100%, all the specimens presented rupture during the loading ramp, not achieving a complete loading cycle in the fatigue tests (which can be expected for stress levels near 100%). These results were confirmed in triplicate. For that reason, this specific data was not included, even though they would not be far from two of the models (bilinear and logarithmic) displayed in Figure 52. Only two M1 specimens achieved 10^6 cycles (with Stress Levels of 55% and 60%), highlighted in red so that the tests were stopped without visible failure. They were not used for the data fitting with the fatigue model curves either.

Concerning the fatigue models, the experimental fatigue data (after discarding early failures and failures at 10^6 cycles) were modeled using three numerical models, (i) linear, (ii) bilinear, and (iii) logarithmic. By assessing the standard codes and literature on this subject (Beriha; Sahoo; Steyn, 2019; CEB, 1990; DNV, 2004; EUROCODE, 2004), linear or bilinear models in a log-linear base are usually adopted, with a special case for this last one, due to a transition between low and high cycle resistance regimes. Such a clear transition could not be directly observed in the experimental data, but still, the model was evaluated. Table 18 presents the fitted models and the corresponding ELs (considering the criterion of failure at 10^7 cycles) for M1 results.

Table 18 - M1 Interpolated Fatigue Models, Accuracy Evaluation and respective ELs

Models	Equations	R² Score	ELs
Linear	$\%S_{max}(N) = -0.0228 * N + 0.7928$	0.4956	63.65%
Bilinear	$\%S_{max}(N) = \begin{cases} -0.0677 * \log_{10} N + 0.8516, & x < 1.6 \\ -0.0199 * \log_{10} N + 0.7809, & x \geq 1.6 \end{cases}$	0.4986	64.16%
Logarithmic	$\%S_{max}(N) = -0.062ln(N) + 0.7836$	0.545	66.65%

Source: Author, 2013

On the adjusted models, the logarithmic showed a better fit. When evaluating the boundary conditions, which include the rupture points at lower stress levels and the points that met the stop criteria, the EL of the logarithmic model did not fit these aspects. Specifically, it did not encompass the behavior of the two rupture points at 65% of S_{max}. It was initial evidence for the evaluation of further numerical approaches.

The linear and bilinear models had similar accuracy results (R² of 0.4956 and 0.4986), having the first a more conservative EL of 63.65%. Additionally, the transition between low and high cycles regime for the bilinear model ($Nf = 10^{1.6}$), illustrated in the Figure 52 by the transition from Low Nf and High Nf, was low compared to the literature results, which are about 10^3 to 10^4 cycles (Kachkouch *et al.*, 2022; Oneschkow, 2016), also indicating an additional deviation in that aspect.

Based on that scenario, for the M1 formulation, it was adopted a linear model to describe its experimental fatigue data on the S-N curve. A similar procedure was conducted for the M2 formulation. Figure 53 presents the corresponding experimental data, interpolated models and ELs obtained.

Figure 53 – Fatigue Data and Adjusted Models for M2 formulation at 10 Hz

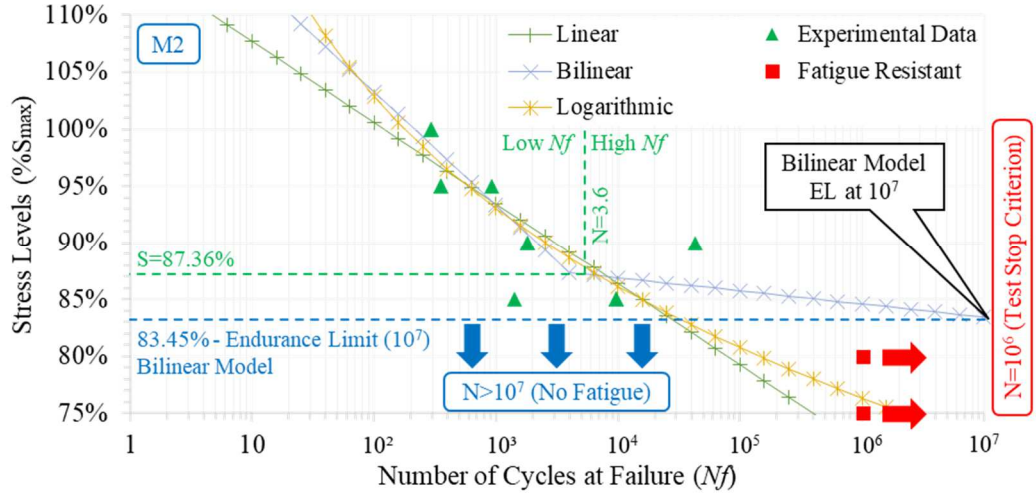

Source: Author (2023).

The M2 rupture data concentrated a range with Nf from 10² up to 10^5, with stress levels from 85% up to 100% also presenting early failures, similar to M1. Two specimens meet the stop criteria once more. There was a lower variance in the global aspect of M2 results when compared to M1, with experimental data closer to the models. This is an effect of the lower variance on the mechanical characterization and microstructural aspects presented previously for other observed properties. Table 19 presents the fitted models and the corresponding ELs (considering the criterion of failure at 10^7 cycles) for M1 results.

Table 19 – M2 Interpolated Fatigue Models, Accuracy Evaluation and respective ELs

Models	Equations	R² Score	ELs
Linear	$\%S_{max}(N) = -0.0712 * N + 1.1484$	0.6965	65.00%
Bilinear	$\%S_{max}(N) = \begin{cases} -0.0997 * \log_{10} N + 1.2322, & x < 3.6 \\ -0.0115 * \log_{10} N + 0.915, & x \geq 3.6 \end{cases}$	0.5145	83.45%
Logarithmic	$\%S_{max}(N) = -0.241ln(N) + 1.1954$	0.7522	72.64%

Source: Author, 2013

The logarithmic and linear models presented higher R² scores. However, when assessing their respective ELs and the points that met the test interruption criterion (fatigue resistant points), they were not able to encompass these boundary conditions. The bilinear model presented a better ability to foresee those aspects, despite the lowest R² score. It indicates that the adjustment accuracy is not an entirely comprehensive evaluation parameter of these models.

Li *et al*. (2016) evaluated the fatigue life of cementitious material with fibers. It was demonstrated that the R² score is not accurate for the evaluation of fatigue models. Instead, the fatigue resistance under similar stress levels and the careful interpretation of the physical behavior are more accurate for that evaluation . Similarly, Balbo *et al*. (2021) also provide further evidence adopting the bilinear model in the investigation of concrete fatigue behavior.

By comparing the Nf results for similar S_{max} (such as 75% and 80%) M1 obtained an average of 10^3 cycles while all tests of M2 achieved the interruption criteria of 10^6 cycles. Additionally, for the bilinear model, the transition between low and high fatigue cycles ($Nf = 10^{3.6}$), settled exactly between 10^3 to 10^4 cycles, values reported from the literature (Kachkouch *et al*., 2022; Oneschkow, 2016).

Moreover, by comparing the R² of both experimental data (M1 and M2), it was visualized that the current models presented higher scores, an influence of lower variances and higher homogeneity, explained by the improved microstructure (Wei; Liang; Kong, 2023).

Figure 54 presents both experimental data with the chosen fatigue models, ELs, and fatigue limit of some classical standard codes for design (known as CEB-FIP, DNV, and EC2) (CEB, 1990; DNV, 2004; EUROCODE, 2004) as a comparison.

Figure 54 - S-N Curves results for pure tension loading regime at different ages

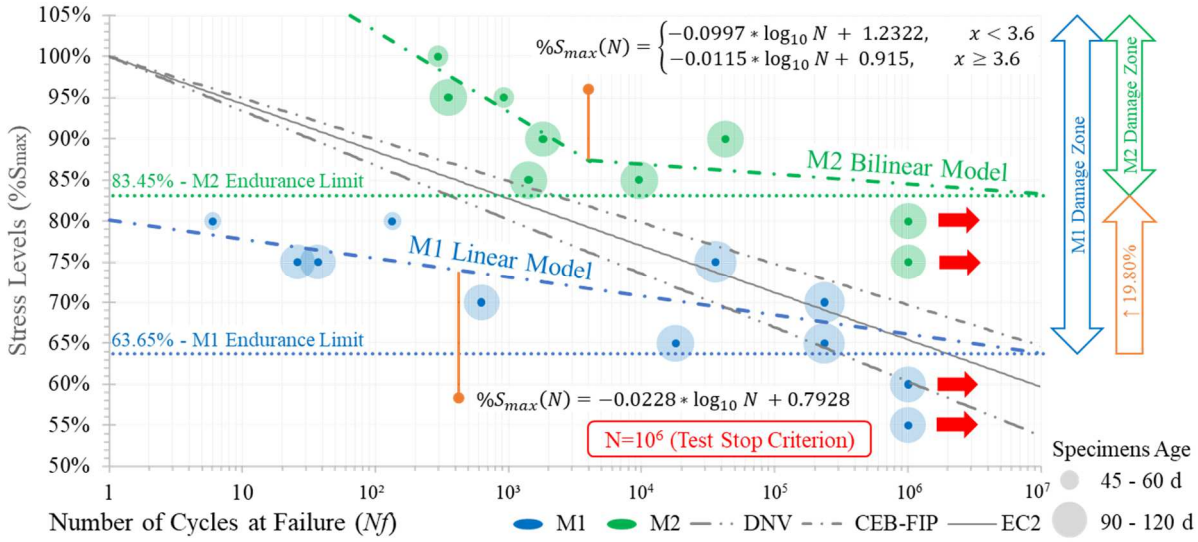

Source: Author (2023).

By comparing both formulations, M2 demonstrated a higher fatigue resistance, with consistent and non-overlapped results. As a second metric, it is possible to compare the ELs, having an increase of 19.80%. This specific result has several implications for structural design and materials' durability on service. A higher EL implies that the material can be submitted to higher stress levels (by the order of 20%) with an equivalent risk of failure. Also, for a given stress level, more cycles are needed to lead the material to failure.

In structural applications, it may result in slender structures and reduced cross-section, with increased durability. It also has improved aspects of sustainability once less maintenance would be required. The EL denotes the maximum stress that a material can endure for an infinite number of cycles. The EL is particularly significant in this context as it provides a stress limit that the material can safely endure over without the risk of fatigue failure.

A higher EL, as exhibited by M2, implies that the material can withstand higher stress levels (+19.80%) for the same number of cycles, or the same stress level for more cycles, thereby augmenting the structure's durability and reducing maintenance requirements, implying reduced cross-sections without compromising durability, thereby enhancing sustainability and cost-effectiveness. Moreover, it is possible to compare the current experimental results in pure tension with the fatigue standard codes of concrete in compression (CEB, 1990; DNV, 2004; EUROCODE, 2004), for a theoretical comparison.

The M1 experimental results were predominantly lower than all the three standard codes presented, indicating its poor performance compared to the minimum requirements of fatigue resistance adopted for creating these standards. This may indicate that structures with regular OPC, submitted to similar stress levels in pure tension, may experience fatigue.

On the other hand, all M2 experimental points exceeded the minimal fatigue resistance of the standard codes. In general, the SCM additions, in the mix design of the proposed formulation, seemed to improve fatigue resistance. Also, structures designed using M2, submitted to similar conditions to those referred codes, would have more durability than regular OPC formulations, and may not be experiencing fatigue.

Different microstructural aspects may influence that outcome. The improvement in the viscoelastic behavior (by the lower viscous parcel, addressed by the quasi-static characterization results), reduces the potential of cracks' formation, which directly impacts fatigue. This lower potential results in the material having a lower degradation when subjected to cyclic loads, withstanding higher stress levels, and lasting more cycles.

Additionally, there is another aspect concerning the improved pores' structure and denser cement matrix (with lower cracks' incidence and more compact CSH formation), demonstrated by the porosity, SEM and TG analysis. Fatigue is governed by the cracks' nucleation and their coalescence (Kachkouch *et al*., 2022; Lemaitre; Sermage; Desmorat, 1999; Myrtja *et al*., 2021; Oneschkow, 2016; Zhao; Chang; Yang, 2008).

The improved microstructural integrity mentioned makes it more difficult for the concrete to experience these processes, especially on the cracks' propagation, leading to more durable and fatigue-resistant materials. The complex modulus degradation curves ($|E^*|$ and φ as a function of the number of cycles) were also addressed. Figure 55 presents an example of the degradation curves.

Figure 55 - $|E^*|$ and φ curves for (a) M1 at 114 days and (b) M2 at 96 days

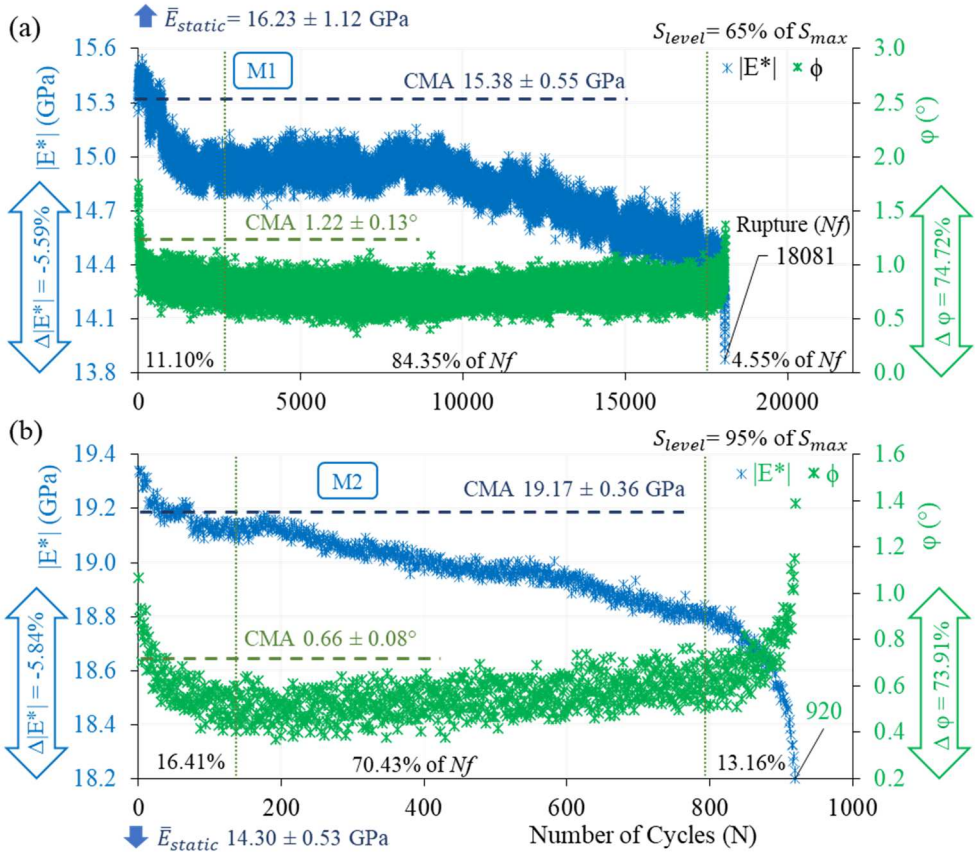

Source: Author (2023).

Based on the results, different aspects can be addressed, such as (i) the difference in the curves' shape format, (ii) the variation in the $|E^*|$ and φ curves, (iii) the curve division into three stages and its proportion, and (iv) a comparison with the CMA results. By comparing the curve shape with the literature, it was found that $|E^*|$ curves presented a similar degradation behavior from pure compression usual results (Kachkouch *et al.*, 2022; Myrtja *et al.*, 2021; Zanuy; Albajar; De La Fuente, 2011).

By comparing the average variations in both signals for both formulations, the M2 degradation curves presented a lower signal noise for both complex modulus parameters. This is a possible reflection of the low variance of error addressed by all the mechanical tests.

The $|E^*|$ and φ absolute variation measures the material's ability to withstand degradation before collapse. Those average degradations were similar (5.59% and 5.84%). Assessing the literature on the same parameter (Myrtja *et al.*, 2021), it was found variation ranges up to 35%. It reflects the short ability of cementitious materials to accumulate damage in pure tension (while most results in the literature are in compression).

Moreover, by assessing the three-stage division of the Nf, there were alterations in the first and third stages. The third segment provides additional information on the rupture of

the specimen. The M1 presented a shorter third segment, which means a segment of rupture with less damage accumulation compared to M2. It has similarities with the behavior of fragile ruptures, being more abrupt this segment.

In this way, the M2 formulation presented a superior behavior, with a higher proportion, influenced by the improved microstructure. Once it is more difficult to coalescence macrocracks, it is necessary to have more cracks incidence to indeed lead the specimen to collapse. Figure 56 presents the visual aspects of the rupture sections.

Figure 56 - Splitting sections for (a) M1 and (b) M2 with their respective details (c, d)

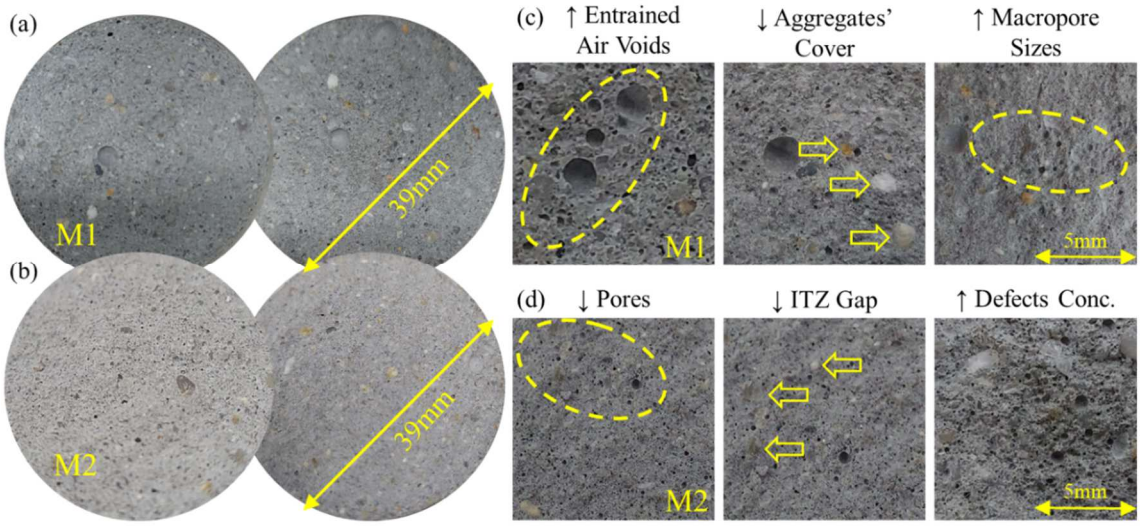

Source: Author (2023).

The M2 whiter aspect was attributed to the influence of the SCMs. Its visual aspect presents a higher uniformity, with a better aggregate covering, as addressed by the microstructure section (by the SEM and porosimetry analysis). For most of the rupture sections, there was a recurrent pattern of defects (mainly EAVs and macropores concentration observations on the ruptures sections visual inspections).

Based on the experimental observations, the entrained air voids (EAVs) were demonstrated as a highly sensitive issue for fatigue, which is aligned with the literature (Li; Ren, 2009; Zhao; Chang; Yang, 2008). It was incident in all rupture sections.

The stochastic damage model is a concept based on the energy equivalent strain, considering the nonlinearity and randomness of cementitious materials (Li; Ren, 2009). The model reproduces the multi-dimensional stochastic nonlinear behaviors and predicts the randomness of multiaxial strength, which is important for explaining their reliability and degradation. Figure 57 illustrates the mentioned damage model.

Figure 57 - Stochastic Damage Model for discrete (a) and continuous bundles (b)

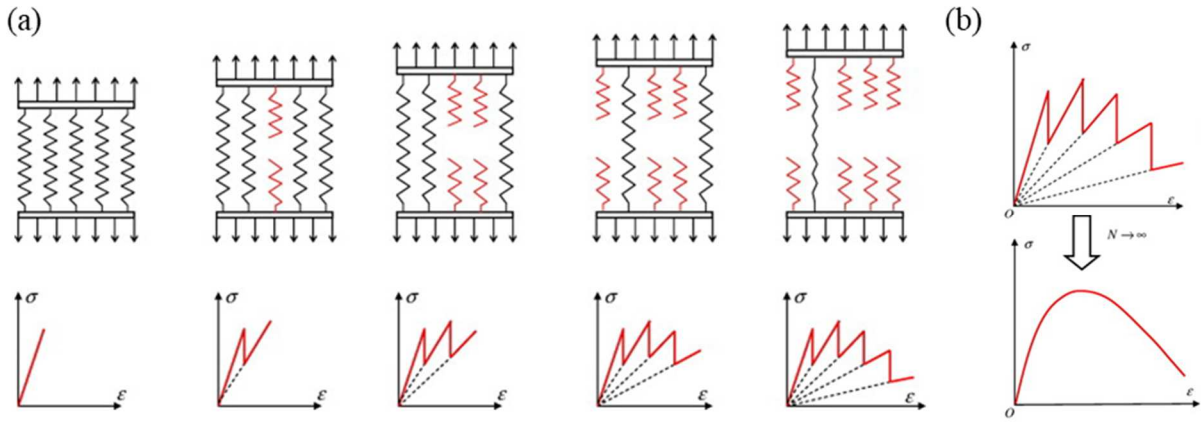

Source: (LI; REN, 2009).

This model can feasibly explain the abnormality in the complex modulus degradation curves, with abrupt drops and signal disruption in the $|E^*|$, also encompassing the EAVs degradation in the cement matrix. Each EAV bubble represents a break or absence of one of the springs in the parallel element model, around which it will probably be easier to nucleate and propagate new cracks. In this way, the presence of EAVs introduces additional randomness and nonlinearity into the mechanical properties, affecting the damage predictions. Then, such kind of model seems as a potential way to explain the abrupt changes and signal disruptions highlighted in $|E^*|$ degradation curves, from Figure 55.

The fatigue results, when juxtaposed with the microstructural analysis, provide quantitative parameters for fatigue investigation and experimental program. The heat of hydration analysis, characterized by results with lower peak amplitude, reduced the potential for thermal and early-age crack formation, resulting in a material with fewer available spots for crack nucleation and propagation, a conclusion supported by the microstructural analysis (on the SEM images, porosimetry, and TG results) and fatigue tests.

The workability results provided potential results for a lower W/B ratio, attributable to the influence of GP coarse particles. This water reduction could have leaded to results of improvements of ITZ and enhancements on the strength. The denser materials, as corroborated by SEM and porosimetry, directly contribute to the higher fatigue resistance for M2.

Lastly, regarding the structural components of the cement matrix (specifically the CSH, Portlandite, and Calcite contents) the porosimetry, SEM images, and TG analysis, their higher content contributed to the improved mechanical behavior (Wei; Liang; Kong, 2023), and fatigue resistance observed (Kachkouch *et al*., 2022; Myrtja *et al*., 2021).

In conclusion, addressing microstructural aspects for fatigue analysis provided a way to design a more fatigue-resistant matrix, which was confirmed with fatigue test results

afterward. Such analysis also provides additional quantifiable parameters for formulation, which are quicker to perform in the laboratory than fatigue tests.

4.4 Final Comments

This paper investigated the influence of the microstructure and SCMs on the stiffness and tensile fatigue behavior of cementitious materials, with a special focus on GP and SF as SCM additions. Such topics were observed as a gap in the literature after a comprehensive bibliometric analysis.

Based on the findings and evaluations, the microstructure experimental investigation demonstrated the potential to directly address and investigate the fatigue phenomenon in more in-depth detail. The fatigue tests and stiffness characterization confirmed the same findings of the microstructure analysis (that the proposed formulation, M2, would have an improved fatigue resistance and stiffness behavior).

Summarizing the contributions to the literature, the microstructure analysis demonstrated feasible parameters for the development of more durable and fatigue-resistant materials. Also, the SCMs proved to have a positive impact on fatigue resistance. On the proposed formulation, M2, the stiffness was improved by up to 24% (from the quasi-static characterization results), and the fatigue resistance had a higher EL, with up to 19.80% improvement (from fatigue tests) being all aligned with different microstructural enhancements (denser cement matrix, higher CSH formation, lower incidence of cracks, as well as other findings). Such work led to the further conclusions described below:

- Formulations with low h□at of hydration ar□ pr□f□rr□d for appli□ations subj□□t□d to fatigu□;
- The SCM additions contributed to a lower thermal energy release rate, having a lower cracks' incidence (demonstrated by the SEM analysis) and improved microstructural integrity, aligned with the improved fatigue resistance results;
- There was a 61.36% reduction in the mesopores range, attributed to a higher CSH formation, impacting stiffness and fatigue behavior (explained by the CMA analysis and fatigue results);
- The microstructural investigation was demonstrated to be less time-consuming than the experimental campaign on fatigue. While fatigue investigation can last months (4 for the current case), the microstructural program was feasible to complete in 28 days;
- On the quasi-static characterization results, the M2 formulation demonstrated an average improvement of 8.22% and 24.64%, for compressive and tensile results respectively, with

a consistently higher $|E^*|$ and lower φ, indicating an overall more recoverable behavior;

- It was visualized an aging effect by comparing results of 45 and 90 days, with a reduction of the φ, suggesting a more recoverable mechanical behavior for higher ages (lower φ);
- An in-depth analysis of the fatigue models resulted in the adoption of two different models, (i) a linear for M1 and (ii) a bilinear for M2 which fitted the fatigue failure results and also predicted correctly the points of the interruption criterion (10^6 cycles with no failure);
- The M2 formulation was consistently more resistant and stiffer on the quasi-static behavior, comparing the experimental data, fatigue models, and endurance limits;
- The M2 ELs and damage zones were improved by 19.80%. It implies a material with a greater bearing capacity to withstand higher loading levels without degradation;
- The M1 experimental data and fatigue model did not meet the minimum requirements of the theoretical standard codes, while both aspects for M2 were exceeded.

5 FINAL CONSIDERATIONS AND SUGGESTIONS FOR FUTURE RESEARCH

The primary objective of this study was to investigate the influence of microstructural aspects and SCMs on the fatigue behavior of cementitious materials, assessing their impact on fatigue. Fatigue tests in pure tension were also addressed. The results suggested that this microstructural approach provided additional parameters for the understanding and investigation of the fatigue, further to the sole characterization through cyclic load resistance.

The results of microstructural analysis such as (i) lower heat of hydration, (ii) denser cement matrix, (iii) lower cracks incidence, (iv) lower porosity, and improved pores structures were aligned with the improved results of fatigue resistance, with 19.80% higher endurance limits. The improvement of fatigue resistance was addressed by gathering the literature recommendations and the addition of GP and SF, into the proposition of cement formulations, and then confirmed with pure tension fatigue tests.

The GP (i) demonstrated to have a positive long-term effect on the gain of strength, contributing to improved stiffness and fatigue resistance (ii) favored the adoption of lower W/B ratios, (iii) improved the CSH formation, and (iv) contributed to consistently higher $|E^*|$ and lower φ in quasi-static characterization, attributing a more elastic and recoverable behavior.

Furthermore, the SF particle directly addressed the cement matrix by fulfilling the pores structures. There was a (i) drop in the porosimetry up to 61.36% in the mesopores range, (ii) lower cracks incidence by the SEM images, and (iii) denser CSH formation, presenting a crystal formation with no visible gaps and cracks. All these mentioned aspects have a proven positive influence on fatigue and were aligned with the improved resistance found.

Therefore, the proposed methodology succeeded in achieving the primary objective, demonstrating the relevance of microstructural aspects on mechanic, quasi-static, and fatigue behavior, highlighting the positive influence of SCM additions on the composites, and providing an experimental fatigue characterization in pure tension. The following section summarizes the most relevant considerations from the three articles, relating those findings with each of the four specific objectives proposed in this MSc thesis.

5.1 Summary Of Conclusions

5.1.1 Specific Objective 1

To evaluate the potential of GP and SF additions, as potentially beneficial SCMs, in cementitious materials, to improve mechanical aspects, physical parameters, and fatigue behavior focusing on the influence of the microstructural changes.

- The proposed formulation demonstrated higher modulus, with improvements up to 37% in the complex modulus for 45 days, which is beneficial for fatigue;
- The proposed formulation, exhibited a 23% modulus increase and lower φ in pure tension from 90 to 120 days, with a more elastic behavior;
- The GP and SF addition demonstrated a lower thermal energy release, which is beneficial for the hydration products, reducing the formation of early-age cracks;
- According to the TG and porosimetry results, the GP and SF addition improved the CSH formation and reduced the portlandite and calcite content. This is aligned with the improved fatigue resistance.

5.1.2 Specific Objective 2

To propose and validate a mechanical characterization method able to assess the viscoelasticity of cementitious materials under cyclic loads for both compression and pure tension.

- The proposed method was able to consistently identify viscoelastic results and yielded experimental outcomes consistent with the literature on asphalt concrete, cementitious concrete, grouts and steel specimens;
- On the validation procedure, there was a statistical difference in the characterization of the $|E^*|$ and φ under pure compressive and tensile stresses. This indicates a frequency-dependent behavior, which is consistent with further experimental data in the literature;
- For complex modulus analysis (CMA) results in pure compression and pure tension, the ANOVA indicated no statistically significant difference in $|E^*|$. However, it was identified in the φ for both formulations in the same scenarios.

5.1.3 Specific Objective 3

To investigate the influences and direct implications of the microstructural aspects on the mechanic, quasi-static, and fatigue behavior, while evaluating optimization potentials.

- The low-heat cement formulations demonstrated to have a lower potential of early-age cracks or DEF manifestations, which positively impacts fatigue behavior;
- The SEM analysis demonstrated a denser and more uniform microstructure. This resulted in a reduction in pores structures by a factor of 2.5 and a 33% decrease in gap widths;
- The CSH formation was denser and more compact. It positively impacted the microstructure cohesion, resulting in lower crack initiation and lower coalescence;
- The reduction in average porosity and a 61.36% reduction in mesopores range, were attributed to the improved CSH formation due to the GP and SF addition;
- By comparing the TG results with porosimetry it was reaffirmed that the GP and SF addition improved the CSH formation and reduced the portlandite and calcite content;
- There was a significant influence of the ITZ on fatigue, especially concerning the cracks coalescence, underscoring their importance in durability;
- There was an aging effect on the quasi-static behavior, by comparing the 45-day aging and the 90-day aging results, presenting a more elastic behavior for long ages;
- In summary, the intricate interplay between microstructural aspects, physical parameters, mechanical behavior and durability, contributes to a more comprehensive understanding of their behavior under quasi-static and fatigue conditions.

5.1.4 Specific Objective 4

To evaluate the fatigue behavior in pure tension and respective degradation curves by comparing them with the available literature and standard codes.

- By assessing the static elastic modulus results of both formulations there was no significant difference in the quasi-static loading characterization, presenting converging confidence intervals between the assessed formulations. However, the CMA results diverged, showing an average improvement from 8.22% to 24.64% with non-overlapping confidence intervals in the frequency domain;
- Concerning the testing observations, the lack of uniformity and variations in the specimens' strength level were the most impacting difficulties for the correct assessment of the fatigue resistance. It led to incorrect results of the number of cycles at failure diverging from the general aspect of the obtained results;
- The entrained air voids were observed in all ruptur sections;
- The proposed formulation consistently demonstrated a higher fatigue resistance, and

improved endurance limits, with a 19.80% increase in those EL levels;

- On the grout application of regular OPC, the fatigue findings did not meet the requirements based on all three standard codes assessed;
- The degradation curves followed the expected behavior described in the literature, with a discrepancy in the φ curves in the S1 range;
- It was demonstrated the importance of the quasi-static characterization. Those methods provided important additional information on the stiffness behavior for static and quasi-static loading regimes, which are valuable parameters for fatigue characterizations;
- There was a 24.64% improvement in the average modulus of the CMA results which was near to the improvement of 19.80% in fatigue ELs. This indicates that alterations in the stiffness behavior directly affect fatigue, whereas the quasi-static characterization provides additional parameters to corroborate the fatigue findings.

5.2 Future Research Suggestions

In conclusion, this master's thesis has shed light on the relationship between SCMs' additions, mechanical behavior and fatigue of cementitious materials. However, there remain several gaps for future research that can further enhance the understanding of this field.

The fatigue models had to be extrapolated to calculate the endurance limit (EL), and the EL of M2 was significantly higher due to its particular choice of the bi-linear model. One way to eliminate this is to perform longer fatigue tests, aiming to exceed 10 million cycles and be able to confirm if its EL is what was estimated by extrapolation. Moreover, the following research directions are recommended upon the findings presented:

- To investigate further analysis methods to complement the proposed characterization and quantify degradation over time (accounting for energy dissipation, self-heating effect and damage calculation), providing more robust models concerning fatigue damage analysis;
- To explore the effect of loading amplitudes and temperature on mechanical behavior, providing insights into stress variations and thermal degradation over the years;
- To review the current standard regulations on fatigue assessments of cementitious materials, with an aim to incorporate quasi-static characterizations, thereby providing a more comprehensive characterization beyond the usual assessments;
- To perform durability tests to substantiate the claims of improved resistance to pathological manifestations, assessed by related experimental results.

These future research endeavors will contribute to a more comprehensive assessment of long-term structural performance, guiding the development of materials with tailored properties while considering sustainability factors.

In summary, future research undertakings should strive to bridge the gaps, improve testing protocols and advance the understanding of crucial aspects like stiffness and fatigue behavior, addressing the influence of the microstructure and SCMs.

These efforts will undoubtedly contribute to the continued development of more durable and sustainable materials and structures. Finally, the differences addressed are feasible for further investigations providing valuable knowledge for improvement in the fatigue and quasi-static behavior.

REFERENCES

ABDELLI, Houssam Eddine; MOKRANI, Larbi; KENNOUCHE, Salim. Mechanical and Durability Properties of Concrete Incorporating Glass and Plastic Waste. **Advances in concrete construction** , *[S. l.]*, v. 11, n. 2, p. 173–181, 2021. DOI: https://doi.org/10.12989/acc.2021.11.2.173. Disponível em: http://koreascience.or.kr/article/JAKO202110348497922.page. Acesso em: 29 agosto 2023.

ABIRAMI, S.; CHITRA, P. Energy-efficient edge based real-time healthcare support system. **Advances in Computers**, *[S. l.]*, v. 117, n. 1, p. 339–368, 2020. DOI: 10.1016/BS.ADCOM.2019.09.007. Disponível em: https://www.sciencedirect.com/science/article/abs/pii/S0065245819300506. Acesso em: 30 ago. 2023.

ASSOCIAÇÃO BRASILEIRA DE NORMAS TÉCNICAS. **ABNT NBR 5739:** Concreto - Ensaio de compressão de corpos-de-prova cilíndricos. Rio de Janeiro: ABNT, 2007. 4p. Disponível em: https://www.abntcatalogo.com.br/norma.aspx?ID=3998. Acesso em: 3 set. 2023.

ABZAEV, Yu. A.; KOROBKOV, S. V.; ANIKANOVA, L. A.; STARENCHENKO, V. A. Thermodynamic simulation of Portland cement hydration with different water content. Vestnik Tomskogo gosudarstvennogo arkhitekturno-stroitel'nogo universiteta. **Journal of Construction and Architecture**, *[S. l.]*, v. 24, n. 5, p. 122–132, 2022. DOI: 10.31675/1607-1859-2022-24-5-122-132. Disponível em: https://vestnik.tsuab.ru/jour/article/view/1315/864. Acesso em: 10 set. 2023.

ADESINA, Adeyemi; DAS, Sreekanta. Influence of glass powder on the durability properties of engineered cementitious composites. **Construction and Building Materials**, *[S. l.]*, v. 242, p. 118199, 2020. DOI: 10.1016/J.CONBUILDMAT.2020.118199. Disponível em: https://www.sciencedirect.com/science/article/abs/pii/S095006182030204X. Acesso em: 30 ago. 2023.

ADIL, Goran; KEVERN, John T.; MANN, Daniel. Influence of silica fume on mechanical and durability of pervious concrete. **Construction and Building Materials**, *[S. l.]*, v. 247, p. 118453, 2020. DOI: 10.1016/j.conbuildmat.2020.118453. Disponível em: https://www.sciencedirect.com/science/article/abs/pii/S095006182030458X. Acesso em: 17 set. 2023.

AKÇAOĞLU, Tülin; ÇUBUKÇUOĞLU, Beste; TARASSOLY, Amir Reza. Effects of Glass Powder as a Supplementary Cementitious Material on the Performance of High Strength Mortars. **Journal of Testing and Evaluation**, *[S. l.]*, v. 48, n. 5, p. 20180140, 2020. DOI: 10.1520/JTE20180140. Disponível em: https://www.astm.org/jte20180140.html. Acesso em: 17 set. 2023.

AL-HASANI, Luna E. et al. Prediction of heat of hydration of cementitious systems using Gaussian process regression enables mass concrete thermal modeling. **Materials and Structures**, *[S. l.]*, v. 56, n. 2, p. 45, 2023. DOI: 10.1617/s11527-023-02134-8. Disponível em: https://link.springer.com/article/10.1617/s11527-023-02134-8. Acesso em: 25 jul. 2023.

ALI, Muna M. M. Modified limited-memory Broyden-Fletcher-Goldfarb-Shanno algorithm for unconstrained optimization problem. **Indonesian Journal of Electrical Engineering and Computer Science**, *[S. l.]*, v. 24, n. 2, p. 1027, 2021. DOI: 10.11591/ijeecs.v24.i2.pp1027-1035. Disponível em: https://ijeecs.iaescore.com/index.php/IJEECS/article/view/24877. Acesso em: 5 jul. 2023.

AL-SWAIDANI, Aref M.; KHWIES, Waed T.; AL-BALY, Mohamad; LALA, Tarek. Development of multiple linear regression, artificial neural networks and fuzzy logic models to predict the efficiency factor and durability indicator of nano natural pozzolana as cement additive. **Journal of Building Engineering**, *[S. l.]*, v. 52, p. 104475, 2022. DOI: 10.1016/J.JOBE.2022.104475. Disponível em: https://www.sciencedirect.com/science/article/abs/pii/S2352710222004880. Acesso em: 30 ago. 2023.

ANGLANI, Giovanni; TULLIANI, Jean-Marc; ANTONACI, Paola. Behaviour of Pre-Cracked Self-Healing Cementitious Materials under Static and Cyclic Loading. **Materials**, *[S. l.]*, v. 13, n. 5, p. 1149, 2020. DOI: 10.3390/ma13051149. Disponível em: https://www.mdpi.com/1996-1944/13/5/1149. Acesso em: 10 ago. 2023.

ANTONI; CHANDRA, Lucky; HARDJITO, Djwantoro. The Impact of Using Fly Ash, Silica Fume and Calcium Carbonate on the Workability and Compressive Strength of Mortar. **Procedia Engineering**, *[S. l.]*, v. 125, p. 773–779, 2015. DOI: 10.1016/J.PROENG.2015.11.132. Disponível em: https://www.sciencedirect.com/science/article/pii/S1877705815034499. Acesso em: 30 ago. 2023.

ANURAG; KUMAR, Rajesh; GOYAL, Shweta; SRIVASTAVA, Abhishek. A comprehensive study on the influence of supplementary cementitious materials on physico-mechanical, microstructural and durability properties of low carbon cement composites. **Powder Technology**, *[S. l.]*, v. 394, p. 645–668, 2021. DOI: 10.1016/j.powtec.2021.08.081. Disponível em: https://www.sciencedirect.com/science/article/abs/pii/S0032591021007695. Acesso em 30 ago. 2023.

AMERICAN SOCIETY FOR TESTING AND MATERIALS. **ASTM C230/230M; Standard Specification for Flow Table for Use in Tests of Hydraulic Cement**. West Conshohocken, PA. Disponível em: https://civilnode.com/download-standard/10659960260712/ASTM-C230-C230M-Standard-Specification-for-Flow-Table-for-Use-in-Tests-of-Hydraulic-Cement. Acesso em: 1 set. 2023.

AMERICAN SOCIETY FOR TESTING AND MATERIALS. **ASTM C1702-17: Standard Test Method for Measurement of Heat of Hydration of Hydraulic Cementitious Materials Using Isothermal Conduction Calorimetry**. [s.l: s.n.]. DOI: 10.1520/C1702-17. Disponível em: https://www.astm.org/c1702-17.html. Acesso em 21 set. 2023.

AMERICAN SOCIETY FOR TESTING AND MATERIALS. **ASTM D4404-18: Standard Test Method for Determination of Pore Volume and Pore Volume Distribution of Soil and Rock by Mercury Intrusion Porosimetry**. [s.l: s.n.]. DOI: 10.1520/D4404-18. Disponível em: https://www.astm.org/d4404-18.html. Acesso em: 25 set. 2023.

AMERICAN SOCIETY FOR TESTING AND MATERIALS. **ASTM C39/C39M-20 Standard Test Method for Compressive Strength of Cylindrical Concrete Specimens**. West Conshohocken. DOI: 10.1520/C0039_C0039M-20. Disponível em: https://www.astm.org/Standards/C39.htm. Acesso em: 3 set. 2023.

AMERICAN SOCIETY FOR TESTING AND MATERIALS. **ASTM E1876-22: Standard Test Method for Dynamic Young's Modulus, Shear Modulus, and Poisson's Ratio by Impulse Excitation of Vibration**. [s.l: s.n.]. DOI: 10.1520/E1876-22. Disponível em: https://www.astm.org/e1876-22.html. Acesso em: 12 ago. 2023.

AMERICAN SOCIETY FOR TESTING AND MATERIALS. **ASTM C192-15 Standard Practice for Making and Curing Concrete Test Specimens in the Laboratory**. West Conshohocken. DOI: 10.1520/C0192_C0192M-15. Disponível em: https://www.astm.org/c0192_c0192m-15.html. Acesso em: 25 jul. 2023.

BAIKERIKAR, Abhijeet; MUDALGI, Shadab; RAM, V. Vinayaka. Utilization of waste glass powder and waste glass sand in the production of Eco-Friendly concrete. **Construction and Building Materials**, *[S. l.]*, v. 377, p. 131078, 2023. DOI: 10.1016/J.CONBUILDMAT.2023.131078. Disponível em: https://www.sciencedirect.com/science/article/abs/pii/S0950061823007900. Acesso em: 31 ago. 2023.

BALBO, José Tadeu; SEVERI, Andrea Arantes; CERVO, Tatiana Cureau; CARGNIN, Andréia Posser. Fracture bi-linear model parameters and brittleness of high-performance concretes for paving: why fatigue tests matters and cannot be spared? **Revista IBRACON de Estruturas e Materiais**, *[S. l.]*, v. 14, n. 1, 2021. DOI: 10.1590/s1983-41952021000100001. Disponível em: https://www.researchgate.net/publication/348130766_Fracture_bi-linear_model_parameters_and_brittleness_of_high-performance_concretes_for_paving_why_fatigue_tests_matters_and_cannot_be_spared. Acesso em: 13 ago. 2023.

BANI ARDALAN, Reza; JOSHAGHANI, Alireza; HOOTON, R. Douglas. Workability retention and compressive strength of self-compacting concrete incorporating pumice powder and silica fume. **Construction and Building Materials**, *[S. l.]*, v. 134, p. 116–122, 2017. DOI: 10.1016/J.CONBUILDMAT.2016.12.090. Disponível em: https://www.sciencedirect.com/science/article/abs/pii/S095006181631995X. Acesso em: 30 ago. 2023.

BAŽANT, Z. P. Constitutive equation for concrete creep and shrinkage based on thermodynamics of multiphase systems. **Matériaux et Constructions**, *[S. l.]*, v. 3, n. 1, p. 3–36, 1970. DOI: 10.1007/BF02475106. Disponível em: https://www.scholars.northwestern.edu/en/publications/constitutive-equation-for-concrete-creep-and-shrinkage-based-on-t. Acesso em: 16 set. 2023.

BAŽANT, Zdeněk P.; JIRÁSEK, Milan. **Creep and Hygrothermal Effects in Concrete Structures**. Dordrecht: Springer Netherlands, 2018. v. 225 DOI: 10.1007/978-94-024-1138-6. Disponível em: https://link.springer.com/book/10.1007/978-94-024-1138-6. Acesso em: 14 set. 2023.

BECKS, Henrik; AGUILAR, Mario; CHUDOBA, Rostislav; CLASSEN, Martin. Characterization of high-strength concrete under monotonic and fatigue mode II loading with actively controlled level of lateral compression. **Materials and Structures**, *[S. l.]*, v. 55, n. 10, p. 252, 2022. DOI: 10.1617/s11527-022-02087-4. Disponível em: https://link.springer.com/article/10.1617/s11527-022-02087-4. Acesso em: 26 set. 2023.

BECKS, Henrik; AGUILAR, Mario; HEGGER, Josef; CHUDOBA, Rostislav; CLASSEN, Martin. Experimental and Numerical Characterization of High-Strength Concrete Under Monotonic and Fatigue Mode II Loading with Active Control of Lateral Compression. **Building for the Future: Durable, sustainable, Resilient.** [s.l: s.n.]. p. 429–439. DOI: 10.1007/978-3-031-32519-9_41. Disponível em: https://www.researchgate.net/publication/371186208_Experimental_and_Numerical_Characterization_of_High-Strength_Concrete_Under_Monotonic_and_Fatigue_Mode_II_Loading_with_Active_Control_of_Lateral_Compression. Acesso em: 25 ago. 2023.

BENTZ, Dale P. Three-Dimensional Computer Simulation of Portland Cement Hydration and Microstructure Development. **Journal of the American Ceramic Society**, *[S. l.]*, v. 80, n. 1, p. 3–21, 1997. DOI: 10.1111/j.1151-2916.1997.tb02785.x. Disponível em: https://ceramics.onlinelibrary.wiley.com/doi/10.1111/j.1151-2916.1997.tb02785.x. Acesso em: 11 ago. 2023.

BERIHA, Brundaban; SAHOO, Umesh C.; STEYN, Wynand JvdM. Determination of endurance limit for different bound materials used in pavements: A review. **International Journal of Transportation Science and Technology**, *[S. l.]*, v. 8, n. 3, p. 263–279, 2019. DOI: 10.1016/j.ijtst.2019.05.002. Disponível em: https://www.sciencedirect.com/science/article/pii/S2046043018301667. Acesso em: 27 jul. 2023.

BHARATHI, K. P. P.; ADARI, S. K.; PALLEPAMULA, Urmila. Mechanical properties of self-compacting concrete using steel slag and glass powder. **Journal of Building Pathology and Rehabilitation**, *[S. l.]*, v. 7, n. 1, p. 46, 2022. DOI: 10.1007/s41024-022-00184-z. Disponível em: https://www.researchgate.net/publication/360269044_Mechanical_properties_of_self-compacting_concrete_using_steel_slag_and_glass_powder. Acesso em: 13 jul. 2023.

BOESCH, Michael E.; VADENBO, Carl; SANER, Dominik; HUTER, Christoph; HELLWEG, Stefanie. An LCA model for waste incineration enhanced with new technologies for metal recovery and application to the case of Switzerland. **Waste Management**, *[S. l.]*, v. 34, n. 2, p. 378–389, 2014. DOI: 10.1016/J.WASMAN.2013.10.019. Disponível em: https://www.sciencedirect.com/science/article/abs/pii/S0956053X13005059. Acesso em: 30 ago. 2023.

BORDY, Arthur; YOUNSI, Akli; AGGOUN, Salima; FIORIO, Bruno. Cement substitution by a recycled cement paste fine: Role of the residual anhydrous clinker. **Construction and Building Materials**, *[S. l.]*, v. 132, p. 1–8, 2017. DOI:10.1016/J.CONBUILDMAT.2016.11.080. Disponível em: https://www.sciencedirect.com/science/article/abs/pii/S0950061816318402. Acesso em: 30 ago. 2023.

BORHANI, Mostafa. Multi-label Log-Loss function using L-BFGS for document categorization. **Engineering Applications of Artificial Intelligence**, *[S. l.]*, v. 91, p. 103623, 2020. DOI: 10.1016/J.ENGAPPAI.2020.103623. Disponível em: https://www.sciencedirect.com/science/article/abs/pii/S0952197620300865. Acesso em: 30 ago. 2023.

BOŠNJAKOVIĆ, Mladen; KATINIĆ, Marko; SANTA, Robert; MARIĆ, Dejan. **Wind Turbine Technology Trends**. *[S. l.]*, 2022. DOI: 10.3390/app12178653. Disponível em: https://www.mdpi.com/2076-3417/12/17/8653. Acesso em: 20 ago. 2023.

BOUCHIKHI, Abdelhadi; BENZERZOUR, Mahfoud; ABRIAK, Nor Edine; MAHERZI, Walid; MAMINDY-PAJANY, Yannick. Study of the impact of waste glasses types on pozzolanic activity of cementitious matrix. **Construction and Building Materials**, *[S. l.]*, v. 197, p. 626–640, 2019. DOI: 10.1016/J.CONBUILDMAT.2018.11.180. Disponível em: https://www.sciencedirect.com/science/article/abs/pii/S0950061818328721. Acesso em: 30 ago. 2023.

BOUKHELF, Fouad; CHERIF, Rachid; TRABELSI, Abdelkrim; BELARBI, Rafik; BOUIADJRA, Mohamed Bachir. On the hygrothermal behavior of concrete containing glass powder and silica fume. **Journal of Cleaner Production**, *[S. l.]*, v. 318, p. 128647, 2021. DOI: 10.1016/J.JCLEPRO.2021.128647. Disponível em: https://www.sciencedirect.com/science/article/abs/pii/S0959652621028493. Acesso em: 12 ago. 2023.

BOUKHELF, Fouad; TARGINO, Daniel Lira Lopes; BENZAAMA, Mohammed Hichem; DE ALBUQUERQUE LIMA BABADOPULOS, Lucas Feitosa; MENDILI, Yassine El. Insight into the Behavior of Mortars Containing Glass Powder: An Artificial Neural Network Analysis Approach to Classify the Hydration Modes. **Materials**, *[S. l.]*, v. 16, n. 3, p. 943, 2023. DOI: 10.3390/ma16030943. Disponível em: https://www.mdpi.com/1996-1944/16/3/943. Acesso em: 20 jul. 2023.

BRINSON, Hal F.; BRINSON, L. Catherine. **Polymer Engineering Science and Viscoelasticity**. [s.l.] : Springer US, 2008. DOI: 10.1007/978-0-387-73861-1. Disponível em: https://link.springer.com/book/10.1007/978-0-387-73861-1. Acesso em: 11 jul. 2023.

BROOKS, J. J. Elasticity of Concrete. *In*: CONCRETE and Masonry Movements. [s.l.] : Elsevier, 2015. p. 61–93. DOI: 10.1016/B978-0-12-801525-4.00004-2. Disponível em: https://www.researchgate.net/publication/344098958_4_Elasticity_of_Concrete. Acesso em: 13 jul. 2023.

BULLARD, Jeffrey W.; JENNINGS, Hamlin M.; LIVINGSTON, Richard A.; NONAT, Andre; SCHERER, George W.; SCHWEITZER, Jeffrey S.; SCRIVENER, Karen L.; THOMAS, Jeffrey J. Mechanisms of cement hydration. **Cement and Concrete Research**, *[S. l.]*, v. 41, n. 12, p. 1208–1223, 2011. DOI: 10.1016/J.CEMCONRES.2010.09.011. Disponível em: https://www.sciencedirect.com/science/article/abs/pii/S0008884610002152. Acesso em: 30 ago. 2023.

CAMBIA. **The Lens - Free & Open Patent and Scholarly Search**. , 2023. Disponível em: https://www.lens.org/. Acesso em: 19 set. 2023.

CÂNDIDO, Taíssa Guedes; MEIRA, Gibson Rocha; QUATTRONE, Marco; JOHN, Vanderley Moacyr. Mechanical performance and chloride penetration resistance of concretes with low cement contents. **Revista IBRACON de Estruturas e Materiais**, *[S. l.]*, v. 15, n. 6, 2022. DOI: 10.1590/s1983-41952022000600008. Disponível em: https://www.scielo.br/j/riem/a/Dq78pnyRf9ppQnXvFkTvhgw/?lang=en. Acesso em: 15 ago. 2023.

CASTRO, Sara De; BRITO, Jorge De. Evaluation of the durability of concrete made with crushed glass aggregates. **Journal of Cleaner Production**, *[S. l.]*, v. 41, p. 7–14, 2013. DOI: 10.1016/J.JCLEPRO.2012.09.021. Disponível em: https://www.sciencedirect.com/science/article/abs/pii/S0959652612004866. Acesso em: 24 set. 2023.

CEB. **CEB-FIP Model Code 90**. [s.l: s.n.], 1993. Disponível em: https://www.fib-international.org/publications/ceb-bulletins/ceb-fip-model-code- 90-pdf-detail.html. Acesso em: 3 set. 2023.

COMITÉ EUROPÉEN DE NORMALISATION. **CEN EN ISO 18757 Fine Ceramics (Advanced Ceramics, Advanced Technical Ceramics): Determination of Specific Surface Area of Ceramic Powders by Gas Adsorption Using the BET Method**. Brussels, 2003.

COMITÉ EUROPÉEN DE NORMALISATION. **CEN EN 13263–1 Silica fume for Concrete Part 1: Definitions, Requirements and Conformity Criteria**. Brussels, 2005.

COMITÉ EUROPÉEN DE NORMALISATION. **CEN EN 197-1: Ciment – Partie 1: Composition, Spécifications et Critères de Conformité des Ciments Courants**. Brussels, 2012. a.

COMITÉ EUROPÉEN DE NORMALISATION. **CEN NF EN 933-1: Essais pour déterminer les Caractéristiques Géométriques des Granulats – Partie 1: Détermination de la Granularité - Analyse Granulométrique par Tamisage**. Brussels, 2012. b.

COMITÉ EUROPÉEN DE NORMALISATION. **CEN EN 993–1 Methods of Test for Dense Shaped Refratory Products Part 1: Determination of Bulk Density, Apparent Porosity and True Porosity**. Brussels, 2018.

COMITÉ EUROPÉEN DE NORMALISATION. **CEN NF EN 12350-2 Testign fresh concrete - Part 2: slump test**. Brussels, 2009.

COMITÉ EUROPÉEN DE NORMALISATION. **CEN EN 12390-3:2019 Testing hardened concrete - Part 3: Compressive strength of test specimens**. Brussels, 2019.

COMITÉ EUROPÉEN DE NORMALISATION. **CEN ISO 18757 Fine Ceramics (Advanced Ceramics, Advanced Technical Ceramics): Determination of Specific Surface Area of Ceramic Powders by Gas Adsorption Using the BET Method**. Brussels, 2005.

COMITÉ EUROPÉEN DE NORMALISATION. **CEN EN 1992-1-1 Eurocode 2: Design of Concrete Structures. Part 1–1: General Rules and Rules for Buildings**. Brussels, 2004. Disponível em: https://www.phd.eng.br/wp-content/uploads/2015/12/en.1992.1.1.2004.pdf. Acesso em 30 ago. 2023.

CHAN, Kwai S. Roles of microstructure in fatigue crack initiation. **International Journal of Fatigue**, *[S. l.]*, v. 32, n. 9, p. 1428–1447, 2010. DOI: 10.1016/j.ijfatigue.2009.10.005. Disponível em: https://www.sciencedirect.com/science/article/abs/pii/S0142112309002989. Acesso em: 17 ago. 2023.

CHAND, Gaurav; HAPPY, Sugandh Kumar; RAM, Shobha. Assessment of the properties of sustainable concrete produced from quaternary blend of portland cement, glass powder, metakaolin and silica fume. **Cleaner Engineering and Technology**, *[S. l.]*, v. 4, p. 100179, 2021. DOI: 10.1016/J.CLET.2021.100179. Disponível em: https://www.sciencedirect.com/science/article/pii/S2666790821001397. Acesso em: 30 ago. 2023.

CHANG, Xiaolin; YANG, Xinping; ZHOU, Wei; XIE, Guoshuai; LIU, Shuhua. Influence of Glass Powder on Hydration Kinetics of Composite Cementitious Materials. **Advances in Materials Science and Engineering**, *[S. l.]*, v. 2015, p. 1–7, 2015. DOI: 10.1155/2015/713415. Disponível em: https://downloads.hindawi.com/journals/amse/2015/713415.pdf. Acesso em: 16 ago. 2023.

CHAUDHARY, Satish Kumar; SINHA, Ajay Kumar. Effect of Silica Fume on Permeability and Microstructure of High Strength Concrete. **Civil Engineering Journal**, *[S. l.]*, v. 6, n. 9, p. 1697–1703, 2020. DOI: 10.28991/cej-2020-03091575. Disponível em: https://www.civilejournal.org/index.php/cej/article/view/2311. Acesso em: 16 ago. 2023.

CHEN, C.; HABERT, G.; BOUZIDI, Y.; JULLIEN, A. Environmental impact of cement production: detail of the different processes and cement plant variability evaluation. **Journal of Cleaner Production**, *[S. l.]*, v. 18, n. 5, p. 478–485, 2010. DOI: 10.1016/j.jclepro.2009.12.014. Disponível em: https://linkinghub.elsevier.com/retrieve/pii/S0959652609004089. Acesso em: 13 set. 2023.

CHEN, Xianmai; CHEN, Nan; WEI, Zilong; ZHANG, Xiangmin; YANG, Fei; ZHAO, Hongjun; YOU, Mingxi; WANG, Weidong. Research on the Influence of Loading Frequency on the Dynamic Response of Concrete Sleepers. **Applied Sciences**, *[S. l.]*, v. 12, n. 14, p. 7245, 2022. DOI: 10.3390/app12147245. Disponível em: https://www.researchgate.net/publication/362110918_Research_on_the_Influence_of_Loading_Frequency_on_the_Dynamic_Response_of_Concrete_Sleepers. Acesso em: 30 ago. 2023.

CHEN, Yifeng; YU, Genying; LONG, Ying; TENG, Jiaheng; YOU, Xiujia; LIAO, Bao Qiang; LIN, Hongjun. Application of radial basis function artificial neural network to quantify interfacial energies related to membrane fouling in a membrane bioreactor. **Bioresource Technology**, *[S. l.]*, v. 293, p. 122103, 2019. DOI: 10.1016/J.BIORTECH.2019.122103. Disponível em: https://www.sciencedirect.com/science/article/abs/pii/S0960852419313331. Acesso em: 30 ago. 2023.

CHERIF, Rachid; HAMAMI, Ameur El Amine; AÏT-MOKHTAR, Abdelkarim. Global quantitative monitoring of the ion exchange balance in a chloride migration test on cementitious materials with mineral additions. **Cement and Concrete Research**, *[S. l.]*, v. 138, p. 106240,

2020. DOI: 10.1016/J.CEMCONRES.2020.106240. Disponível em: https://www.sciencedirect.com/science/article/abs/pii/S0008884620308553. Acesso em: 30 ago. 2023.

CHU, Duc Chinh; KLEIB, Joelle; AMAR, Mouhamadou; BENZERZOUR, Mahfoud; ABRIAK, Nor Edine. Recycling of dredged sediment as a raw material for the manufacture of Portland cement – Numerical modeling of the hydration of synthesized cement using the CEMHYD3D code. **Journal of Building Engineering**, *[S. l.]*, v. 48, p. 103871, 2022. a. DOI: 10.1016/J.JOBE.2021.103871. Disponível em: https://www.sciencedirect.com/science/article/abs/pii/S2352710221017290. Acesso em: 13 set. 2023.

CHU, Hongyan; GAO, Li; QIN, Jianjian; JIANG, Jinyang; WANG, Fengjuan. Feasibility of producing ultra-high performance concrete with high elastic modulus by steel chips: An experimental study. **Construction and Building Materials**, *[S. l.]*, v. 375, p. 130964, 2023. a. DOI: 10.1016/j.conbuildmat.2023.130964. Disponivel em: https://www.sciencedirect.com/science/article/abs/pii/S0950061823006761. Acesso em: 22 jul. 2023.

CHU, Hongyan; SHI, Wenfang; WANG, Qun; GAO, Li; WANG, Danqian. Feasibility of manufacturing self-compacting mortar with high elastic modulus by Al2O3 micro powder: A preliminary study. **Construction and Building Materials**, *[S. l.]*, v. 340, p. 127736, 2022. b. DOI: 10.1016/j.conbuildmat.2022.127736. Disponível em: https://www.sciencedirect.com/science/article/abs/pii/S0950061822014118. Acesso em: 7 jul. 2023.

CHUNG, D. D. L. Review: Improving cement-based materials by using silica fume. **Journal of Materials Science**, *[S. l.]*, v. 37, n. 4, p. 673–682, 2002. DOI: 10.1023/A:1013889725971. Disponível em: https://www.researchgate.net/publication/226807152_Review_Improving_cement-based_materials_by_using_silica_fume. Acesso em: 2 set. 2023.

CIAVARELLA, Michele; CARBONE, Giuseppe; VINOGRADOV, Vladimir. A Critical Assessment of Kassapoglou's Statistical Model for Composites Fatigue. **Facta Universitatis, Series: Mechanical Engineering**, *[S. l.]*, v. 16, n. 2, p. 115, 2018. DOI: 10.22190/FUME180321014C. Disponível em: https://www.researchgate.net/publication/325144686_Original_scientific_paper_A_CRITICAL_ASSESSMENT_OF_KASSAPOGLOU%27S_STATISTICAL_MODEL_FOR_COMPOSITES_FATIGUE. Acesso em: 22 jul. 2023.

COOK, Rachel; HAN, Taihao; CHILDERS, Alaina; RYCKMAN, Cambria; KHAYAT, Kamal; MA, Hongyan; HUANG, Jie; KUMAR, Aditya. Machine learning for high-fidelity prediction of cement hydration kinetics in blended systems. **Materials & Design**, *[S. l.]*, v. 208, p. 109920, 2021. DOI: 10.1016/J.MATDES.2021.109920. Disponível em: https://www.sciencedirect.com/science/article/pii/S0264127521004731. Acesso em: 30 ago. 2023.

CORRADO, M.; MOLINARI, J. F. Effects of residual stresses on the tensile fatigue behavior of concrete. **Cement and Concrete Research**, *[S. l.]*, v. 89, p. 206–219, 2016. DOI: 10.1016/j.cemconres.2016.08.014. Disponível em: https://www.sciencedirect.com/science/article/abs/pii/S0008884616301946. Acesso em: 26 ago. 2023.

CORREIA, José; DE JESUS, Abílio; CALÇADA, Rui. Structural Integrity of Materials and Structures. **Engineering Structures and Technologies**, *[S. l.]*, v. 9, n. 4, p. 157–157, 2017. DOI: 10.3846/2029882X.2017.1418172. Disponível em: https://www.researchgate.net/publication/321875815_Structural_integrity_of_materials_and_structures. Acesso em: 24 set. 2023.

CROSSIN, E. The greenhouse gas implications of using ground granulated blast furnace slag as a cement substitute. **Journal of Cleaner Production**, *[S. l.]*, v. 95, p. 101–108, 2015. DOI: 10.1016/J.JCLEPRO.2015.02.082. Disponível em: https://www.sciencedirect.com/science/article/abs/pii/S0959652615002085. Acesso em: 30 ago. 2023.

DABIĆ, P.; KRSTULOVIĆ, R.; RUŠIĆ, D. A new approach in mathematical modelling of cement hydration development. **Cement and Concrete Research**, *[S. l.]*, v. 30, n. 7, p. 1017–1021, 2000. DOI: 10.1016/S0008-8846(00)00293-3. Disponível em: https://www.sciencedirect.com/science/article/abs/pii/S0008884600002933. Acesso em: 30 ago. 2023.

DAMIDOT, D.; LOTHENBACH, B.; HERFORT, D.; GLASSER, F. P. Thermodynamics and cement science. **Cement and Concrete Research**, *[S. l.]*, v. 41, n. 7, p. 679–695, 2011. DOI: 10.1016/J.CEMCONRES.2011.03.018. Disponível em: https://www.sciencedirect.com/science/article/abs/pii/S0008884611000949. Acesso em: 30 ago. 2023.

DAVIES, E. R.. Biologically Inspired Recognition Schemes. In: DAVIES, E. R.. **Machine Vision**. 3. ed. Amsterdan, The Netherlands: Elsevier, 2005. Cap. 25. p. 725-755. Disponível em: https://www.oreilly.com/library/view/machine-vision-3rd/9780122060939/OEBPS/B9780122060939500289.htm. Acesso em: 21 ago. 2023

DE CASTRO, Sara; DE BRITO, Jorge. Evaluation of the durability of concrete made with crushed glass aggregates. **Journal of Cleaner Production**, *[S. l.]*, v. 41, p. 7–14, 2013. DOI: 10.1016/J.JCLEPRO.2012.09.021. Disponível em: https://www.sciencedirect.com/science/article/abs/pii/S0959652612004866. Acesso em: 30 ago. 2023.

DE DOMENICO, Dario; BERNARDO, Luís F. A. Editorial for “Mechanical Behavior of Concrete Materials and Structures: Experimental Evidence and Analytical Models”. **Materials**, *[S. l.]*, v. 15, n. 14, p. 4921, 2022. DOI: 10.3390/ma15144921. Disponível em: https://www.researchgate.net/publication/362014259_Editorial_for_Mechanical_Behavior_of_Concrete_Materials_and_Structures_Experimental_Evidence_and_Analytical_Models. Acesso em: 14 ago. 2023.

DI BENEDETTO, R. M.; BOTELHO, E. C.; JANOTTI, A.; ANCELOTTI JUNIOR, A. C.; GOMES, G. F. Development of an artificial neural network for predicting energy absorption capability of thermoplastic commingled composites. **Composite Structures**, *[S. l.]*, v. 257, p. 113131, 2021. DOI: 10.1016/J.COMPSTRUCT.2020.113131. Disponível em: https://www.sciencedirect.com/science/article/abs/pii/S0263822320330579. Acesso em: 30 ago. 2023.

DING, Xiangqun; LIANG, Xinyu; ZHANG, Yichao; FANG, Yanfeng; ZHOU, Jinghai; KANG, Tianbei. Capillary Water Absorption and Micro Pore Connectivity of Concrete with

Fractal Analysis. **Crystals**, *[S. l.]*, v. 10, n. 10, p. 892, 2020. DOI: 10.3390/cryst10100892. Disponível em: https://www.researchgate.net/publication/346019771_Capillary_Water_Absorption_and_Micro_Pore_Connectivity_of_Concrete_with_Fractal_Analysis. Acesso em: 20 ago. 2023.

DING, Zude; FU, Jiang; LI, Xiaoqin; JI, Xiafei. Mechanical Behavior and Its Influencing Factors on Engineered Cementitious Composite Linings. **Advances in Materials Science and Engineering**, *[S. l.]*, v. 2019, p. 1–15, 2019. DOI: 10.1155/2019/3979741. Disponível em: https://www.hindawi.com/journals/amse/2019/3979741/. Acesso em: 18 set. 2023.

DNV. **DNV-OS-J101: Design of Offshore Wind Turbine Structures**. [s.l: s.n.]. 2016. Disponível em: https://global.ihs.com/doc_detail.cfm?document_name=DNV%2DOS%2DJ101&item_s_key=00451770. Acesso em: 30 ago. 2023.

DU, Yuanbo; YANG, Wencui; GE, Yong; WANG, Sha; LIU, Penghuan. Thermal conductivity of cement paste containing waste glass powder, metakaolin and limestone filler as supplementary cementitious material. **Journal of Cleaner Production**, *[S. l.]*, v. 287, p. 125018, 2021. DOI: 10.1016/J.JCLEPRO.2020.125018. Disponível em: https://www.sciencedirect.com/science/article/abs/pii/S0959652620350629. Acesso em: 30 ago. 2023.

DUNG, Cao Vu; ANH, Le Duc. Autonomous concrete crack detection using deep fully convolutional neural network. **Automation in Construction**, *[S. l.]*, v. 99, p. 52–58, 2019. DOI: 10.1016/J.AUTCON.2018.11.028. Disponível em: https://www.sciencedirect.com/science/article/abs/pii/S0926580518306745. Acesso em: 30 ago. 2023.

ERWAY, Jennifer B.; MARCIA, Roummel F. On solving large-scale limited-memory quasi-Newton equations. **Linear Algebra and its Applications**, *[S. l.]*, v. 515, p. 196–225, 2017. DOI: 10.1016/J.LAA.2016.11.003. Disponível em: https://www.sciencedirect.com/science/article/pii/S0024379516305195. Acesso em: 30 ago. 2023.

EVANGELISTA JUNIOR, Francisco; MACEDO, Fabiano Campos; FARIAS, Márcio Muniz. A methodology to assess the evolution of viscoelastic properties of hardened cement pastes through dynamic mechanical analysis. **Construction and Building Materials**, *[S. l.]*, v. 226, p. 849–858, 2019. DOI: 10.1016/j.conbuildmat.2019.07.268. Disponível em: https://www.sciencedirect.com/science/article/abs/pii/S0950061819319439. Acesso em: 22 ago. 2023.

FATTOUH, Mohy; ELSAYED, Elsayed. Influence of Utilizing Glass Powder with Silica Fume on Mechanical Properties and Microstructure of Concrete. **Delta University Scientific Journal**, *[S. l.]*, v. 6, n. 1, p. 111–122, 2023. DOI: 10.21608/dusj.2023.291027. Disponível em: https://dusj.journals.ekb.eg/article_291027.html. Acesso em: 25 jul. 2023.

FU, Chaoshu; GUO, Rongxin; LIN, Zhiwei; XIA, Haiting; YANG, Yang; MA, Qianmin. Effect of nanosilica and silica fume on the mechanical properties and microstructure of lightweight engineered cementitious composites. **Construction and Building Materials**, *[S. l.]*, v. 298, p. 123788, 2021. DOI: 10.1016/j.conbuildmat.2021.123788. Disponível em:

https://www.sciencedirect.com/science/article/abs/pii/S0950061821015488. Acesso em: 11 ago. 2023.

GALLOWAY, J. W.; HARDING, H. M.; RAITHBY, K. D. Effects of age on flexural, fatigue and compressive strength of concrete : Galloway, J W; Harding, H M; Raithby, K D Transport and Road Research Lab lab report N865, 1979, 20P. **International Journal of Rock Mechanics and Mining Sciences & Geomechanics Abstracts**, *[S. l.]*, v. 16, n. 6, p. 146, 1979. DOI: 10.1016/0148-9062(79)90238-9. Disponível em: https://www.semanticscholar.org/paper/EFFECTS-OF-AGE-ON-FLEXURAL%2C-FATIGUE-AND-COMPRESSIVE-Galloway-Harding/e9dda82e5095d2ab11da344ecc677057303fd6c9. Acesso em: 31 ago. 2023.

GAN, Y.; VAN BREUGEL, K.; SCHLANGEN, E.; ŠAVIJA, B. **Experimental and numerical study of fatigue behaviour at the microscale of cementitious materials**. 2022. Delft University of Technology, *[S. l.]*, 2022. ISBN: 978-94-6421-840-4. Disponível em: https://doi.org/10.4233/uuid:4fd952d3-f892-4567-8e51-e6623c7a6650. Acesso em: 6 ago. 2023.

GAO, Peng; YE, Guang; WEI, Jiangxiong; YU, Qijun. Multi-scale Simulation of Capillary Pores and Gel Pores in Portland Cement Paste. **Materials Science, Engineering**, *[S. l.]*, 2015. DOI: 10.1016/j.conbuildmat.2019.117124. Disponível em: https://www.sciencedirect.com/science/article/abs/pii/S0950061819325668. Acesso em: 23 ago. 2023.

GENCEL, Osman; KARADAG, Omer; OREN, Osman Hulusi; BILIR, Turhan. Steel slag and its applications in cement and concrete technology: A review. **Construction and Building Materials**, *[S. l.]*, v. 283, p. 122783, 2021. DOI: 10.1016/J.CONBUILDMAT.2021.122783. Disponível em: https://www.sciencedirect.com/science/article/abs/pii/S0950061821005432. Acesso em: 30 ago. 2023.

GIORLA, Alain B.; DUNANT, Cyrille F. Microstructural effects in the simulation of creep of concrete. **Cement and Concrete Research**, *[S. l.]*, v. 105, p. 44–53, 2018. DOI: 10.1016/j.cemconres.2017.12.001. Disponível em: https://www.sciencedirect.com/science/article/abs/pii/S000888461730488X. Acesso em: 11 jul. 2023.

GOKULNATH, V.; RAMESH, B.; PRIYADHARSAN, K. Influence of M-Sand in self compacting concrete with addition of glass powder in M-25 grade. **Materials Today: Proceedings**, *[S. l.]*, v. 22, p. 535–540, 2020. DOI: 10.1016/j.matpr.2019.08.188. Disponível em: https://www.sciencedirect.com/science/article/abs/pii/S2214785319331773. Acesso em: 13 ago. 2023.

GOŁEK, Łukasz. Glass powder and high-calcium fly ash based binders – Long term examinations. **Journal of Cleaner Production**, *[S. l.]*, v. 220, p. 493–506, 2019. DOI: 10.1016/J.JCLEPRO.2019.02.095. Disponível em: https://www.sciencedirect.com/science/article/abs/pii/S0959652619304846. Acesso em: 4 ago. 2023.

GOŁEK, Łukasz. New insights into the use of glass cullet in cement composites - Long term examinations. **Cement and Concrete Composites**, *[S. l.]*, v. 133, p. 104673, 2022. DOI:

10.1016/J.CEMCONCOMP.2022.104673. Disponível em: https://www.sciencedirect.com/science/article/abs/pii/S0958946522002669. Acesso em: 30 ago. 2023.

GOŁEK, Łukasz; SZUDEK, Wojciech; BŁĄDEK, Monika; CIĘCIWA, Monika. The influence of ground waste glass cullet addition on the compressive strength and microstructure of Portland cement pastes and mortars. **Cement Wapno Beton**, *[S. l.]*, v. 25, n. 6, p. 480–494, 2020. DOI: 10.32047/cwb.2020.25.6.5. Disponível em: https://www.researchgate.net/publication/348805957_The_influence_of_ground_waste_glass_cullet_addition_on_the_compressive_strength_and_microstructure_of_Portland_cement_pastes_and_mortars. Acesso em: 3 ago. 2023.

GRINYS, Audrius; BALAMURUGAN, Muthaiah; AUGONIS, Algirdas; IVANAUSKAS, Ernestas. Mechanical Properties and Durability of Rubberized and Glass Powder Modified Rubberized Concrete for Whitetopping Structures. **Materials**, *[S. l.]*, v. 14, n. 9, p. 2321, 2021. DOI: 10.3390/ma14092321. Disponível em: https://www.mdpi.com/1996-1944/14/9/2321. Acesso em: 9 set. 2023.

GUIGNONE, Guilherme; CALMON, João Luiz; VIEIRA, Geilma; ZULCÃO, Robson; REBELLO, Thais Ayres. **Life Cycle Assessment of Waste Glass Powder Incorporation on Concrete: A Bridge Retrofit Study Case**. *[S. l.]*, 2022. DOI: 10.3390/app12073353. Disponível em: https://doi.org/10.3390/app12073353. Acesso em: 9 set. 2023.

GUO, Yingying; ZHANG, Y. X.; SOE, Khin; WUHRER, Richard; HUTCHISON, Wayne D.; TIMMERS, Heiko. Development of magnesium oxychloride cement with enhanced water resistance by adding silica fume and hybrid fly ash-silica fume. **Journal of Cleaner Production**, *[S. l.]*, v. 313, p. 127682, 2021. DOI: 10.1016/j.jclepro.2021.127682. Disponível em: https://www.sciencedirect.com/science/article/abs/pii/S0959652621019004. Acesso em: 6 ago. 2023.

GUPTA, Pramod; SINHA, Naresh K. Neural Networks for Identification of Nonlinear Systems: An Overview. **Soft Computing and Intelligent Systems**, *[S. l.]*, p. 337–356, 2000. DOI: 10.1016/B978-012646490-0/50017-2. Disponível em: https://www.researchgate.net/publication/288229616_Neural_Networks_for_Identification_of_Nonlinear_Systems_An_Overview. Acesso em: 30 ago. 2023.

HALLINAN, Jennifer S. Computational Intelligence in the Design of Synthetic Microbial Genetic Systems. **Methods in Microbiology**, *[S. l.]*, v. 40, p. 1–37, 2013. DOI: 10.1016/B978-0-12-417029-2.00001-7. Disponível em: https://www.sciencedirect.com/science/article/abs/pii/B9780124170292000017. Acesso em: 30 ago. 2023.

HAMAD, Mays A.; NASR, Mohammed; SHUBBAR, Ali; AL-KHAFAJI, Zainab; AL MASOODI, Zainab; AL-HASHIMI, Osamah; KOT, Patryk; ALKHADDAR, Rafid; HASHIM, Khalid. Production of Ultra-High-Performance Concrete with Low Energy Consumption and Carbon Footprint Using Supplementary Cementitious Materials Instead of Silica Fume: A Review. **Energies**, *[S. l.]*, v. 14, n. 24, p. 8291, 2021. DOI:

10.3390/en14248291. Disponível em: https://www.mdpi.com/1996-1073/14/24/8291. Acesso em: 23 ago. 2023.

HAN, Seung-Wook; PARK, Jung-Hoon; MYEONG, No-Jun; CHOI, Nak-Sam. Reviews on Very High Cycle Fatigue Behaviors of Structural Metals. **Transactions of the Korean Society of Automotive Engineers**, *[S. l.]*, v. 22, n. 2, p. 134–140, 2014. DOI: 10.7467/KSAE.2014.22.2.134. Disponível em: https://koreascience.kr/article/JAKO201409739048521.pdf. Acesso em: 10 set. 2023.

HE, Jionghuang; LONG, Guangcheng; MA, Kunlin; XIE, Youjun; MA, Cong. Hydration heat evolution of Portland cement paste during unsteady steam curing process: Modelling and optimization. **Thermochimica Acta**, *[S. l.]*, v. 694, p. 178784, 2020. DOI: 10.1016/J.TCA.2020.178784. Disponível em: https://www.sciencedirect.com/science/article/abs/pii/S0040603120306997. Acesso em: 30 ago. 2023.

HONG, Huachang; ZHANG, Zhiying; GUO, Aidi; SHEN, Liguo; SUN, Hongjie; LIANG, Yan; WU, Fuyong; LIN, Hongjun. Radial basis function artificial neural network (RBF ANN) as well as the hybrid method of RBF ANN and grey relational analysis able to well predict trihalomethanes levels in tap water. **Journal of Hydrology**, *[S. l.]*, v. 591, p. 125574, 2020. DOI: 10.1016/J.JHYDROL.2020.125574. Disponível em: https://www.sciencedirect.com/science/article/abs/pii/S0022169420310349. Acesso em: 30 ago. 2023.

HUANG, Bo-Tao; LI, Qinghua; XU, Shilang; ZHOU, Baomin. Investigation on Compressive Fatigue Damage Process of Ultra-High Toughness Cementitious Composites. *In*: PROCEEDINGS OF THE 9TH INTERNATIONAL CONFERENCE ON FRACTURE MECHANICS OF CONCRETE AND CONCRETE STRUCTURES 2016, **Anais** [...]. Berkeley, USA: IA-FraMCoS, 2016. p. 1-8. DOI: 10.21012/FC9.116. Disponível em: https://www.semanticscholar.org/paper/Investigation-on-Compressive-Fatigue-Damage-Process-Botao-Li/33351464559230622bdb8790d59c992107272f1f. Acesso em: 5 jul. 2023.

HUANG, Bo-Tao; LI, Qing-Hua; XU, Shi-Lang; ZHOU, Bao-Min. Frequency Effect on the Compressive Fatigue Behavior of Ultrahigh Toughness Cementitious Composites: Experimental Study and Probabilistic Analysis. **Journal of Structural Engineering**, *[S. l.]*, v. 143, n. 8, 2017. DOI: 10.1061/(ASCE)ST.1943-541X.0001799. Disponível em: https://www.researchgate.net/publication/315693894_Frequency_effect_on_the_compressive_fatigue_behavior_of_ultrahigh_toughness_cementitious_composites_Experimental_study_and_probabilistic_analysis. Acesso em: 26 jul. 2023.

HUANG, Xieping; KONG, Xiangzhen; HU, Jing; ZHANG, Xuedong; ZHANG, Zitao; FANG, Qin. The influence of free water content on ballistic performances of concrete targets. **International Journal of Impact Engineering**, *[S. l.]*, v. 139, p. 103530, 2020. DOI: 10.1016/j.ijimpeng.2020.103530. Disponível em: https://www.sciencedirect.com/science/article/abs/pii/S0734743X19313788. Acesso em: 17 jul. 2023.

HÜMME, Julian; VON DER HAAR, Christoph; LOHAUS, Ludger; MARX, Steffen. Fatigue behaviour of a normal-strength concrete - number of cycles to failure and strain development.

Structural Concrete, *[S. l.]*, v. 17, n. 4, p. 637–645, 2016. DOI: 10.1002/suco.201500139. Disponível em: https://onlinelibrary.wiley.com/doi/abs/10.1002/suco.201500139. Acesso em: 27 ago. 2023.

HUNTZINGER, Deborah N.; EATMON, Thomas D. A life-cycle assessment of Portland cement manufacturing: comparing the traditional process with alternative technologies. **Journal of Cleaner Production**, *[S. l.]*, v. 17, n. 7, p. 668–675, 2009. DOI: 10.1016/J.JCLEPRO.2008.04.007. Disponível em: https://www.sciencedirect.com/science/article/abs/pii/S0959652608000826. Acesso em: 30 ago. 2023.

IDIR, Rachida; CYR, Martin; TAGNIT-HAMOU, Arezki. Use of fine glass as ASR inhibitor in glass aggregate mortars. **Construction and Building Materials**, *[S. l.]*, v. 24, n. 7, p. 1309–1312, 2010. DOI: 10.1016/J.CONBUILDMAT.2009.12.030. Disponível em: https://www.sciencedirect.com/science/article/abs/pii/S0950061809004413. Acesso em: 30 ago. 2023.

IDIR, Rachida; CYR, Martin; TAGNIT-HAMOU, Arezki. Pozzolanic properties of fine and coarse color-mixed glass cullet. **Cement and Concrete Composites**, *[S. l.]*, v. 33, n. 1, p. 19–29, 2011. DOI: 10.1016/J.CEMCONCOMP.2010.09.013. Disponível em: https://www.sciencedirect.com/science/article/abs/pii/S0958946510001435. Acesso em: 2 set. 2023.

ISSAADI, N.; HAMAMI, A. A.; BELARBI, R.; AÏT-MOKHTAR, A. Experimental assessment of the spatial variability of porosity, permeability and sorption isotherms in an ordinary building concrete. **Heat and Mass Transfer**, *[S. l.]*, v. 53, n. 10, p. 3037–3048, 2017. DOI: 10.1007/s00231-017-2041-4. Disponível em: https://www.researchgate.net/publication/316938302_Experimental_assessment_of_the_spatial_variability_of_porosity_permeability_and_sorption_isotherms_in_an_ordinary_building_concrete. Acesso em: 4 set. 2023.

JAHANDARI, Soheil; MOHAMMADI, Masoud; RAHMANI, Aida; ABOLHASANI, Masoumeh; MIRAKI, Hania; MOHAMMADIFAR, Leili; KAZEMI, Mostafa; SABERIAN, Mohammad; RASHIDI, Maria. Mechanical Properties of Recycled Aggregate Concretes Containing Silica Fume and Steel Fibres. **Materials**, *[S. l.]*, v. 14, n. 22, p. 7065, 2021. DOI: 10.3390/ma14227065. Disponível em: https://www.mdpi.com/1996-1944/14/22/7065. Acesso em: 5 ago. 2023.

JAIN, Kishan Lal; SANCHETI, Gaurav; GUPTA, Lalit Kumar. Durability performance of waste granite and glass powder added concrete. **Construction and Building Materials**, *[S. l.]*, v. 252, p. 119075, 2020. DOI: 10.1016/j.conbuildmat.2020.119075. Disponível em: https://www.sciencedirect.com/science/article/abs/pii/S0950061820310801. Acesso em: 1 jul. 2023.

JENSEN, O. Mejlhede. Thermodynamic limitation of self-desiccation. **Cement and Concrete Research**, *[S. l.]*, v. 25, n. 1, p. 157–164, 1995. DOI: 10.1016/0008-8846(94)00123-G. Disponível em: https://www.sciencedirect.com/science/article/abs/pii/000888469400123G. Acesso em: 30 ago. 2023.

JIA, Mengdi; WU, Zhimin; YU, Rena C.; ZHANG, Xiaoxin. Residual fracture energy of concrete suffering from fatigue loading. **Engineering Fracture Mechanics**, *[S. l.]*, v. 255, p. 107956, 2021. DOI: 10.1016/j.engfracmech.2021.107956. Disponível em: https://www.sciencedirect.com/science/article/abs/pii/S0013794421003829. Acesso em: 14 set. 2023.

JIAO, Yubo; LIU, Hanbing; WANG, Xianqiang; ZHANG, Yuwei; LUO, Guobao; GONG, Yafeng. Temperature Effect on Mechanical Properties and Damage Identification of Concrete Structure. **Advances in Materials Science and Engineering**, *[S. l.]*, v. 2014, p. 1–10, 2014. DOI: 10.1155/2014/191360. Disponível em: https://www.researchgate.net/publication/277566220_Temperature_Effect_on_Mechanical_Properties_and_Damage_Identification_of_Concrete_Structure. Acesso em: 18 jul. 2023.

KACHANOV, L. Time of the Rupture Process under Creep Conditions. **Izvestiia Akademii Nauk SSSR**, *[S. l.]*, v. 8, p. 26–31, 1958. Disponível em: https://www.scirp.org/reference/referencespapers?referenceid=1910907. Acesso em: 14 set. 2023.

KACHKOUCH, Fatima Zahraa; NOBERTO, Camila Carvalho; BABADOPULOS, Lucas Feitosa de Albuquerque Lima; MELO, Abcael Ronald Santos; MACHADO, Amanda Moreira Lima; SEBAIBI, Nassim; BOUKHELF, Fouad; MENDILI, Yassine El. Fatigue behavior of concrete: A literature review on the main relevant parameters. **Construction and Building Materials**, *[S. l.]*, v. 338, p. 127510, 2022. DOI: 10.1016/j.conbuildmat.2022.127510. Disponível em: https://www.sciencedirect.com/science/article/abs/pii/S0950061822011874. Acesso em: 19 de set. 2023.

KALAKADA, Z.; DOH, J. H.; ZI, G. Utilisation of coarse glass powder as pozzolanic cement—A mix design investigation. **Construction and Building Materials**, *[S. l.]*, v. 240, p. 117916, 2020. DOI: 10.1016/J.CONBUILDMAT.2019.117916. Disponível em: https://www.sciencedirect.com/science/article/abs/pii/S0950061819333690. Acesso em: 11 jul. 2023.

KALPOKAITĖ-DIČKUVIENĖ, Regina; PITAK, Inna; BALTUŠNIKAS, Arūnas; LUKOŠIŪTĖ, Stasė Irena; DENAFAS, Gintaras; ČĖSNIENĖ, Jūratė. Cement substitution by sludge-biomass gasification residue: Synergy with silica fume. **Construction and Building Materials**, *[S. l.]*, v. 326, p. 126902, 2022. DOI: 10.1016/J.CONBUILDMAT.2022.126902. Disponível em: https://www.sciencedirect.com/science/article/abs/pii/S0950061822005888. Acesso em: 30 ago. 2023.

KATTAN, P. I.; VOYIADJIS, G. Z. Damage Mechanics. *In*: DAMAGE mechanics with finite elements. Berlin, Heidelberg: Springer Berlin Heidelberg, 2002. p. 1–35. DOI: 10.1007/978-3-642-56384-3_1. Disponível em: https://www.researchgate.net/publication/301130067_Damage_Mechanics. Acesso em: 8 ago. 2023.

KAZMIERCZAK, Claudio de Souza; BOARO, Joana Kirchner Benetti; LUNARDI, Monique Palavro; KULAKOWSKI, Marlova Piva; MANCIO, Mauricio. Influence of the moisture content on the dynamic modulus of elasticity of concrete made with recycled aggregate. **Ambiente Construído**, *[S. l.]*, v. 19, n. 2, p. 79–89, 2019. DOI: 10.1590/s1678-

86212019000200309. Disponível em: https://www.scielo.br/j/ac/a/vSVwNXZR-jdCWS9CSD6hQzBS/?lang=en. Acesso em: 6 set. 2023.

KEERIO, Manthar Ali; ABBASI, Suhail Ahmed; KUMAR, Aneel; BHEEL, Naraindas; UR REHAMAN, Khalil; TASHFEEN, Muhammad. Effect of Silica Fume as Cementitious Material and Waste Glass as Fine Aggregate Replacement Constituent on Selected Properties of Concrete. **Silicon**, *[S. l.]*, v. 14, n. 1, p. 165–176, 2022. DOI: 10.1007/s12633-020-00806-6. Disponível em: https://www.researchgate.net/publication/346515823_Effect_of_Silica_Fume_as_Cementitious_Material_and_Waste_Glass_as_Fine_Aggregate_Replacement_Constituent_on_Selected_Properties_of_Concrete. Acesso em: 20 ago. 2023.

KEMER, Houssam; BOURAS, Rachid; MESBOUA, Noureddine; SONEBI, Mohammed; KINNANE, Oliver. Shear-thickening behavior of sustainable cement paste — Controlling physical parameters of new sources of supplementary cementitious materials. **Construction and Building Materials**, *[S. l.]*, v. 310, p. 125277, 2021. DOI: 10.1016/j.conbuildmat.2021.125277. Disponível em: https://www.sciencedirect.com/science/article/abs/pii/S095006182103018X. Acesso em: 2 set. 2023.

KHEIR, Judy; HILLOULIN, Benoît; LOUKILI, Ahmed; DE BELIE, Nele. **Chemical Shrinkage of Low Water to Cement (w/c) Ratio CEM I and CEM III Cement Pastes Incorporating Silica Fume and Fille**r. *[S. l.]*, 2021. DOI: 10.3390/ma14051164. Disponível em: https://doi.org/10.3390/ma14051164. Acesso em: 23 set. 2023.

KISHI, Toshiharu; MAEKAWA, Koichi. Multi-Component Model for Hydration Heat of Portland Cement. **Doboku Gakkai Ronbunshu**, *[S. l.]*, n. 526, p. 97–109, 1995. DOI: 10.2208/jscej.1995.526_97. Disponível em: https://www.researchgate.net/publication/265529821_Multi-component_model_for_hydration_heating_of_Portland_cement. Acesso em: 25 set. 2023.

KOLANI, B.; BUFFO-LACARRIÈRE, L.; SELLIER, A.; ESCADEILLAS, G.; BOUTILLON, L.; LINGER, L. Hydration of slag-blended cements. **Cement and Concrete Composites**, *[S. l.]*, v. 34, n. 9, p. 1009–1018, 2012. DOI: 10.1016/J.CEMCONCOMP.2012.05.007. Disponível em: https://www.sciencedirect.com/science/article/abs/pii/S0958946512001175. Acesso em: 30 ago. 2023.

KONDO, R. Kinetics and Mechanism of the Hydration of Cements. *In*: FIFTH INTERNATIONAL SYMPOSIUM ON THE CHEMISTRY OF CEMENT. **Anais** [...]. Tokyo, Japan: No Publisher, 1968. p. 203–248. DOI: 10.1002/jctb.5030320733. Disponível em: https://onlinelibrary.wiley.com/doi/10.1002/jctb.5030320733. Acesso em: 22 ago. 2023.

KONSTA-GDOUTOS, Maria S.; DANOGLIDIS, Panagiotis A.; SHAH, Surendra P. High modulus concrete: Effects of low carbon nanotube and nanofiber additions. **Theoretical and Applied Fracture Mechanics**, *[S. l.]*, v. 103, p. 102295, 2019. DOI: 10.1016/j.tafmec.2019.102295. Disponível em: https://www.sciencedirect.com/science/article/abs/pii/S0167844219301399. Acesso em: 27 set. 2023.

KRAVTSOVA, O. N.; TIMOFEEV, A. M.; TAPPYROVA, N. I.; PROTODYAKONOVA, N. A. The Influence of Silica Fume Concentration on Capillary Porosity and Concrete Heat Conductivity. *In:* 2020 INTERNATIONAL MULTI-CONFERENCE ON INDUSTRIAL ENGINEERING AND MODERN TECHNOLOGIES (FAREASTCON) 2020, **Anais** [...]. Vladivostok, Russia: IEEE, 2020. p. 1–3. DOI: 10.1109/FarEastCon50210.2020.9271378. Disponível em: https://www.researchgate.net/publication/347482850_The_Influence_of_Silica_Fume_Concentration_on_Capillary_Porosity_and_Concrete_Heat_Conductivity. Acesso em: 16 jul. 2023.

KRSTULOVIĆ, R.; DABIĆ, P. A conceptual model of the cement hydration process. **Cement and Concrete Research**, *[S. l.]*, v. 30, n. 5, p. 693–698, 2000. DOI: 10.1016/S0008-8846(00)00231-3. Disponível em: https://www.sciencedirect.com/science/article/abs/pii/S0008884600002313. Acesso em: 30 ago. 2023.

KUO, Wen-Ten; ZHUANG, Zheng-Yun. A Comprehensive Study of the Mechanical and Durability Properties of High-Performance Concrete Materials for Grouting Underwater Foundations of Offshore Wind Turbines. **Materials**, *[S. l.]*, v. 14, n. 20, p. 5968, 2021. DOI: 10.3390/ma14205968. Disponível em: https://www.researchgate.net/publication/355276485_A_Comprehensive_Study_of_the_Mechanical_and_Durability_Properties_of_High-Performance_Concrete_Materials_for_Grouting_Underwater_Foundations_of_Offshore_Wind_Turbines. Acesso em: 10 jul. 2023.

LABORATOIRE MATÉRIAUX ET DURABILITÉ DES CONSTRUCTIONS. **AFPC-AFREM. Durabilité Des Bétons: Méthodes Recommandées Pour La Mesure Des Grandeurs Associées à La Durabilité**. Toulouse, France, 2009.

LAVAGNA, Luca; NISTICÒ, Roberto. An Insight into the Chemistry of Cement—A Review. **Applied Sciences**, *[S. l.]*, v. 13, n. 1, p. 203, 2022. DOI: 10.3390/app13010203. Disponível em: https://www.researchgate.net/publication/366618423_An_Insight_into_the_Chemistry_of_Cement-A_Review. Acesso em: 28 jul. 2023.

LAVERGNE, F.; BEN FRAJ, A.; BAYANE, I.; BARTHÉLÉMY, J. F. Estimating the mechanical properties of hydrating blended cementitious materials: An investigation based on micromechanics. **Cement and Concrete Research**, *[S. l.]*, v. 104, p. 37–60, 2018. DOI: 10.1016/J.CEMCONRES.2017.10.018. Disponível em: https://www.sciencedirect.com/science/article/abs/pii/S0008884617304015. Acesso em: 30 ago. 2023.

LEE, M. K.; BARR, B. I. G. An overview of the fatigue behaviour of plain and fibre reinforced concrete. **Cement and Concrete Composites**, *[S. l.]*, v. 26, n. 4, p. 299–305, 2004. DOI: 10.1016/S0958-9465(02)00139-7. Disponível em: https://www.sciencedirect.com/science/article/abs/pii/S0958946502001397. Acesso em: 31 ago. 2023.

LEI, Dong; ZHANG, Pei; HE, Jintao; BAI, Pengxiang; ZHU, Feipeng. Fatigue life prediction method of concrete based on energy dissipation. **Construction and Building Materials**, *[S. l.]*, v. 145, p. 419–425, 2017. DOI: 10.1016/j.conbuildmat.2017.04.030. Disponível em:

https://www.sciencedirect.com/science/article/abs/pii/S0950061817306888. Acesso em: 30 jul. 2023.

LEMAITRE, J.; SERMAGE, J. P.; DESMORAT, R. A two scale damage concept applied to fatigue. **International Journal of Fracture**, *[S. l.]*, v. 97, n. 1/4, p. 67–81, 1999. DOI: 10.1023/A:1018641414428. Disponível em: https://link.springer.com/article/10.1023/A:1018641414428. Acesso em: 13 ago. 2023.

LEMAITRE, Jean; CHABOCHE, Jean-Louis. **Mechanics of Solid Materials**. [s.l.] : Cambridge University Press, 1990. DOI: 10.1017/CBO9781139167970.

LI, Jie; REN, Xiaodan. Stochastic damage model for concrete based on energy equivalent strain. **International Journal of Solids and Structures**, *[S. l.]*, v. 46, n. 11–12, p. 2407–2419, 2009. DOI: 10.1016/j.ijsolstr.2009.01.024. Disponível em: https://www.sciencedirect.com/science/article/pii/S002076830900050X. Acesso em: 9 jul. 2023.

LI, Qinghua; HUANG, Botao; XU, Shilang; ZHOU, Baomin; YU, Rena C. Compressive fatigue damage and failure mechanism of fiber reinforced cementitious material with high ductility. **Cement and Concrete Research**, *[S. l.]*, v. 90, p. 174–183, 2016. DOI: 10.1016/j.cemconres.2016.09.019. Disponível em: https://www.researchgate.net/publication/308917611_Compressive_fatigue_damage_and_failure_mechanism_of_fiber_reinforced_cementitious_material_with_high_ductility. Acesso em: 6 set. 2023.

LI, Wei; WANG, Rongjie; WANG, Yuan; ZUO, Wenqiang; HONG, Jinxiang; LUO, Shuqiong; WANG, Penggang. The acceleration effect of nano C-S-H-PCE on the microstructure formation and evolution at early age of cement paste. **Materials and Structures**, *[S. l.]*, v. 56, n. 4, p. 89, 2023. DOI: 10.1617/s11527-023-02179-9. Disponível em: https://www.researchgate.net/publication/370571002_The_acceleration_effect_of_nano_C-S-H-PCE_on_the_microstructure_formation_and_evolution_at_early_age_of_cement_paste. Acesso em: 19 ago. 2023.

LI, Yang; ZHANG, Xu; WANG, Ruijun; LEI, Yan. Performance enhancement of rubberised concrete via surface modification of rubber: A review. **Construction and Building Materials**, *[S. l.]*, v. 227, p. 116691, 2019. DOI: 10.1016/J.CONBUILDMAT.2019.116691. Disponível em: https://www.sciencedirect.com/science/article/abs/pii/S0950061819321075. Acesso em: 31 ago. 2023.

LIANG, Chaofeng; YOU, Jinkui; GU, Feng; GAO, Yueqing; YANG, Guowei; HE, Zhihai; HOU, Shaodan; DUAN, Zhenhua. Enhancing the elastic modulus of concrete prepared with recycled coarse aggregates of different quality by chemical modifications. **Construction and Building Materials**, *[S. l.]*, v. 360, p. 129590, 2022. a. DOI: 10.1016/J.CONBUILDMAT.2022.129590. Disponível em: https://www.sciencedirect.com/science/article/abs/pii/S0950061822032469. Acesso em: 4 set. 2023.

LIANG, Chaofeng; YOU, Jinkui; GU, Feng; GAO, Yueqing; YANG, Guowei; HE, Zhihai; HOU, Shaodan; DUAN, Zhenhua. Enhancing the elastic modulus of concrete prepared with recycled coarse aggregates of different quality by chemical modifications. **Construction and**

Building Materials, *[S. l.]*, v. 360, p. 129590, 2022. b. DOI: 10.1016/J.CONBUILDMAT.2022.129590. Disponível em: https://www.sciencedirect.com/science/article/abs/pii/S0950061822032469. Acesso em: 31 ago. 2023.

LIANG, Jun Song; LI, Jie. Damage Theory Based Fatigue Simulation of Concrete Structure. **Applied Mechanics and Materials**, *[S. l.]*, v. 784, p. 51–58, 2015. DOI: 10.4028/www.scientific.net/AMM.784.51. Disponível em: https://www.scientific.net/AMM.784.51. Acesso em: 30 jul. 2023.

LIN, Hongjun; DAI, Qunyun; ZHENG, Lili; HONG, Huachang; DENG, Wenjing; WU, Fuyong. Radial basis function artificial neural network able to accurately predict disinfection by-product levels in tap water: Taking haloacetic acids as a case study. **Chemosphere**, *[S. l.]*, v. 248, p. 125999, 2020. DOI: 10.1016/J.CHEMOSPHERE.2020.125999. Disponível em: https://www.sciencedirect.com/science/article/abs/pii/S0045653520301922. Acesso em: 30 ago. 2023.

LING, Tung Chai; POON, Chi Sun; WONG, Hau Wing. Management and recycling of waste glass in concrete products: Current situations in Hong Kong. **Resources, Conservation and Recycling**, *[S. l.]*, v. 70, p. 25–31, 2013. DOI: 10.1016/J.RESCONREC.2012.10.006. Disponível em: https://www.sciencedirect.com/science/article/abs/pii/S0921344912001917. Acesso em: 30 ago. 2023.

LIU, Chaochao; LV, Songtao; PENG, Xinghai; ZHENG, Jianlong. Normalized characterization method for fatigue behavior of cement-treated aggregates based on the yield criterion. **Construction and Building Materials**, *[S. l.]*, v. 228, p. 117099, 2019. DOI: 10.1016/j.conbuildmat.2019.117099. Disponível em: https://www.sciencedirect.com/science/article/abs/pii/S0950061819325413. Acesso em: 15 ago. 2023.

LIU, Lei; HE, Zhen; CAI, Xinhua; FU, Shaojun. Application of Low-Field NMR to the Pore Structure of Concrete. **Applied Magnetic Resonance**, *[S. l.]*, v. 52, n. 1, p. 15–31, 2021. DOI: 10.1007/s00723-020-01229-7. Disponível em: https://www.researchgate.net/publication/344081380_Application_of_Low-Field_NMR_to_the_Pore_Structure_of_Concrete. Acesso em: 13 jul. 2023.

LIU, Xiaoyan; XIE, Xian; LIU, Ruidan; LYU, Kai; ZUO, Junqing; LI, Shijie; LIU, Li; SHAH, Surendra P. Research on the durability of nano-SiO2 and sodium silicate co-modified recycled coarse aggregate (RCA) concrete. **Construction and Building Materials**, *[S. l.]*, v. 378, p. 131185, 2023. a. DOI: 10.1016/J.CONBUILDMAT.2023.131185. Disponível em: https://www.sciencedirect.com/science/article/abs/pii/S0950061823008978. Acesso em: 31 ago. 2023.

LU, Bao; HUO, Zhen; XU, Qingyuan; HOU, Guihua; WANG, Xiaosan; LIU, Jianhui; HU, Xiang. Characteristics of CSH under carbonation and its effects on the hydration and microstructure of cement paste. **Construction and Building Materials**, *[S. l.]*, v. 364, p. 129952, 2023. DOI: 10.1016/j.conbuildmat.2022.129952. Disponível em: https://www.sciencedirect.com/science/article/abs/pii/S095006182203608X. Acesso em: 31 jul. 2023.

LUO, Dayou; WEI, Jianqiang. Hydration kinetics and phase evolution of Portland cement composites containing sodium-montmorillonite functionalized with a Non-Ionic surfactant. **Construction and Building Materials**, *[S. l.]*, v. 333, p. 127386, 2022. DOI: 10.1016/J.CONBUILDMAT.2022.127386. Disponível em: https://www.sciencedirect.com/science/article/abs/pii/S0950061822010637. Acesso em: 30 ago. 2023.

LUO, Sang; QIAN, Zhendong; YANG, Xu; LU, Qing. Fatigue behavior of epoxy asphalt concrete and its moisture susceptibility from flexural stiffness and phase angle. **Construction and Building Materials**, *[S. l.]*, v. 145, p. 506–517, 2017. DOI: 10.1016/j.conbuildmat.2017.04.049. Disponível em: https://www.sciencedirect.com/science/article/abs/pii/S0950061817306943. Acesso em: 19 ago. 2023.

MAGALHÃES, A. G.; MARQUES, A. T.; OLIVEIRA, F. M. F.; SOUKATCHOFF, P.; DE CASTRO, P. T. Mechanical behaviour of cementitious matrix composites. **Cement and Concrete Composites**, *[S. l.]*, v. 18, n. 1, p. 9–22, 1996. DOI: 10.1016/0958-9465(95)00035-6. Disponível em: https://www.sciencedirect.com/science/article/abs/pii/0958946595000356. Acesso em: 22 set. 2023.

MARUYAMA, Ippei; TERAMOTO, Atsushi; IGARASHI, Go. Strain and thermal expansion coefficients of various cement pastes during hydration at early ages. **Materials and Structures**, *[S. l.]*, v. 47, n. 1–2, p. 27–37, 2014. DOI: 10.1617/s11527-013-0042-4. Disponível em: https://www.researchgate.net/publication/252323824_Strain_and_thermal_expansion_coefficients_of_various_cement_pastes_during_hydration_at_early_ages. Acesso em: 5 ago. 2023.

MASSOUD, Sofi.; MENDIS, P. A.; LIE, S.; BAWEJA, D. Early Age Concrete Thermal and Creep effects: Relevance to Anchorage Zones of Post-tensioned Members. **Eletronic Journal of Structural Engineering** *[S. l.]*, v. 8, p. 90–96, 2008. Disponível em: https://www.researchgate.net/publication/289861448_Early_age_concrete_thermal_and_creep_effects_Relevance_to_anchorage_zones_of_post-tensioned_members. Acesso em: 20 ago. 2023.

MECHTCHERINE, Viktor; SLOWIK, Volker; KABELE, Petr (ORG.). **Strain-Hardening Cement-Based Composites**. Dordrecht: Springer Netherlands, 2018. v. 15 DOI: 10.1007/978-94-024-1194-2. Disponível em: https://www.researchgate.net/publication/237842700_Durability_of_strain-hardening_cement-based_composites_SHCC. Acesso em: 11 ago. 2023.

MEDEIROS, Arthur; ZHANG, Xiaoxin; RUIZ, Gonzalo; YU, Rena C.; VELASCO, Marta De Souza Lima. Effect of the loading frequency on the compressive fatigue behavior of plain and fiber reinforced concrete. **International Journal of Fatigue**, *[S. l.]*, v. 70, p. 342–350, 2015. DOI: 10.1016/J.IJFATIGUE.2014.08.005. Disponível em: https://www.sciencedirect.com/science/article/abs/pii/S0142112314002102. Acesso em: 31 ago. 2023.

MEINHARD, Klaus; LACKNER, Roman. Multi-phase hydration model for prediction of hydration-heat release of blended cements. **Cement and Concrete Research**, *[S. l.]*, v. 38, n. 6, p. 794–802, 2008. DOI: 10.1016/J.CEMCONRES.2008.01.008. Disponível em:

https://www.sciencedirect.com/science/article/abs/pii/S0008884608000252. Acesso em: 30 ago. 2023.

MENZIES, Tim; KOCAGÜNELI, Ekrem; MINKU, Leandro; PETERS, Fayola; TURHAN, Burak. Using Goals in Model-Based Reasoning. *In*: SHARING Data and Models In Software Engineering. [s.l.] : Elsevier, 2015. p. 321–353. DOI: 10.1016/B978-0-12-417295-1.00024-2. Disponível em: https://www.researchgate.net/publication/302547354_Chapter_24_Using_Goals_in_Model-Based_Reasoning. Acesso em: 18 ago. 2023.

MILLER, S. A.; HORVATH, A.; MONTEIRO, P. J. M. Readily Implementable Techniques Can Cut Annual CO2 Emissions from the Production of Concrete by over 20%. **Environmental Research Letters**, *[S. l.]*, v. 11, n. 7, 2016. DOI: 10.1088/1748-9326/11/7/074029. Disponível em: https://www.researchgate.net/publication/305645264_Readily_implementable_techniques_can_cut_annual_CO_2_emissions_from_the_production_of_concrete_by_over_20. Acesso em: 6 set. 2023.

MILLER, Sabbie A.; MONTEIRO, Paulo J. M.; OSTERTAG, Claudia P.; HORVATH, Arpad. Concrete mixture proportioning for desired strength and reduced global warming potential. **Construction and Building Materials**, *[S. l.]*, v. 128, p. 410–421, 2016. DOI: 10.1016/j.conbuildmat.2016.10.081. Disponível em: https://www.sciencedirect.com/science/article/abs/pii/S0950061816316968. Acesso em: 22 ago. 2023

MULLER, A. C. A.; SCRIVENER, K. L.; SKIBSTED, J.; GAJEWICZ, A. M.; MCDONALD, P. J. Influence of silica fume on the microstructure of cement pastes: New insights from 1H NMR relaxometry. **Cement and Concrete Research**, *[S. l.]*, v. 74, p. 116–125, 2015. DOI: 10.1016/j.cemconres.2015.04.005. Disponível em: https://www.sciencedirect.com/science/article/pii/S0008884615001118. Acesso em: 2 set. 2023.

MÜLLER, Steffen; MECHTCHERINE, Viktor. Fatigue behaviour of strain-hardening cement-based composites (SHCC). **Cement and Concrete Research**, *[S. l.]*, v. 92, p. 75–83, 2017. DOI: 10.1016/j.cemconres.2016.11.003. Disponível em: https://www.sciencedirect.com/science/article/abs/pii/S0008884616305993. Acesso em: 14 set. 2023.

MYRTJA, Erisa; SOUDIER, Jérôme; PRAT, Evelyne; CHAOUCHE, Mohend. Fatigue deterioration mechanisms of high-strength grout in compression. **Construction and Building Materials**, *[S. l.]*, v. 270, p. 121387, 2021. DOI: 10.1016/J.CONBUILDMAT.2020.121387. Disponível em: https://www.sciencedirect.com/science/article/abs/pii/S0950061820333912. Acesso em: 16 set. 2023.

NASER, M. Z.; THAI, Son; THAI, Huu Tai. Evaluating structural response of concrete-filled steel tubular columns through machine learning. **Journal of Building Engineering**, *[S. l.]*, v. 34, p. 101888, 2021. DOI: 10.1016/J.JOBE.2020.101888. Disponível: https://www.sciencedirect.com/science/article/abs/pii/S235271022033521X. Acesso em: 30 ago. 2023.

NGUYEN, Khoa Tan; NGUYEN, Quang Dang; LE, Tuan Anh; SHIN, Jiuk; LEE, Kihak. Analyzing the compressive strength of green fly ash based geopolymer concrete using experiment and machine learning approaches. **Construction and Building Materials**, *[S. l.]*, v.

247, p. 118581, 2020. DOI: 10.1016/J.CONBUILDMAT.2020.118581. Disponível em: https://www.sciencedirect.com/science/article/abs/pii/S0950061820305869. Acesso em: 30 ago. 2023.

NGUYEN, Van Thong; LEE, Seon Yeol; CHUNG, Sang Yeop; MOON, Jae Heum; KIM, Dong Joo. Effects of cement particle distribution on the hydration process of cement paste in three-dimensional computer simulation. **Construction and Building Materials**, *[S. l.]*, v. 311, p. 125322, 2021. DOI: 10.1016/J.CONBUILDMAT.2021.125322. Disponível em: https://www.sciencedirect.com/science/article/abs/pii/S0950061821030634. Acesso em: 30 ago. 2023.

NI, Chenxin; WU, Qingyong; YU, Zhuqing; SHEN, Xiaodong. Hydration of Portland cement paste mixed with densified silica fume: From the point of view of fineness. **Construction and Building Materials**, *[S. l.]*, v. 272, p. 121906, 2021. DOI: 10.1016/J.CONBUILDMAT.2020.121906. Disponível em: https://www.sciencedirect.com/science/article/abs/pii/S0950061820339106. Acesso em: 8 ago. 2023.

OMRAN, Ahmed F.; D.-MORIN, Etienne; HARBEC, David; TAGNIT-HAMOU, Arezki. Long-term performance of glass-powder concrete in large-scale field applications. **Construction and Building Materials**, *[S. l.]*, v. 135, p. 43–58, 2017. DOI: 10.1016/j.conbuildmat.2016.12.218. Disponível em: https://www.sciencedirect.com/science/article/abs/pii/S0950061816321511. Acesso em: 21 ago. 2023.

ONESCHKOW, Nadja. Fatigue behaviour of high-strength concrete with respect to strain and stiffness. **International Journal of Fatigue**, *[S. l.]*, v. 87, p. 38–49, 2016. DOI: 10.1016/j.ijfatigue.2016.01.008. Disponível em: https://www.sciencedirect.com/science/article/abs/pii/S0142112316000098. Acesso em: 10 ago. 2023.

OROUJI, Maedeh; ZAHRAI, Seyed Mehdi; NAJAF, Erfan. Effect of glass powder & polypropylene fibers on compressive and flexural strengths, toughness and ductility of concrete: An environmental approach. **Structures**, *[S. l.]*, v. 33, p. 4616–4628, 2021. DOI: 10.1016/j.istruc.2021.07.048. Disponível em: https://www.sciencedirect.com/science/article/abs/pii/S2352012421006640. Acesso em: 10 ago. 2023.

OZAKI, Shinobu; SUGATA, Noriyuki. Fatigue of Concrete Composed of Blast Furnace Slag or Silica Fume Under Submerged Condition.. *In:* INTERNATIONAL CONFERENCE FLY ASH, SILICA FUME, SLAG, AND NATURAL POZZOLANS IN CONCRETE, 4., 1992, Istanbul. **Anais** [...]. Istanbul, Turkey: American Concrete Institute, 1992. p. 1509–1524. DOI: 10.14359/2282. Disponível em: https://www.concrete.org/publications/internationalconcreteabstractsportal.aspx?m=details&id=2282. Acesso em: 14 jul. 2023.

PAPPA, Evanthia J.; MURRAY, James J.; WALLS, Michael; ALAM, Parvez; FLANAGAN, Tomas; DOYLE, Adrian; NOI, Sandro Di; MCCARTHY, Edward D.; BRADAIGH, Conchur O. Fatigue life analysis of hybrid E-glass/carbon fibre powder Epoxy Materials for Wind Turbine Blades. *In:* EUROPEAN CONFERENCE ON COMPOSITE MATERIALS, 18., 2018, Athens. **Anais** [...]. Athens, Greece: ECCM18, 2018. p. 1-8. Disponível em:

https://www.researchgate.net/publication/324703720_Fatigue_life_analysis_of_hybrid_E-glasscarbon_composite_materials_for_wind_turbine_blades. Acesso em: 22 jul. 2023.

PARANT, Edouard; ROSSI, Pierre; BOULAY, Claude. Fatigue behavior of a multi-scale cement composite. **Cement and Concrete Research**, *[S. l.]*, v. 37, n. 2, p. 264–269, 2007. DOI: 10.1016/j.cemconres.2006.04.006. Disponível em: https://www.sciencedirect.com/science/article/abs/pii/S0008884606002687. Acesso em: 22 jul. 2023.

PAUL, Suvash Chandra; ŠAVIJA, Branko; BABAFEMI, Adewumi John. A comprehensive review on mechanical and durability properties of cement-based materials containing waste recycled glass. **Journal of Cleaner Production**, *[S. l.]*, v. 198, p. 891–906, 2018. DOI: 10.1016/J.JCLEPRO.2018.07.095. Disponível em: https://www.sciencedirect.com/science/article/abs/pii/S0959652618320687. Acesso em: 4 ago. 2023.

PERSSON, Bertil. Self-desiccation and its importance in concrete technology. **Materials and Structures**, *[S. l.]*, v. 30, n. 5, p. 293–305, 1997. DOI: 10.1007/BF02486354. Disponível em: https://link.springer.com/article/10.1007/BF02486354. Acesso em: 9 set. 2023.

PETRELLA, Andrea; SZUDEK, Wojciech; GOŁEK, Łukasz; MALATA, Grzegorz; PYTEL, Zdzisław. I**nfluence of Waste Glass Powder Addition on the Microstructure and Mechanical Properties of Autoclaved Building Materials**. *[S. l.]*, 2022. DOI: 10.3390/ma15020434. Disponível em: https://doi.org/10.3390/ma15020434. Acesso em: 9 set. 2023.

POMMERSHEIM, James M.; CLIFTON, James R. Mathematical modeling of tricalcium silicate hydration. **Cement and Concrete Research**, *[S. l.]*, v. 9, n. 6, p. 765–770, 1979. DOI: 10.1016/0008-8846(79)90072-3. Disponível em: https://www.sciencedirect.com/science/article/abs/pii/0008884679900723. Acesso em: 30 ago. 2023.

POMMERSHEIM, James M.; CLIFTON, James R. Mathematical modeling of tricalcium silicate hydration. II. Hydration sub-models and the effect of model parameters. **Cement and Concrete Research**, *[S. l.]*, v. 12, n. 6, p. 765–772, 1982. DOI: 10.1016/0008-8846(82)90040-0. Disponível em: https://www.sciencedirect.com/science/article/abs/pii/0008884682900400. Acesso em: 30 ago. 2023.

PRAKASH, Ramaiah; THENMOZHI, Rajagopal; RAMAN, Sudharshan N.; SUBRAMANIAN, Chidambaram. Characterization of Eco-friendly Steel Fiber-reinforced Concrete Containing Waste Coconut Shell as Coarse Aggregates and Fly Ash as Partial Cement Replacement. **Structural Concrete**, *[S. l.]*, p. 1–11, 2019. DOI: 10.1002/suco.201800355. Disponível em: https://www.researchgate.net/publication/334197444_Characterization_of_eco-friendly_steel_fiber-reinforced_concrete_containing_waste_coconut_shell_as_coarse_aggregates_and_fly_ash_as_partial_cement_replacement. Acesso em: 5 ago. 2023.

QIAN, Rusheng; ZHANG, Yunsheng; LIU, Cheng; LIU, Zhiyong; ZHANG, Yu; LIU, Guojian. Effects of supplementary cementitious materials on pore-solution chemistry of blended cements. **Journal of Sustainable Cement-Based Materials**, *[S. l.]*, v. 11, n. 6, p. 389–407, 2022. DOI: 10.1080/21650373.2021.1988754. Disponível em:

https://www.researchgate.net/publication/355353935_Effects_of_supplementary_cementitious_materials_on_pore-solution_chemistry_of_blended_cements. Acesso em: 2 jul. 2023.

QIN, Can; GONG, Jingwei; XIE, Gangchuan. Modeling Hydration Kinetics of the Portland-Cement-Based Cementitious Systems with Mortar Blends by Non-Assumptive Projection Pursuit Regression. **Thermochimica Acta**, *[S. l.]*, v. 705, p. 179035, 2021. DOI: 10.1016/J.TCA.2021.179035. Disponível em: https://www.sciencedirect.com/science/article/abs/pii/S0040603121001763. Acesso em: 30 ago. 2023.

QIU, Jishen; YANG, En-Hua. Micromechanics-based investigation of fatigue deterioration of engineered cementitious composite (ECC). **Cement and Concrete Research**, *[S. l.]*, v. 95, p. 65–74, 2017. DOI: 10.1016/j.cemconres.2017.02.029. Disponível em: https://www.sciencedirect.com/science/article/abs/pii/S0008884616308018. Acesso em: 11 jul. 2023.

RAJAOARISOA, L. Large-Scale Building Thermal Modeling Based on Artificial Neural Networks: Application to Smart Energy Management. **Artificial Intelligence Techniques for a Scalable Energy Transition**. Cham, Switzerland: Springer International Publishing, 2020. p. 15–44. DOI: 10.1007/978-3-030-42726-9_2. Disponível em: https://www.researchgate.net/publication/337906444_Large-Scale_Building_Thermal_Modeling_Based_on_Artificial_Neural_Networks_Application_to_Smart_Energy_Management. Acesso em: 13 ago. 2023.

RIDING K. A; POOLE J. L; FOLLIARD K. J; JUENGER M. C. G; SCHINDLER A. K. Modeling Hydration of Cementitious Systems. **ACI Materials Journal**, *[S. l.]*, v. 109, n. 2, 2012. DOI: 10.14359/51683709. Disponível em: https://krex.k-state.edu/bitstream/handle/2097/15459/RidingACIMaterJ2012.pdf;jsessionid=DCF7F6292E03B9E1A7F0E1E6181BB96A?sequence=1. Acesso em: 20 ago. 2023.

SAGAR, Bhanavath; SIVAKUMAR, M. V. N. Use of alccofine-1203 in concrete: review on mechanical and durability properties. **International Journal of Sustainable Engineering**, *[S. l.]*, v. 14, n. 6, p. 2060–2073, 2021. DOI: 10.1080/19397038.2021.1970275. Disponível em: https://www.researchgate.net/publication/354212147_Use_of_alccofine-1203_in_concrete_review_on_mechanical_and_durability_properties. Acesso em: 7 de set. 2023.

SALLEH, Mohd Najib Mohd; TALPUR, Noureen; HUSSAIN, Kashif. Adaptive Neuro-Fuzzy Inference System: Overview, Strengths, Limitations, and Solutions. *In*: INTERNATIONAL CONFERENCE ON DATA MINING AND BIG DATA, 2., 2017, Fukuoka. **Anais** […]. Fukuoka, Japan: Springer,Cham, 2017. p. 527–535. DOI: 10.1007/978-3-319-61845-6_52. Disponível em: https://www.researchgate.net/publication/318154996_Adaptive_Neuro-Fuzzy_Inference_System_Overview_Strengths_Limitations_and_Solutions. Acesso em: 9 set. 2023.

SANAHUJA, Julien; DORMIEUX, Luc; CHANVILLARD, Gilles. Modelling elasticity of a hydrating cement paste. **Cement and Concrete Research**, *[S. l.]*, v. 37, n. 10, p. 1427–1439, 2007. DOI: 10.1016/J.CEMCONRES.2007.07.003. Disponível em: https://www.sciencedirect.com/science/article/abs/pii/S0008884607001548. Acesso em: 31 ago. 2023.

SÁNCHEZ, A. R; RAMOS, V. C; POLO, M. S; VICTORIA, María; RAMÓN, López; UTRILLA, J. R. Life Cycle Assessment of Cement Production with Marble Waste Sludges Life Cycle Assessment of Cement Production with Marble Waste. **Sludges. Int. J. Environ. Res. Public Health**, *[S. l.]*, v. 18, p. 10968, 2021. DOI: 10.3390/ijerph182010968. Disponível em: https://www.researchgate.net/publication/355425307_Life_Cycle_Assessment_of_Cement_Production_with_Marble_Waste_Sludges. Acesso em: 13 jul. 2023.

SANTOS, Paulo Ricardo Alves dos Reis; SANTOS, Diovana da Silva; ALMADA, Max Silva De; SILVA, Lirana Lamara Barreto Da; CONCEIÇÃO, Italo Gutierry Carneiro Da; SILVA, Paulysendra Felipe; PEREIRA, Gabriel Gregório Sousa; FREITAS, Walber Alves. Analysis of the mechanical properties of the concrete with partial substitution of the kind's aggregate glass powder. **International Journal for Innovation Education and Research**, *[S. l.]*, v. 9, n. 6, p. 406–425, 2021. DOI: 10.31686/ijier.vol9.iss6.3204. Disponível em: https://scholars-journal.net/index.php/ijier/article/view/3204. Acesso em: 8 ago. 2023.

SAUCEDO, Luis; YU, Rena C.; MEDEIROS, Arthur; ZHANG, Xiaoxin; RUIZ, Gonzalo. A probabilistic fatigue model based on the initial distribution to consider frequency effect in plain and fiber reinforced concrete. **International Journal of Fatigue**, *[S. l.]*, v. 48, p. 308–318, 2013. DOI: 10.1016/J.IJFATIGUE.2012.11.013. Disponível em: https://www.sciencedirect.com/science/article/abs/pii/S0142112312003453. Acesso em: 31 ago. 2023.

SAURABH, A. Jaiswal; DARJI, A. R. Effect on Strength of Concrete Incorporating Cotton Fiber and Silica Fume. **International Journal for Scientific Research and Development**, *[S. l.]*, 2016. Disponível em: https://www.ijsrd.com/Article.php?manuscript=IJSRDV2I6041. Acesso em: 22 jul. 2023.

SCHWARZ, Nathan; CAM, Hieu; NEITHALATH, Narayanan. Influence of a fine glass powder on the durability characteristics of concrete and its comparison to fly ash. **Cement and Concrete Composites**, *[S. l.]*, v. 30, n. 6, p. 486–496, 2008. DOI: 10.1016/J.CEMCONCOMP.2008.02.001. Disponível em: https://www.sciencedirect.com/science/article/abs/pii/S0958946508000176. Acesso em: 31 ago. 2023.

SCRIVENER, Karen L.; JUILLAND, Patrick; MONTEIRO, Paulo J. M. Advances in understanding hydration of Portland cement. **Cement and Concrete Research**, *[S. l.]*, v. 78, p. 38–56, 2015. DOI: 10.1016/J.CEMCONRES.2015.05.025. Disponível em: https://www.sciencedirect.com/science/article/abs/pii/S0008884615001623. Acesso em: 30 ago. 2023.

SEALEY, B.; SKJØLSVOLD, Ola; GOODIER, Chris I.; JUSTNES, Harald. Long Term Field Study Into the Durability of Silica Fume Concrete in a Marine Tidal Zone. *In:* CONCRETE INNOVATION CONFERENCE, 2., 2017, Tromsø. **Anais** [...]. Tromsø, Norway: Norwegian Concrete Association /Tekna, 2017. p. 1-6. Disponível em: https://www.researchgate.net/publication/327019359_LONG_TERM_FIELD_STUDY_INTO_THE_DURABILITY_OF_SILICA_FUME_CONCRETE_IN_A_MARINE_TIDAL_ZONE. Acesso em: 18 ago. 2023.

SERELIS, Evaldas; VAITKEVICIUS, Vitoldas; HILBIG, Harald; IRBE, Linda; RUDZIONIS, Zymantas. Effect of ultra-sonic dispersion time on hydration process and microstructure development of ultra-high performance glass powder concrete. **Construction and Building Materials**, *[S. l.]*, v. 298, p. 123856, 2021. DOI: 10.1016/j.conbuildmat.2021.123856. Disponível em: https://www.sciencedirect.com/science/article/abs/pii/S0950061821016160. Acesso em: 13 ago. 2023.

SERPA, D.; SANTOS SILVA, A.; DE BRITO, J.; PONTES, J.; SOARES, D. ASR of mortars containing glass. **Construction and Building Materials**, *[S. l.]*, v. 47, p. 489–495, 2013. DOI: 10.1016/J.CONBUILDMAT.2013.05.058. Disponível em: https://www.sciencedirect.com/science/article/abs/pii/S095006181300456X. Acesso em: 30 ago. 2023.

SHAH, Asif H.; WANI, Elieya; KHAN, Anjum S.; FARIDI, Afeefa F.; NAJIULLAH, Syed M.; SHAH, Ali A.; SOHARWARDI, Tayib K. Engineered Cementitious Composites: An Analysis of the Composition and Behaviour at Ambient and Elevated Temperatures. **Iranian Journal of Science and Technology, Transactions of Civil Engineering**, *[S. l.]*, v. 47, n. 5, p. 2549–2569, 2023. DOI: 10.1007/s40996-023-01089-8. Disponível em: https://www.researchgate.net/publication/369601664_Engineered_Cementitious_Composites_An_Analysis_of_the_Composition_and_Behaviour_at_Ambient_and_Elevated_Temperatures. Acesso em: 6 ago. 2023.

SHAH, Rishika; PANDIT, R. K.; GAUR, M. K. Thermal comfort analysis through development of artificial neural network models: An experimental study in Cwa climate. **Materials Today: Proceedings**, *[S. l.]*, v. 57, p. 2018–2025, 2022. DOI: 10.1016/J.MATPR.2021.11.139. Disponível em: https://www.sciencedirect.com/science/article/abs/pii/S2214785321071479. Acesso em: 30 ago. 2023.

SHANMUGASUNDARAM, N.; PRAVEENKUMAR, S. Mechanical properties of engineered cementitious composites (ECC) incorporating different mineral admixtures and fibre: a review. **Journal of Building Pathology and Rehabilitation**, *[S. l.]*, v. 7, n. 1, p. 40, 2022. DOI: 10.1007/s41024-022-00182-1. Disponível em: https://www.researchgate.net/publication/359540838_Mechanical_properties_of_engineered_cementitious_composites_ECC_incorporating_different_mineral_admixtures_and_fibre_a_review. Acesso em: 27 ago. 2023.

SHAYAN, Ahmad; XU, Aimin. Value-added utilisation of waste glass in concrete. **Cement and Concrete Research**, *[S. l.]*, v. 34, n. 1, p. 81–89, 2004. DOI: 10.1016/S0008-8846(03)00251-5. Disponível em: https://www.sciencedirect.com/science/article/abs/pii/S0008884603002515. Acesso em: 30 ago. 2023.

SHEN, Dejian; JIAO, Yang; KANG, Jiacheng; FENG, Zhizhuo; SHEN, Yongqiang. Influence of ground granulated blast furnace slag on early-age cracking potential of internally cured high performance concrete. **Construction and Building Materials**, *[S. l.]*, v. 233, p. 117083, 2020. DOI: 10.1016/J.CONBUILDMAT.2019.117083. Disponível em: https://www.sciencedirect.com/science/article/abs/pii/S0950061819325255. Acesso em: 30 ago. 2023.

SHOUKRY, Samir N.; WILLIAM, Gergis W.; DOWNIE, Brian; RIAD, Mourad Y. Effect of moisture and temperature on the mechanical properties of concrete. **Construction and Building Materials**, *[S. l.]*, v. 25, n. 2, p. 688–696, 2011. DOI: 10.1016/J.CONBUILDMAT.2010.07.020. Disponível em: https://www.sciencedirect.com/science/article/abs/pii/S0950061810004058. Acesso em: 31 ago. 2023.

SINGH, Anjali; MEHTA, P. K.; KUMAR, Rakesh. Strength and microstructure analysis of sustainable self-compacting concrete with fly ash, silica fume, and recycled minerals. **Materials Today: Proceedings**, *[S. l.]*, v. 78, p. 86–98, 2023. DOI: 10.1016/j.matpr.2022.11.282. Disponível em: https://www.sciencedirect.com/science/article/abs/pii/S2214785322071334. Acesso em: 18 set. 2023.

SINGH, Hardeep; TALWAR, Kiran. Evaluation of Sulphate Resistance Effects of Glass Powder as A Supllementary Cementitious Material on the Performance of High Strength Mortar. **International Journal of Engineering Research and**, *[S. l.]*, v. V9, n. 03, 2020. DOI: 10.17577/IJERTV9IS030413. Disponível em: https://www.researchgate.net/publication/341875145_Evaluation_of_Sulphate_Resistance_Effects_of_Glass_Powder_as_A_Supllementary_Cementitious_Material_on_the_Performance_of_High_Strength_Mortar. Acesso em: 02 ago. 2023.

STEPKOWSKA, E. T.; BLANES, J. M.; FRANCO, F.; REAL, C.; PÉREZ-RODRÍGUEZ, J. L. Phase transformation on heating of an aged cement paste. **Thermochimica Acta**, *[S. l.]*, v. 420, n. 1–2, p. 79–87, 2004. DOI: 10.1016/J.TCA.2003.11.057. Disponível em: https://www.sciencedirect.com/science/article/abs/pii/S0040603104002291. Acesso em: 30 ago. 2023.

SUBASI, Abdulhamit; YILMAZ, Ahmet Serdar; BINICI, Hanifi. Prediction of early heat of hydration of plain and blended cements using neuro-fuzzy modelling techniques. **Expert Systems with Applications**, *[S. l.]*, v. 36, n. 3, p. 4940–4950, 2009. DOI: 10.1016/J.ESWA.2008.06.015. Disponível em: https://www.sciencedirect.com/science/article/abs/pii/S0957417408003424. Acesso em: 30 ago. 2023.

SUNDARESAN, Srividhya; RAMAMURTHY, Vidjeapriya; MEYAPPAN, Neelamegam. Improving Mechanical and Durability Properties of Hypo Sludge Concrete with Basalt Fibres and SBR Latex. **Advances in Concrete Construction**, *[S. l.]*, v. 12, n. 4, p. 327–337, 2021. DOI: 10.12989/acc.2021.12.4.327. Disponível em: http://www.techno-press.org/content/?page=article&journal=acc&volume=12&num=4&ordernum=6. Acesso em: 18 set. 2023.

SZYDŁOWSKI, Jakub; SZUDEK, Wojciech; GOŁEK, Łukasz. Effect of temperature on the long-term properties of mortars containing waste glass powder and ground granulated blast furnace slag. **Cement Wapno Beton**, *[S. l.]*, v. 26, n. 4, p. 264–278, 2021. DOI: 10.32047/CWB.2021.26.4.1. Disponível em: https://www.researchgate.net/publication/356528752_Effect_of_temperature_on_the_long-term_properties_of_mortars_containing_waste_glass_powder_and_ground_granulated_blast_furnace_slag_Wplyw_temperatury_na_dlugoterminowe_wlasciwosci_zapraw_zawierajacych. Acesso em: 29 jul. 2023.

TAHERSIMA, Mohammad; TIKALSKY, Paul. Finite element modeling of hydration heat in a concrete slab-on-grade floor with limestone blended cement. **Construction and Building Materials**, *[S. l.]*, v. 154, p. 44–50, 2017. DOI: 10.1016/J.CONBUILDMAT.2017.07.176. Disponível em: https://www.sciencedirect.com/science/article/abs/pii/S0950061817315180. Acesso em: 30 ago. 2023.

TARGINO, Daniel Lira Lopes; HOLANDA, Ana Dulce de Castro; HENRIQUEZ, Pablo Andrade Martinez; FREITAS, Ingrid Lourrany Barreto; BOUKHELF, Fouad; MENDILI, Yassine El; BABADOPULOS, Lucas Feitosa de Albuquerque Lima. Complex Modulus characterization of an Optimized Binder with SCMs: proposition of an enhanced Cement formulation to improve Stiffness Behavior and Durability of Mortars and Concretes. **Journal of Building Pathology and Rehabilitation**, *[S. l.]*, v. 8, n. 2, p. 85, 2023. DOI: 10.1007/s41024-023-00293-3. Disponível em: https://www.researchgate.net/publication/372442791_Complex_Modulus_characterization_of_an_Optimized_Binder_with_SCMs_proposition_of_an_enhanced_Cement_formulation_to_improve_Stiffness_Behavior_and_Durability_of_Mortars_and_Concretes. Acesso em: 21 jul. 2023.

TAVARES, Ludmila Rodrigues Costa; TAVARES JUNIOR, Joaquim Francisco; COSTA, Leonardo Martins; BEZERRA, Augusto Cesar da Silva; CETLIN, Paulo Roberto; AGUILAR, Maria Teresa Paulino. Influence of quartz powder and silica fume on the performance of Portland cement. **Scientific Reports**, *[S. l.]*, v. 10, n. 1, p. 21461, 2020. DOI: 10.1038/s41598-020-78567-w. Disponível em: https://www.researchgate.net/publication/346732071_Influence_of_quartz_powder_and_silica_fume_on_the_performance_of_Portland_cement. Acesso em: 28 ago. 2023.

TREMIÑO, Rosa María; REAL-HERRAIZ, Teresa; LETELIER, Viviana; BRANCO, Fernando G.; ORTEGA, José Marcos. Effects after 1500 Hardening Days on the Microstructure and Durability-Related Parameters of Mortars Produced by the Incorporation of Waste Glass Powder as a Clinker Replacement. **Sustainability**, *[S. l.]*, v. 13, n. 7, p. 3979, 2021. DOI: 10.3390/su13073979. Disponível em: https://www.researchgate.net/publication/350599424_Effects_after_1500_Hardening_Days_on_the_Microstructure_and_Durability-Related_Parameters_of_Mortars_Produced_by_the_Incorporation_of_Waste_Glass_Powder_as_a_Clinker_Replacement. Acesso em: 26 ago. 2023.

TRIPATHI, Deep; KUMAR, Rakesh; MEHTA, P. K.; SINGH, Amrendra. Silica fume mixed concrete in acidic environment. **Materials Today: Proceedings**, *[S. l.]*, v. 27, p. 1001–1005, 2020. DOI: 10.1016/J.MATPR.2020.01.311. Disponível em: https://www.sciencedirect.com/science/article/abs/pii/S221478532030393X. Acesso em: 03 set. 2023.

UZBAS, B.; AYDIN, A. C. Microstructural Analysis of Silica Fume Concrete with Scanning Electron Microscopy and X-Ray Diffraction. **Engineering, Technology & Applied Science Research**, *[S. l.]*, v. 10, n. 3, p. 5845–5850, 2020. DOI: 10.48084/etasr.3288. Disponível em: https://etasr.com/index.php/ETASR/article/view/3288. Acesso em: 28 ago. 2023.

VALDERRAMA, César; GRANADOS, Ricard; CORTINA, José Luis; GASOL, Carles M.; GUILLEM, Manel; JOSA, Alejandro. Implementation of best available techniques in cement

manufacturing: a life-cycle assessment study. **Journal of Cleaner Production**, *[S. l.]*, v. 25, p. 60–67, 2012. DOI: 10.1016/J.JCLEPRO.2011.11.055. Disponível em: https://www.sciencedirect.com/science/article/abs/pii/S095965261100494X. Acesso em: 17 jul. 2023.

VANCE, Kirk; AGUAYO, Matthew; OEY, Tandre; SANT, Gaurav; NEITHALATH, Narayanan. Hydration and strength development in ternary portland cement blends containing limestone and fly ash or metakaolin. **Cement and Concrete Composites**, *[S. l.]*, v. 39, p. 93–103, 2013. DOI: 10.1016/J.CEMCONCOMP.2013.03.028. Disponível em: https://www.sciencedirect.com/science/article/abs/pii/S0958946513000474. Acesso em: 30 ago. 2023.

VASSILOPOULOS, A. P. Predicting the fatigue life of adhesively-bonded structural composite joints. **Fatigue and Fracture of Adhesively-Bonded Composite Joints**. [s.l.] : Elsevier, 2015. p. 443–491. DOI: 10.1016/B978-0-85709-806-1.00016-1. Disponível em: https://www.sciencedirect.com/science/article/abs/pii/B9780857098061000161. Acesso em: 15 ago. 2023.

VICENTE, Miguel A.; MÍNGUEZ, Jesús; MARTÍNEZ, José A.; GONZÁLEZ, Dorys C. High-Performance Concrete and Fiber-Reinforced High- Performance Concrete under Fatigue Efforts. *In*: YILMAZ, Salih; ÖZMEN, Hayri Bayatan. (org.). **High performance concrete technology and applications**. [s.l.] : InTech, 2016.p 63-85. DOI: 10.5772/64387. Disponível em: https://www.researchgate.net/publication/339830649_High-Performance_Concrete_and_Fiber-Reinforced_High-_Performance_Concrete_under_Fatigue_Efforts. Acesso em: 22 jul. 2023.

VISWANATH, Somashekar; LAFAVE, James M.; KUCHMA, Daniel A. Concrete compressive strain behavior and magnitudes under uniaxial fatigue loading. **Construction and Building Materials**, *[S. l.]*, v. 296, p. 123718, 2021. DOI: 10.1016/j.conbuildmat.2021.123718. Disponível em: https://www.sciencedirect.com/science/article/abs/pii/S0950061821014781. Acesso em: 15 set. 2023.

VOGLER, Nico; DRABETZKI, Philipp; LINDEMANN, Mathias; KÜHNE, Hans-Carsten. Description of the concrete carbonation process with adjusted depth-resolved thermogravimetric analysis. **Journal of Thermal Analysis and Calorimetry**, *[S. l.]*, v. 147, n. 11, p. 6167–6180, 2022. DOI: 10.1007/s10973-021-10966-1. Disponível em: https://www.researchgate.net/publication/353319453_Description_of_the_concrete_carbonation_process_with_adjusted_depth-resolved_thermogravimetric_analysis. Acesso em: 16 ago. 2023.

WANG, Caihui. Research Progress and Discussion on the Factors Influencing the Durability of Structural Concrete. **Materials review**, *[S. l.]*, v. 27, n. 6A, p. 111–117, 2012. Disponível em: https://www.semanticscholar.org/paper/Research-Progress-and-Discussion-on-the-Factors-the-Cai-hui/4caff07d85018a80847652b5abef4d57280ee964. Acesso em: 16 ago. 2023.

WANG, Wenfeng; DUAN, Shaochan; ZHU, Haoran. Research on Improving the Durability of Bridge Pavement Using a High-Modulus Asphalt Mixture. **Materials**, *[S. l.]*, v. 14, n. 6, p. 1449, 2021. DOI: 10.3390/ma14061449. Disponível em: https://www.mdpi.com/1996-1944/14/6/1449. Acesso em: 16 ago. 2023.

WANG, Xiao Yong. Analysis of hydration kinetics and strength progress in cement–slag binary composites. **Journal of Building Engineering**, *[S. l.]*, v. 35, p. 101810, 2021. DOI: 10.1016/J.JOBE.2020.101810. Disponível em: https://www.sciencedirect.com/science/article/abs/pii/S2352710220334434. Acesso em: 30 ago. 2023.

WEI, Ya. Fracture Mechanics-Based Fatigue Behavior of Jointed Concrete Pavement. **Applied Mechanics and Materials**, *[S. l.]*, v. 226–228, p. 1481–1487, 2012. DOI: 10.4028/www.scientific.net/AMM.226-228.1481. Disponível em: https://www.scientific.net/AMM.226-228.1481. Acesso em: 17 set. 2023.

WEI, Ya; LIANG, Siming; KONG, Weikang. **Mechanical Properties of Cementitious Materials at Microscale**. Singapore: Springer Nature Singapore, 2023. DOI: 10.1007/978-981-19-6883-9. Disponivel em: https://link.springer.com/book/10.1007/978-981-19-6883-9. Acesso em: 23 ago. 2023.

WENG, Jia-Rui; LIAO, Wen-Cheng. Microstructure and shrinkage behavior of high-performance concrete containing supplementary cementitious materials. **Construction and Building Materials**, *[S. l.]*, v. 308, p. 125045, 2021. DOI: 10.1016/j.conbuildmat.2021.125045. Disponível em: https://www.sciencedirect.com/science/article/abs/pii/S0950061821027902. Acesso em: 08 ago. 2023.

WORLD BUSINESS COUNCIL FOR SUSTAINABLE DEVELOPMENT. **Cement Technology Roadmap 2009:** Carbon Emissions Reductions up to 2050. [s.l: s.n.], 2009. Disponível em: https://www.iea.org/reports/cement-technology-roadmap-carbon-emissions-reductions-up-to-2050. Acesso em: 10 nov. 2022.

XU, Zeqiong et al. Using simple and easy water quality parameters to predict trihalomethane occurrence in tap water. **Chemosphere**, *[S. l.]*, v. 286, p. 131586, 2022. DOI: 10.1016/J.CHEMOSPHERE.2021.131586. Disponível em: https://www.sciencedirect.com/science/article/abs/pii/S0045653521020580. Acesso em: 30 ago. 2023.

YAMASHITA, Heisuke; YOSHIDA, Toru; HIRASHIMA, Takeo. Influence of Water Content on Total Strain of Super High-Strength Concrete Under Elevated Temperature. *In*: FIRE Science and Technology 2015. [s.l.] : Springer Singapore, 2017. p. 289–297. DOI: 10.1007/978-981-10-0376-9_29.

YAN, Handong; SUN, Wei; CHEN, Huisu. The effect of silica fume and steel fiber on the dynamic mechanical performance of high-strength concrete. **Cement and Concrete Research**, *[S. l.]*, v. 29, n. 3, p. 423–426, 1999. DOI: 10.1016/S0008-8846(98)00235-X. Disponível em: https://www.sciencedirect.com/science/article/abs/pii/S000888469800235X. Acesso em: 11 ago. 2023.

YANG, Jian; JIANG, Liqiang; GUO, Haizhu; YAO, Guohuang. Stress Mechanism and Energy Dissipation Performance Optimization of Prefabricated ECC/RC Combined Shear Walls under Low Cyclic Loading. **Buildings**, *[S. l.]*, v. 13, n. 3, p. 772, 2023. DOI: 10.3390/buildings13030772. Disponível em: https://www.mdpi.com/2075-5309/13/3/772. Acesso em: 04 jul. 2023.

YANG, Z. R.; YANG, Z. Artificial Neural Networks. *In*: COMPREHENSIVE Biomedical Physycs. Amsterdam, The Netherlands: Elsevier, 2014. p. 1–17. Disponível em: https://www.researchgate.net/publication/322642509_Comprehensive_Biomedical_Physics. Acesso em: 08 ago. 2023.

YIN, Weisong; LI, Xinping; SUN, Tao; CHEN, Youzhi; XU, Fang; YAN, Ge; XU, Mingnan; TIAN, Kun. Utilization of waste glass powder as partial replacement of cement for the cementitious grouts with superplasticizer and viscosity modifying agent binary mixtures: Rheological and mechanical performances. **Construction and Building Materials**, *[S. l.]*, v. 286, p. 122953, 2021. DOI: 10.1016/J.CONBUILDMAT.2021.122953. Disponível em: https://www.sciencedirect.com/science/article/abs/pii/S0950061821007133. Acesso em: 30 ago. 2023.

ZANUY, Carlos; ALBAJAR, Luis; DE LA FUENTE, Pablo. El proceso de fatiga del hormigón y su influencia estructural. **Materiales de Construcción**, *[S. l.]*, v. 61, n. 303, p. 385–399, 2011. DOI: 10.3989/mc.2010.54609. Disponível em: https://materconstrucc.revistas.csic.es/index.php/materconstrucc/article/view/422/468. Acesso em: 19 set. 2023.

ZERBST, Uwe; MADIA, Mauro. Structural integrity II. *In*: FUNDAMENTALS of Laser Powder Bed Fusion of Metals. [s.l.] : Elsevier, 2021. p. 377–394. DOI: 10.1016/B978-0-12-824090-8.00015-9. Disponível em: https://www.sciencedirect.com/science/article/abs/pii/B9780128240908000159. Acesso em: 28 ago. 2023.

ZEYBEK, Özer; ONURALP ÖZKILIÇ, Yasin; KARALAR, Memduh; ÇELIK, Ihsan; QAIDI, Shaker; AHMAD, Jawad; DORU BURDUHOS-NERGIS, Dumitru; PETRONELA BURDUHOS-NERGIS, Diana. **Influence of Replacing Cement with Waste Glass on Mechanical Properties of Concrete**. *[S. l.]*, 2022. DOI: 10.3390/ma15217513. Disponível em: https://www.mdpi.com/1996-1944/15/21/7513. Acesso em: 21 jul. 2023.

ZHAN, Bao Jian; XUAN, Dong Xing; POON, Chi Sun; SHI, Cai Jun; KOU, Shi Cong. Characterization of C–S–H formed in coupled CO2–water cured Portland cement pastes. **Materials and Structures**, *[S. l.]*, v. 51, n. 4, p. 92, 2018. DOI: 10.1617/s11527-018-1211-2. Disponível em: https://link.springer.com/article/10.1617/s11527-018-1211-2. Acesso em: 30 ago. 2023.

ZHANG, Guohui; LI, Xiaohang; LI, Zongli. Experimental Study on Static Mechanical Properties and Moisture Contents of Concrete Under Water Environment. **Sustainability**, *[S. l.]*, v. 11, n. 10, p. 2962, 2019. DOI: 10.3390/su11102962. Disponível em: https://www.mdpi.com/2071-1050/11/10/2962. Acesso em: 21 set. 2023.

ZHAO, D.; CHANG, Q.; YANG, J. Analysis for Factors Affecting Fatigue Behaviour of Concrete. **Journal of building Structures**, *[S. l.]*, p. 102–105, 2008. Disponível em: https://www.researchgate.net/publication/289859511_Analysis_for_factors_affecting_fatigue_behavior_of_concrete. Acesso em: 14 ago. 2023.

ZHAO, Yanqing; LIU, Hui; BAI, Long; TAN, Yiqiu. Characterization of Linear Viscoelastic Behavior of Asphalt Concrete Using Complex Modulus Model. **Journal of Materials in**

Civil Engineering, *[S. l.]*, v. 25, n. 10, p. 1543–1548, 2013. DOI: 10.1061/(ASCE)MT.1943-5533.0000688. Disponível em: https://ascelibrary.org/doi/abs/10.1061/%28ASCE%29MT.1943-5533.0000688. Acesso em: 05 ago. 2023.

ZHAO, Yasong; GAO, Jianming; CHEN, Gaofeng; LI, Shujun; LUO, Xu; XU, Zhenhai; GUO, Zhaoheng; DU, Hongjian. Early-age hydration characteristics and kinetics model of blended cement containing waste clay brick and slag. **Journal of Building Engineering**, *[S. l.]*, v. 51, p. 104360, 2022. DOI: 10.1016/J.JOBE.2022.104360. Disponível em: https://www.sciencedirect.com/science/article/abs/pii/S2352710222003734. Acesso em: 30 ago. 2023.

ZIDOL, Ablam; TOGNONVI, Monique Tohoue; TAGNIT-HAMOU, Arezki. Effect of Glass Powder on Concrete Sustainability. **New Journal of Glass and Ceramics**, *[S. l.]*, v. 07, n. 02, p. 34–47, 2017. DOI: 10.4236/njgc.2017.72004. Disponível em: https://www.scirp.org/journal/paperinformation?paperid=75985. Acesso em: 13 set.2023.

ZULKARNAIN, I.; LAI, L. S.; SYAKIR, M. I.; RAHMAN, A. A.; YUSUFF, S.; HANAFIAH, M. M. Life cycle assessment of crushed glass abrasive manufacturing from recycled glass. **IOP Conference Series: Earth and Environmental Science**, *[S. l.]*, v. 880, n. 1, p. 012054, 2021. DOI: 10.1088/1755-1315/880/1/012054. Disponível em: https://www.researchgate.net/publication/356127375_Life_cycle_assessment_of_crushed_glass_abrasive_manufacturing_from_recycled_glass. Acesso em: 28 set. 2023.